



Structural Analysis of a Floating Foundation for Offshore Wind Power under Service Conditions

Diogo Filipe da Silva Vasconcelos

Thesis to obtain the Master of Science Degree in
Mechanical Engineering

Supervisors: Prof. Luís Filipe Galrão dos Reis
Eng. Mário Alberto Silveira Costa Vieira

Examination Committee

Chairperson: Prof. João Orlando Marques Gameiro Folgado

Supervisor: Prof. Luís Filipe Galrão dos Reis

Member of the Committee: Prof. Rui Fernando dos Santos Pereira Martins

July 2019

Acknowledgments

First and foremost, I am grateful for all the help, comprehension and love that my parents and brother have always given me. I express my utmost gratitude for everything, as all my achievements are possible due to their care and efforts.

Second, I show my greatest appreciation to Carolina, my life partner, for all the support, understanding and respect.

Thirdly, to my supervisors, Professor Luís Reis and Engineer Mário Vieira, for all the knowledge and skills conveyed. Additionally, also thanking for all the time spent for the conclusion of this work.

A big thank you to all my colleagues, especially to José Cardoso, Diogo Dias, Gabriel Maciel and Vicente Salgueiro for all the tips and exchanged opinions.

Lastly, to all my friends who accompanied me during this journey.

Abstract

Wind power is a great solution for the increased necessity of producing electricity without carbon emissions. Going offshore is to enter the most promising market for this type of energy production. In spite of this, when it comes to high sea depths, economically viable solutions are still under development and/or testing, due to the necessity of being a floatable solution. This thesis focused on the analysis of the DeepCWind concept. The FAST software was used to produce the loads/conditions that the structure is supposed to endure. Afterwards, structural analyses were made with the ANSYS software. The main objective was to evaluate the original structure under a specific Design Load Case, which is required for the certification of these structures, and if necessary to perform a structural improvement. After the initial analyses, the original structure was not able to cope with the required conditions, thus an improvement process was made. The general dimensions and the members' outside diameters were not to be changed. The improvement work concentrated on the use of structural reinforcements, minor layout alterations and thickness adjustments. Several hypothesis were studied and the most advantageous solutions were adopted. Lastly, the improved structure was subjected to the previous Design Load Case and its results compared to previous versions. The final analyses presented safety coefficients above the required 1.2, with a minimum of 1.668 at the maximum required wind speed of 24 m s^{-1} .

Keywords: offshore wind power, DeepCWind, ANSYS, FAST, Design Load Case, structural analysis

Resumo

A energia eólica apresenta-se como uma das soluções com maior potencial para produzir electricidade sem emissões poluentes. Iniciando a exploração *offshore*, entra-se na componente de mercado com maior potencial para este método de produção de electricidade. Contudo, esta exploração em zonas com maior profundidade, ainda apresenta algumas limitações, pois uma plataforma flutuante é aconselhada, complicando a obtenção de uma solução que seja estrutural e economicamente vantajosa. A maioria das soluções existentes estão ainda a ser desenvolvidas e/ou testadas. Esta tese foca-se na análise estrutural da plataforma DeepCWind, bem como na posterior melhoria desta estrutura. Para obter as condições externas de carregamento, utilizou-se o programa FAST. Subsequentemente, o programa ANSYS foi usado para avaliar a resposta estrutural do DeepCWind às condições impostas. O objectivo principal consistiu na análise da versão original da estrutura, de acordo com um determinado teste de carga, e se necessário proceder ao seu reforço estrutural. Após as análises iniciais, a estrutura mostrou-se incapaz de suportar as condições exigidas, revelando uma necessidade de reforço estrutural. As dimensões gerais, bem como os diâmetros exteriores dos membros, não deveriam ser alterados. O processo de melhoria passava pelo uso de reforços estruturais, pequenas alterações de *layout* e/ou ajustamento de espessuras. Várias hipóteses foram examinadas, sendo selecionadas as mais vantajosas. Finalmente, a estrutura final foi avaliada segundo o mesmo teste de carga a que a plataforma original foi sujeita. As análises finais revelaram coeficientes de segurança mínimos superiores ao exigido, com 1.668 à velocidade máxima de vento requerida, 24 m s^{-1} .

Palavras-chave: energia eólica offshore, DeepCWind, ANSYS, FAST, teste de carga, análise estrutural

Table of Contents

Acknowledgments	ii
Abstract.....	iii
Resumo	iv
Table of Contents	v
List of Tables	ix
List of Figures	x
List of Software	xiv
List of Symbols	xv
Abbreviations and Acronyms List	xvii
1. Introduction.....	1
1.1. Motivation and Overview.....	1
1.2. Objectives	2
1.3. Document Structure	2
2. Bibliographic Research	3
2.1. How electricity is produced	3
2.2. Renewable Energies	4
2.2.1. Hydroelectric.....	4
2.2.2. Geothermal	4
2.2.3. Solar	5
2.2.4. Waves	5
2.2.5. Currents	5
2.2.6. Wind.....	5
2.3. Modern Perspective	6
2.4. Wind Power Potential.....	7
2.5. Ways of Collecting Wind Power.....	7
2.6. Wind Power Turbine.....	10
2.6.1. Blades.....	10
2.6.2. Dimensions	12
2.6.3. Control Systems	13
2.7. Offshore Foundations.....	15

2.8.	Types of Foundations for Offshore Wind Turbines	16
2.8.1.	Bottom Fixed Foundations.....	17
2.8.1.1.	Monopile Foundation	17
2.8.1.2.	Jacket Foundation	17
2.8.1.3.	Gravity Based Foundation	18
2.8.1.4.	Tripod Foundation.....	19
2.8.2.	Floating Structures.....	20
2.8.2.1.	Spar-buoy Foundation	20
2.8.2.2.	Semi-Submersible Foundation	21
2.8.2.3.	TLP	21
2.9.	Portugal and the Offshore Wind Power	22
2.10.	DeepCWind Foundation	23
2.10.1.	Foundation Members and Dimensions.....	24
2.10.2.	Platform Properties	26
2.10.3.	Previous Structural Improvements to Original Structure	26
2.11.	Finite Element Analysis and the Aliasing Problem	27
2.11.1.	Finite Element Method.....	27
3.	Methods	29
3.1.	Tower and Turbine Properties	29
3.2.	Material Properties	30
3.3.	FAST Software.....	30
3.4.	Coordinate Systems for the Analysis	31
3.5.	Simulation Parameters.....	31
3.6.	Sea Currents	35
3.7.	Marine Growth.....	36
3.8.	Finite Element Method	37
3.8.1.	Static Structural Analysis.....	37
3.8.2.	Transient Structural Analysis.....	37
3.8.3.	Modal Analysis.....	38
3.8.3.1.	Real World Effects for the Modal Analysis	39
3.9.	Modelling Techniques	40

3.9.1.	Shell Analysis	40
3.9.2.	Shell + Solid Submodel Analysis	40
3.9.3.	Shell – Solid Hybrid Model Analysis.....	40
3.10.	Boundary Conditions	40
3.11.	Linear Analysis	42
3.12.	Design Load Case	43
3.13.	The Rainflow Counting Method	44
4.	Results	47
4.1.	Time Step Study and Aliasing.....	47
4.1.1.	Experiment Method	47
4.1.2.	Results and Discussion	48
4.2.	Structural Analysis	50
4.2.1.	Original DeepCWind Platform Analysis	50
4.2.1.1.	Static Shell Simulation – Displacement Formulation.....	51
4.2.1.2.	Submodel Analysis – Displacement Formulation	51
4.2.1.3.	Static Shell Simulation – Springs Formulation	52
4.2.1.4.	Submodel Analysis – Springs Formulation.....	53
4.2.1.5.	Modal Analysis Results	54
4.2.2.	Structural Improvement	55
4.2.2.1.	UC and BC Joint Improvement.....	56
4.2.2.2.	BC Improvement.....	56
4.2.2.3.	UC Improvement.....	61
4.2.2.4.	MC Improvement	62
4.2.2.5.	Pontoons Improvement	64
4.2.2.5.1	Conical Connections	65
4.2.2.5.2	Disjoint Connections	67
4.2.2.5.3	Thickness Increment.....	68
4.2.3.	Final Analysis.....	68
4.2.3.1.	Springs Formulation at 11.4 m s^{-1}	69
4.2.3.2.	Displacements Formulation at 11.4 m s^{-1}	70
4.2.3.3.	Springs Formulation at 24 m s^{-1}	71

4.2.3.4. Displacements Formulation at 24 m s ⁻¹	72
4.2.3.5. Modal	73
4.3. Comparison of Results.....	75
5. Conclusions and Future Work.....	77
5.1. Conclusions.....	77
5.2. Future Work	78
Bibliography	79
Appendix A - Original Foundation Details	87
A.1. Static Shell Simulation – Displacement Formulation	87
A.2. Submodel Analysis – Displacement Formulation	87
A.3. Static Shell Simulation – Springs Formulation	88
A.4. Submodel Analysis – Springs Formulation	88
Appendix B - Improvement Process Details.....	90
B.1. Pontoons Disjoint and Joint Connection Comparison.....	90
B.2. Pontoons Conical Transitions with Triangular Reinforcements	91
B.3. Pontoons Simple Conical Transitions	93
Appendix C - Final Analysis Details	95
C.1. Springs Formulation at 11.4 m s ⁻¹	95
C.2. Displacements Formulation 11.4 m s ⁻¹	97
C.3. Springs Formulation at 24 m s ⁻¹	98
C.4. Displacements Formulation at 24 m s ⁻¹	100
C.5. Modal Analysis Supplement.....	101
Appendix D - Singularities	102

List of Tables

Table 2.1 Members dimensions	25
Table 2.2 Inertia properties of the structure	26
Table 2.3 Members dimensions	27
Table 3.1 NREL 5 MW wind turbine information.....	29
Table 3.2 Marine Growth Data.....	36
Table 4.1 Computational data.....	50
Table 4.2 Considered Natural frequencies of the structure.....	54
Table 4.3 Mode description and respective frequency.	74
Table 4.4 Platform versions comparison.....	75
Table B.1 Comparison of disjoint and joint connections.....	91
Table B.2 Comparison of reinforced and simple conical transitions.....	93
Table B.3 Comparison of conical transitions and no conical transitions.	94
Table C.1 Platform's Natural Frequencies	101

List of Figures

Figure 2.1 Hydroelectric power plant layout	4
Figure 2.2 Geothermal power plant layout	4
Figure 2.3 Solar panels installation	5
Figure 2.4 The <i>Pelamis</i> device	5
Figure 2.5 System to harvest currents' energy	6
Figure 2.6 Wind power turbine	6
Figure 2.7 Energy sources relative use from 1974 to 2016.....	6
Figure 2.8 Portugal's relative use of each energy source, from January 2019 to March 2019	7
Figure 2.9 Horizontal-Axis Turbines on the left and Vertical-Axis Turbines on the right.....	8
Figure 2.10 Upwind Turbine on the left. Downwind Turbine on the right.	8
Figure 2.11 Types of wind power turbines. a) Altaeros Energies' High Altitude Turbine; b) Ogin's Shrouded Turbine; c) Challenergy's Typhoon Turbine; d) Common Wind Turbine	9
Figure 2.12 Wind turbine description	10
Figure 2.13 Inside look of the constitution of wind turbine's blade	11
Figure 2.14 Airfoil section	11
Figure 2.15 Two bladed turbine on the left; one bladed turbine on the right.....	12
Figure 2.16 Usual power distribution of turbines on onshore and offshore conditions.....	12
Figure 2.17 Wind turbine control axis. Blade pitch control in black and yaw control in green	13
Figure 2.18 Rotor speed control strategy for a 2 MW turbine	13
Figure 2.19 Thrust force variation with wind speed.....	14
Figure 2.20 Types of offshore foundations for wind turbines	16
Figure 2.21 Monopile Foundation	17
Figure 2.22 Jacket Foundation	18
Figure 2.23 Gravity Based Foundation	19
Figure 2.24 Tripod Foundation	19
Figure 2.25 Spar-buoy Foundation	20
Figure 2.26 WindFloat Foundation	21
Figure 2.27 TLP Foundation	22
Figure 2.28 At the left, simulated map of average wind speeds at an altitude of 80 m. On the right, simulated map of average turbulence intensity at an altitude of 80 m	22
Figure 2.29 DeepCWind Foundation	24
Figure 2.30 General dimensions of the structure and identification of the larger members. YL member is hidden, connecting the bottom of the MC and the BC.....	25
Figure 2.31 Reinforcements used in previous improvement process	26
Figure 2.32 Aliasing effect	27
Figure 3.1 FAST environmental conditions	30
Figure 3.2 Structure coordinate system.....	31
Figure 3.3 Mathematical wave simplification.....	32

Figure 3.4 Location specified for this project	32
Figure 3.5 HydroDyn additional linear restoring stiffness matrix	34
Figure 3.6 Water velocity profiles as a function of water depth.....	35
Figure 3.7 FEA procedure example.....	37
Figure 3.8 Simplified mass-spring system.....	38
Figure 3.9 Interval ranges for resonance, already including safety coefficient of 10%.	39
Figure 3.10 Platform dynamic offset representation.....	41
Figure 3.11 Displacement Formulation input.....	42
Figure 3.12 Springs Formulation input.	42
Figure 3.13 Load time series	44
Figure 3.14 Rainflow Algorithm	45
Figure 4.1 Location of selected point.....	48
Figure 4.2 Stresses verified.	49
Figure 4.3 Amount of cycles verified at the selected element.	49
Figure 4.4 Relative error of using different time steps.....	49
Figure 4.5 Global model analysis with the displacement formulation. Units in Pascal.	51
Figure 4.6 BC submodel with the displacements formulation. Units in Pascal.	51
Figure 4.7 Global model analysis with the springs formulation. Units in Pascal.	52
Figure 4.8 Details of the global model analysis with springs formulation. Units in Pascal.	53
Figure 4.9 Details of the global model analysis with the displacements formulation. Units in Pascal.	53
Figure 4.10 Details of the global model analysis with the displacements formulation. Units in Pascal.	53
Figure 4.11 Deformation Shapes: a) Mode 1 – Side to Side; b) Mode 1 - Fore-Aft; c) Mode 2 - Side-to-Side; d) Mode 2 - Fore-Aft; e) Mode 2 – Torsion.	55
Figure 4.12 UC and BC joint cut view. Original on the left; Improved on the right.	56
Figure 4.13 Reinforcement used at BC.	57
Figure 4.14 Reinforcements assembled.	57
Figure 4.15 Model analysis at 11.4 m s^{-1} , with the displacement formulation. Units in Pascal.	57
Figure 4.16 Central reinforcements at the BC. a) Dimensions; b) Location.	58
Figure 4.17 Reinforcements' Geometries and Dimensions.	58
Figure 4.18 Reinforcements Layout.	59
Figure 4.19 BC reinforcement analysis at 11.4 m s^{-1} , with the displacements formulation.	59
Figure 4.20 Reinforcement improvement. Analysis at 24 m s^{-1} , with the displacements formulation. Units in Pascal.	59
Figure 4.21 Improved Reinforcement. a) Reinforcement geometry; b) Analysis of this reinforcement. Analysis at 24 m s^{-1} , with the displacements formulation. Units in Pascal.	60
Figure 4.22 BC thickness segmentation.	60
Figure 4.23 MC. a) Thickness segmentation. b) Analysis' results. Analysis at 11.4 m s^{-1} , with the displacements formulation. Units in Pascal.	61

Figure 4.24 UC. a) UC reinforcements; b) UC analysis. Analysis at 11.4 m s^{-1} , with the displacements formulation. Units in Pascal.....	61
Figure 4.25 UC. a) UC top view; b) UC side cut view.	62
Figure 4.26 MC. a) Reinforcements design; b) Reinforcements analysis. Analysis at 11.4 m s^{-1} , with the displacements formulation. Units in Pascal.....	62
Figure 4.27 MC's bottom. a) Dimensions; b) Design; c) Analysis. Analysis at 11.4 m s^{-1} , with the displacements formulation. Units in Pascal.....	63
Figure 4.28 MC reinforcements. a) at the top; b) at the bottom.	63
Figure 4.29 MC segmentation.	64
Figure 4.30 Pontoons identification.	65
Figure 4.31 Weld bead. Real weld bead on the left. Simulated one on the right.	65
Figure 4.32 Conical connections. a) DU to UC; b) YL+CB to MC.	66
Figure 4.33 Conical connection analysis. With conical connections on the left and without on the right. Analysis at 11.4 m s^{-1} , with the displacements formulation. Units in Pascal.....	66
Figure 4.34 Connection study. a) Joint connection; b) Disjoint connection.....	67
Figure 4.35 Joint analysis. Joint connection on the left and disjoint connection on the right.....	67
Figure 4.36 Global model analysis with springs formulation. Units in Pascal.	69
Figure 4.37 Plot of the highest stresses verified during the time of the analysis.	69
Figure 4.38 BC analysis with the displacements formulation. Units in Pascal	70
Figure 4.39 Plot of the highest stresses verified during the time of the analysis	70
Figure 4.40 Global model analysis with the springs formulation. Units in Pascal.	71
Figure 4.41 Plot of the highest stresses verified during the time of the analysis.	71
Figure 4.42 BC analysis with the displacements formulation. Units in Pascal	72
Figure 4.43 Plot of the highest stresses verified during the time of the analysis.	72
Figure 4.44 Structure Fundamental Frequency.....	73
Figure 4.45 Figure Deformation Shapes from the Modal Analysis; a) Mode 1 – Side to Side; b) Mode 1 - Fore-Aft; c) Mode 2 – Torsion; d) Mode 2 - Fore-Aft; e) Mode 2 - Side-to-Side.	74
Figure A.1 Global model analysis. Units in Pascal.....	87
Figure A.2 BC Submodel analysis' details. Units in Pascal.	87
Figure A.3 Details of the global analysis with the springs formulation. Units in Pascal.	88
Figure A.4 Submodel Analysis' details. Units in Pascal.	88
Figure A.5 Submodel Analysis' details. Units in Pascal.	89
Figure B.1 Pontoons disjoint and joint connection comparison. Units in Pascal.....	90
Figure B.2 BC member conical transition.	91
Figure B.3 Conical connections with triangular reinforcements. a) triangular reinforcement at the CB members; b) exterior view of reinforced conical connection; c) interior view of reinforced conical connection (the conical transition is partially transparent, allowing to see the reinforcements inside). 92	92
Figure B.4 Comparison of reinforced conical transitions with simple conical transitions. Units in Pascal.	92

Figure B.5 Simple conical transitions. Units in Pascal.	93
Figure B.6 Without conical transitions. Units in Pascal.	94
Figure C.1 UC detail. Units in Pascal.	95
Figure C.2 BC connections detail.	95
Figure C.3 MC top detail.	96
Figure C.4 MC bottom cut view detail.	96
Figure C.5 MC bottom detail.	96
Figure C.6 Time series of the safety coefficient.	97
Figure C.7 BC cut view. Units in Pascal.	97
Figure C.8 Time series of the safety coefficient.	98
Figure C.9 UC detail. Units in Pascal.	98
Figure C.10 BC connections detail.	98
Figure C.11 MC top detail.	99
Figure C.12 MC bottom cut view detail.	99
Figure C.13 MC bottom detail.	100
Figure C.14 Time series of the safety coefficient.	100
Figure C.15 BC cut view. Units in Pascal.	100
Figure C.16 Time series of the safety coefficient.	101
Figure C.17 Deformation shapes. a) Mode 1 - Torsion; b) Mode 1 - Bending Fore-Aft; c) Mode 1 - Bending Side-to-Side.	101
Figure D.1 BC detail.	102
Figure D.2 Singularity detail.	102

List of Software

ANSYS 16 – Engineering Simulation & 3D Design Software

ANSYS 2019 R1 – Engineering Simulation & 3D Design Software

Excel 2016 – Spreadsheet Software

FAST 8 - Fatigue, Aerodynamics, Structures and Turbulence CAE Software for Wind Turbines

MatLab R2017b – Matrix Laboratory; Numerical Computing Environment

SolidWorks 2017 – 3D CAD design and analysis software

List of Symbols

Greek Symbols

α	Angle of attack
δ	Kronecker Delta
ζ	Wave elevation
ρ	Density
τ	Dummy variable

Roman Symbols

A_0	Undisplaced waterplane area of platform
$C_{ij}^{Hydrostatic}$	Linear hydrostatic-restoring matrix
CO_2	Carbon Dioxide
F_i^{Hydro}	Hydrodynamic model
F_t^{Waves}	Diffraction Forces
f_{1P}	1P frequency
f_{3P}	3P frequency
g	Gravity acceleration
H_s	Significant Wave Height
k	stiffness
K_{ij}	(i,j) component of the wave-radiation-retardation kernel matrix
m_b	Total mass of marine growth
m_f	Total mass of ballast
NO_x	Nitrogen Oxides
q_j	Platform displacement
\dot{q}_j	Platform velocity
SO_2	Sulphur Dioxide
t	time
T_p	Peak Wave Period
U_{ons}	Current velocity at SWL with near-surface current model
U_{oss}	Current velocity at SWL with sub-surface current model
U_{ns}	Current velocity with near-surface current model
U_{ss}	Current velocity with sub-surface current model
V_0	Dislocated volume of fluid for the platform undisplaced position

x,y,z	Cartesian coordinates
x_b,y_b,z_b	Coordinates of the centre of buoyancy of the undisplaced platform
x_f,y_f,z_f	Coordinates of the centre of mass of the undisplaced filled fluid
x_{mg},y_{mg},z_{mg}	Coordinates of the centre of mass of the undisplaced marine growth

Subscripts

(i,j)	Coordinate (i,j) of matrix
b	Buoyancy
f	Filled fluid (ballast)
max	Maximum
mg	Marine growth
min	Minimum
ns	Near-surface
ss	Sub-surface

Abbreviations and Acronyms List

ARSEM	Association de Recherche sur les Structures Métalliques Marines
BC	Bottom Column
CB	Cross Brace
CM	Centre of Mass
CNC	Computer Numerical Control
CPU	Central Processing Unit
DL	Delta Lower pontoon
DLC	Design Load Case
DNV	Det Norske Veritas
DOF	Degree of Freedom
DU	Delta Upper pontoon
E	East
FAST	Fatigue, Aerodynamics, Structures and Turbulence
FEA	Finite Element Analysis
FEM	Finite Element Method
GL	Germanischer Lloyd
JONSWAP	Joint North Sea Wave Observatory Project
MC	Main Column
N	North
NREL	National Renewable Energy Laboratory
OC4	Offshore Code Comparison Collaboration Continuation
RAM	Random-access memory
REN	Redes Energéticas Nacionais
SWL	Sea Water Level
TLP	Tension Leg Platform
UC	Upper Column
UK	United Kingdom
USA	United States of America
YL	Y Lower pontoon
YU	Y Upper pontoon

Chapter 1

1. Introduction

1.1. Motivation and Overview

Nowadays, electricity is a fundamental resource, as daily routines depend on it for all sorts of activities, from work to entertainment, and its demand is increasing. This demand is currently high due to the move towards electrical transportation, the growth of connected devices and the digitalization of modern economies [1].

Although electricity's use is not harmful for the environment, the same ~~cannot~~ be said about its production and distribution. In 2017, 40% of total USA energy-related CO₂ emissions were made by electrical production power plants, most of them burnt fossil fuels (or its products) [2].

The new approach to electricity production is producing it in a sustainable and clean way and to achieve this, the use of renewable energy sources is essential. Some of the most common energy sources are wind, solar, waves and rivers. The use of wind, commonly known as wind power, is one of the most important components of future energy scenarios [3]. The most usual method of using wind to produce electricity is with the three-bladed wind turbine. Depending on the site of installation, it can be classified as onshore or offshore wind power. The exploration of onshore wind power is widely spread, but these days, offshore wind power is considered as an option with great potential. In terms of practical implementation offshore wind technology is years behind onshore technology, as it was developed almost a century later [4].

There are many challenges in the future of offshore wind power, but it is an industry that is growing fast. One of the biggest challenges is the foundation structures needed for offshore use. Unlike onshore or some fixed offshore foundations, the foundations for greater depths need to be of the floating type, presenting a bigger challenge for a working and economically viable structure. Floating platforms are subjected to a variety of loads, as in addition to the weight of the turbine itself, they need to withstand dynamic loads and dynamic offsets from its equilibrium position, as a result of the action of the sea and the wind on the structure.

1.2. Objectives

The objective of this project is to carry out a structural analysis of a foundation for offshore turbines, to be used in deep waters. The project focuses on the DeepCWind concept. An analysis of the initial concept will be produced and the needed modifications will be made in order to satisfy de Design Loading Case 1.1. The main objective is to strengthen the structure without modifying its outside dimensions. Therefore, reinforcements and thickness modifications ought to be performed. Additionally, the structure mass should be as low as possible. A paper was written about the original platform examination, called "*Structural Evaluation of the DeepCWind Offshore Wind Foundation*" and submitted to the *Frattura ed Integrità Strutturale* international journal.

1.3. Document Structure

This document is structured in the following way:

- **Chapter 1 – Introduction:** the subject of this thesis is presented, its objectives and the structure of the document;
- **Chapter 2 – Bibliographic Research:** the historical approach to energy production is presented. Renewable energies are introduced, as well as the role of wind power. Wind power technologies are explained, along with its suitability for Portugal. The aliasing effect is also presented;
- **Chapter 3 – Methods:** the mathematical approaches for the description of environmental conditions are explained, as well as the considered boundary conditions. Finite element analysis are presented, including the assumptions for this research;
- **Chapter 4 – Results:** the use of a suitable time step is examined, in order to produce accurate results, thus avoiding aliasing from the discretization of environmental loads. The original structure performance under the required loads is shown. Subsequently, the improvement process is described and the analysis of the obtained structure is made;
- **Chapter 5 – Conclusions and Future Work:** the main conclusions of the project are exposed, together with recommendations for future improvements.

Chapter 2

2. Bibliographic Research

2.1. How electricity is produced

Michael Faraday, in 1831, discovered that the movement of a magnet inside a coil of wire produces an electric current in the wire. This principle would later be used in electrical generators, usually through the use of a rotating shaft, thus providing a movement to the magnet [5]. One of the easiest ways to rotate a shaft is to have it connected to a turbine that would be rotated by a fluid, like moving water or a boiling fluid, which may be heated by a certain fuel. For example, when it's said that coal is the source of power, it means that coal is used to heat the fluid that will rotate a turbine. This stands for the basic method of electricity production used until today.

In 1882, the first commercial installation of electric power and light distribution, on land, was developed by Thomas Edison, making it available to numerous people. At the time, electricity was produced by generators driven by steam engines [6]. Coal was used to fuel the steam engines. The use of coal to produce energy was one of the major contributors to the Industrial Revolution but a high price was paid by the environment.

Coal is a fossil fuel, thus a limited resource, but the big disadvantage of its use is the impact that it has on the planet. The combustion of coal is a source of emissions to the atmosphere such as Sulphur dioxide (SO_2), Carbon Dioxide (CO_2), Nitrogen Oxides (NO_x) and flying ashes [7].

A few years later, Natural Gas came into play and started being used in electricity production [8]. Again, it was a fossil fuel and a limited resource. Although, it emitted 50% to 60% percent CO_2 than Coal, it was not a non-pollutant option.

Next big source of power was nuclear. In 1951, the first nuclear reactor used for electricity production, was built. This power source possess two major problems: its residues and its deadly history. In terms of residues, to produce a nuclear reaction the atoms used go through the process of fission (its division) which produces radioactive components that are difficult to safely eliminate or store. Its history has not been peaceful either, due to catastrophic accidents that released massive amounts of radioactive material into the environment, like Chernobyl (1986) or Fukushima (2011) [8].

In 1997, the Kyoto Protocol was signed as a commitment to stabilize atmospheric concentrations of Greenhouse Gases to a level that will prevent or reduce dangerous interference to a healthy climate system [9]. More recently, in 2015, the Paris Climate Agreement was embraced, which aims to promote a sustainable development by keeping a global average temperature rise well below 2 degree Celsius, above pre-industrial levels, throughout this century. Moreover, a limit of 1.5 degrees should be pursued [10].

2.2. Renewable Energies

After decades of a mentality of mass production of energy without caution, the world started to worry about the effects that pollution could have on the environment and began to think on the future of the planet. To think about its future, it had to think about its past. Humans have been harnessing energy from the sun, wind or water for thousands of years and it was time to produce electricity with these sources, which are clean and renewable. The term renewable is used to describe a source of energy that can be said to be infinite, in our life span. Renewable energies have their origin on three, so called, primary sources: solar radiation, heat from the earth's core and the gravitational interaction between earth and other celestial objects, mainly the sun and the moon. Solar energy is the fundamental source of many earth's phenomena: about 1/3 of the radiation that reaches the earth's surface is used by the hydrological cycle, atmospheric temperature differences create zones with different pressures causing the wind, ultimately producing the waves, and plants use solar radiation to accomplish photosynthesis [11]. The most well-known sources of renewable energy are: hydroelectric, geothermal, solar, waves, currents and wind.

2.2.1. Hydroelectric

A dam is constructed, which allows to store water, from a river, in a reservoir. To produce electricity, the water is released through a channel that transports the water into a hydraulic turbine. The motion of the water rotates the turbine, which is connected to a generator. The generator produces electricity due to the input of the rotational movement [12]. Figure 2.1 shows the working system of such constructions.

2.2.2. Geothermal

This energy source is the heat from the Planet Earth itself. It is usually installed in volcanic regions and uses the heat from hot water or hot rock, found a few miles beneath the surface, and from magma¹ as well. The heat is used to boil a working fluid which will rotate a turbine [13]. Figure 2.2 shows a geothermal power plant working scheme.

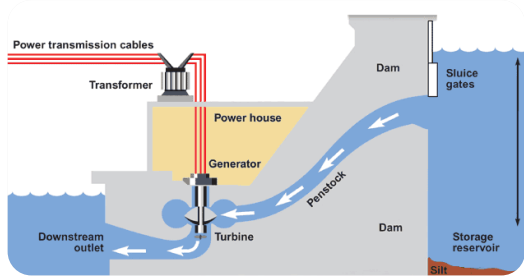


Figure 2.1 Hydroelectric power plant layout [12].

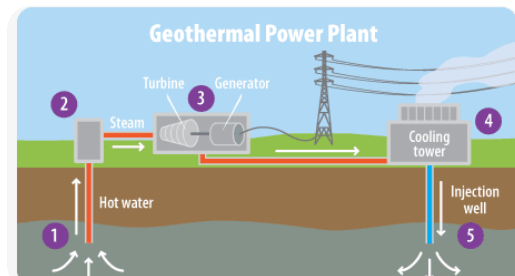


Figure 2.2 Geothermal power plant layout [13].

¹ High temperature molten rock.

2.2.3. Solar

There are mainly two very different approaches: photovoltaic panels and sun heated reservoirs. Solar-powered photovoltaic panels consist of silicon cells. The electrons of these cells are excited by photons, which come from the sun, thus creating an electric current that can be collected [14]. Other approach, is using U-shaped mirrors that focus sunlight on pipes transporting a circulation fluid. This circulation fluid will then be used to boil water, which will rotate a turbine [15]. Figure 2.3 shows a solar panels installation.

2.2.4. Waves

In order to use the power of the waves, several solutions have been developed, most of them still under testing. For example, some of the solutions use the rotation of turbines by passing waves while others make use of the spread of the waves to move components of lengthy cylindrical structures [16]. Figure 2.4 displays such cylindrical structures, namely the *Pelamis wave-following attenuation device*. This device was installed in Portugal, in 2008, with three devices, each of 120-meters, being installed 5km off the coast of Aguçadoura. This project ended much earlier than expected, as in November 2008, technical problems forced the devices to be brought to shore. Although the problems were fixed, the beginning of a financial crisis prevented the successful resume of the project [17].



Figure 2.3 Solar panels installation [14].



Figure 2.4 The *Pelamis* device [17].

2.2.5. Currents

The use of ocean currents may also be advantageous. Ocean currents have a relatively constant and directional flow, with large amounts of potentially useful energy being carried across the ocean. Turbines can be installed in deep waters, thus harvesting the energy transported by these currents [18]. Figure 2.5 shows a conceptual installation for such system.

2.2.6. Wind

The most common way of producing electricity using the wind is by rotating a wind turbine due to the motion of the wind, also rotating a shaft that is connected to the electricity generator. These turbines can be used for *utility-scale wind* with large turbines producing several megawatts or for *distributed wind* as for small turbines being used to directly power a home [19]. Figure 2.6 shows a common wind turbine

system. Wind Power is the focus of this project and thus will be thoroughly explained in following sections.

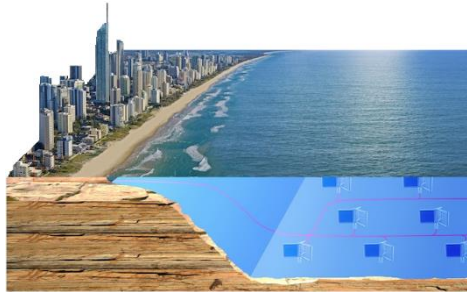


Figure 2.5 System to harvest currents' energy [18].

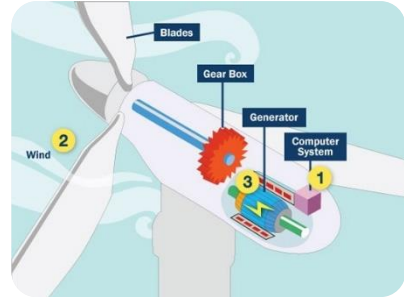


Figure 2.6 Wind power turbine [19].

2.3. Modern Perspective

Data of 2017 revealed that Renewables Energies were still a small part of the world electrical production, having a significance of around 24% [20]. Figure 2.7 shows the evolution of the relative use of each source of energy from 1974 to 2016 [21].

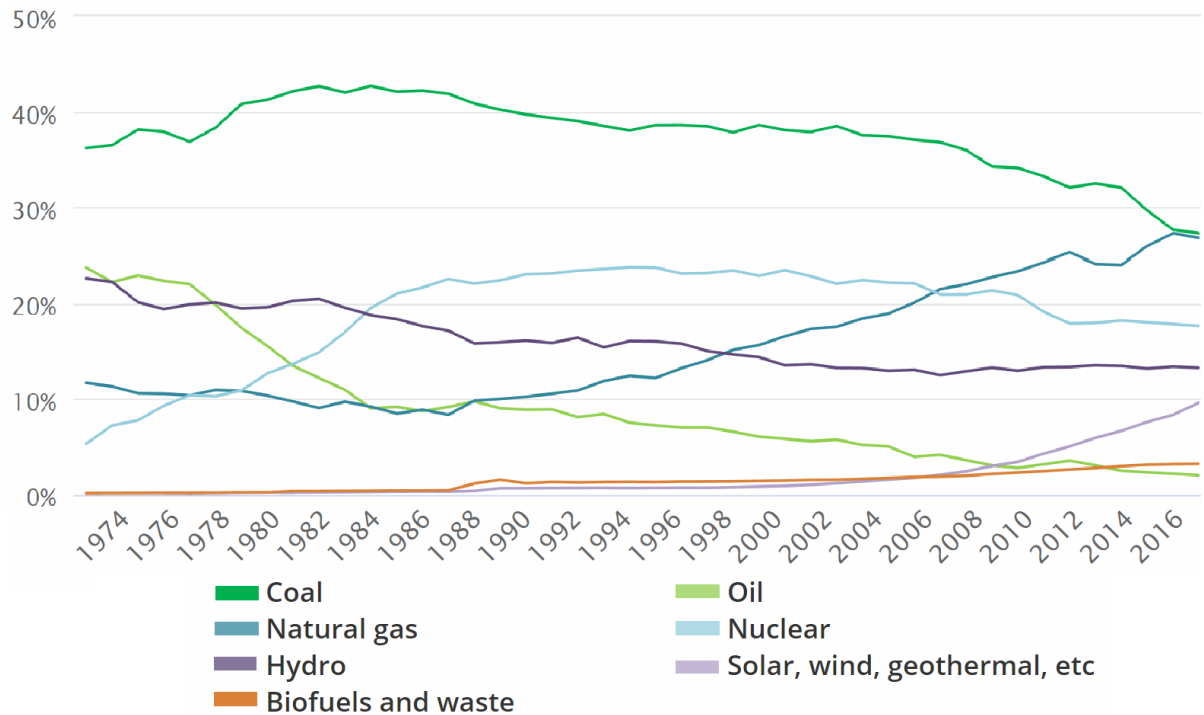


Figure 2.7 Energy sources relative use from 1974 to 2016 [21].

From this information, it can be understood that the change from fossil fuels to renewable energies is not being made fast enough. And that is not all. In addition to this, the electrical transportation revolution is starting and the current electricity capacity is not enough to support this new paradigm. Today's grid would most probably fail catastrophically if the entire US car fleet was to immediately make the change from fuel to electricity [22]. With all this happening at the same time, it is important to take the right decisions, and the investment on renewable energies is necessary. One of the most popular

renewable energies is Wind Power. Figure 2.8 shows the relative use of each source in Portugal for 2019, between January and March [23].

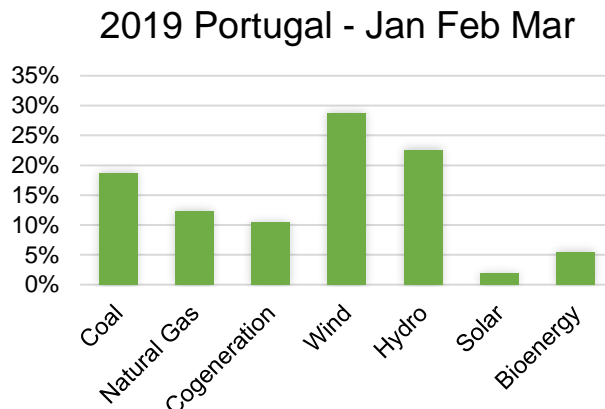


Figure 2.8 Portugal's relative use of each energy source, from January 2019 to March 2019 [23].

From the examination of this picture, it can be understood that renewable energies already have a key role for supplying electricity in Portugal, having a weight of 58.64%. Wind power presents itself as responsible for the production of 28.67% of the total power [23].

2.4. Wind Power Potential

Climate scientist Katherine Marvel was responsible for a study evaluating the maximum potential use of Wind Power to produce energy. Collectively adding more turbines slows down the wind to be used by subsequent turbines. Consequently, there is a certain amount of turbines, added to a certain place, after which the generation of electricity is not substantially increased. This limit situation was considered and the simulations showed that there is a potential for producing 400 Terawatts from surface winds, increasing to 1800 Terawatts if winds throughout the atmosphere were explored. Comparing this limit to the current global usage, which is about 18 Terawatts, it can be concluded that there is an enormous potential as a source of clean energy [24].

2.5. Ways of Collecting Wind Power

For centuries, Mankind has been using wind for his advantage, from windmills to the new generation of Wind Turbines, not forgetting the ships that hundreds of years ago used the wind to sail. In our time, different solutions have been found to produce energy, most of them consisting of different kinds of turbines.

Most turbines can be classified using three criteria:

- **Alignment of the Rotor's Axis:**
 - **Horizontal-axis wind turbine:** the rotating axis is horizontal, i.e., parallel with the ground. They are usually heavier than vertical ones and also do not collect well in

turbulent winds [25]. The advantages are that they produce more electricity from a given amount of wind and they can be set up higher, which means more wind speed [26].

- **Vertical-axis wind turbine**: The rotating axis is perpendicular with the ground. They are a better option when the wind conditions are very irregular, as they are powered by wind coming from all 360° , thus not needing to perform the turbine's alignment every time these conditions change [25]. Furthermore, in some cases, they can be powered by wind blowing from top to bottom [27].

Figure 2.9 displays horizontal-axis rotors on the left and vertical-axis rotor on the right.

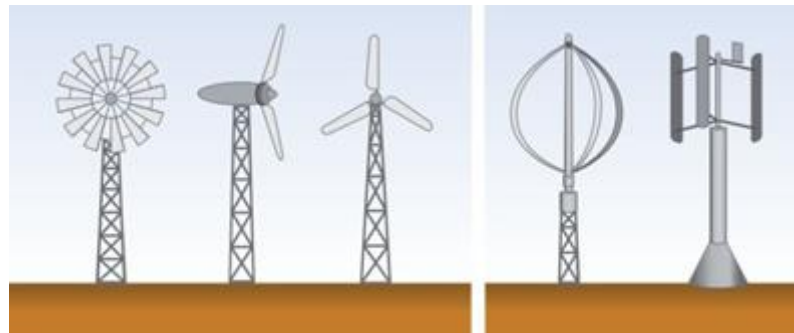


Figure 2.9 Horizontal-Axis Turbines on the left and Vertical-Axis Turbines on the right [25].

- **Direction of the wind:**

- **Upwind**: the wind passes first through the blades and then through the tower, reducing shadowing effects. There is a more smoothly operation and more power is produced. It's the most common type. It is shown in Figure 2.10 on the left.
- **Downwind**: the wind goes through the tower and only then through the blades, creating a high degree of shadowing effects that can cause flexion on the blades, resulting in more fatigue to the structure due to the increased flexion cycles [28].

Figure 2.10 shows a downwind turbine on the right.

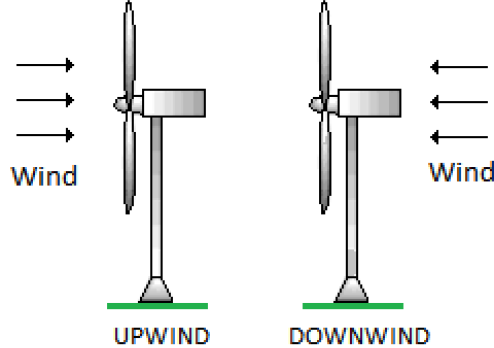


Figure 2.10 Upwind Turbine on the left. Downwind Turbine on the right. Adapted from [28].

- **Site of installation:**

- **Onshore**: if they are installed on land.
- **Offshore**: if they are installed at sea.

As stated before, several kinds of turbines have been developed, most of them being prototypes. Some concepts include:

- **Altaeros Energies' High-Altitude Turbine**: This kind of turbine was developed to be used at high altitudes, around 600 meters. Basically, it is a small turbine inside a large helium-filled inflatable body. The big advantage is that the higher the turbine is set up, the steadier and stronger the winds are, thus generating twice as much power as common ground turbines [29,30]. Figure 2.11 a) shows this type of turbine.
- **Ogin's Shrouded Turbine**: This corporation produces a much smaller type of turbine which can be applied at business or residential sites. This turbine possess a body in funnel form around it, which has two effects. First, in the front part of the turbine, it increases the speed of the air, allowing for higher efficiencies, even at lower wind speeds than conventional turbines. Second, at the back of the funnel body, it reduces the downstream turbulence and the shadowing effects [30]. Figure 2.11 b) shows this type of turbine.
- **Challenergy's Typhoon Turbine**: This Japanese design was built to withstand the violent and destructive forces of hurricanes' winds, which are very common in Japan [31]. They have a vertical axis and are very durable – according to the manufacturer [30]. This type of turbine is shown in Figure 2.11 c).
- **Common Wind Turbine**: the most common device used to convert the movement of the wind into electricity is the horizontal axis, upwind turbine. Some reasons could be pointed for its market dominion: its simple design, they occupy a relatively small area at the ground level, their maintenance is cheap and mostly, they are very versatile, thus can be used in very different environments [32]. There are several different designs with different number of blades, but the most used is the one with 3 blades. This is the type of turbine that is going to be used throughout this project and it will be discussed in detail. Figure 2.11 d) displays this type of turbine.

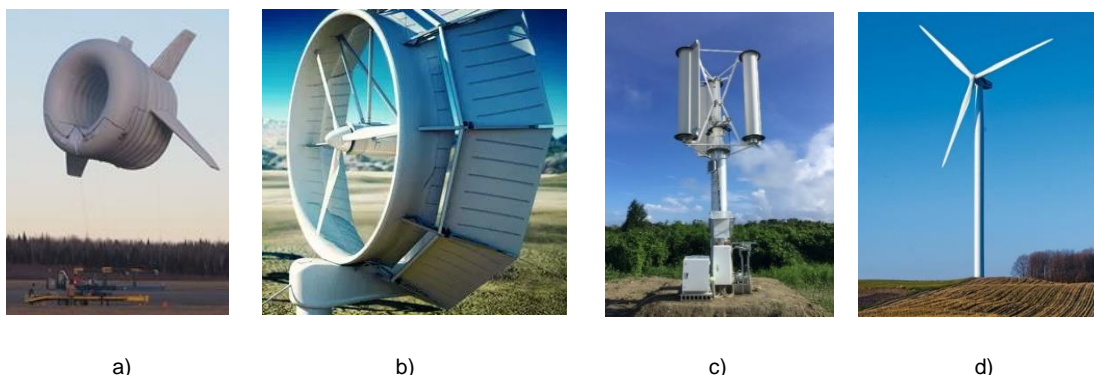


Figure 2.11 Types of wind power turbines. a) Altaeros Energies' High Altitude Turbine [29]; b) Ogin's Shrouded Turbine [30]; c) Challenergy's Typhoon Turbine [31]; d) Common Wind Turbine [32].

2.6. Wind Power Turbine

A wind turbine consists of 5 main parts:

- **Tower**: it supports the structure of the turbine.
- **Nacelle**: it is assembled on top of the tower and it houses the main components that allow the turbine to function and generate power. These components include the gear box, shafts, generator, controllers and brakes. Some turbines have these components at ground level, instead of inside the nacelle.
- **Hub**: it is the structure where the blades are fixed and is connected to the Nacelle. The Hub and Blades together are called the Rotor.
- **Blades**: when the wind is blown over them, they cause the Rotor to spin.
- **Foundation**: it's the structure that supports the tower [33].

A common wind turbine is shown in Figure 2.12, with the identification of some of the components previously described.

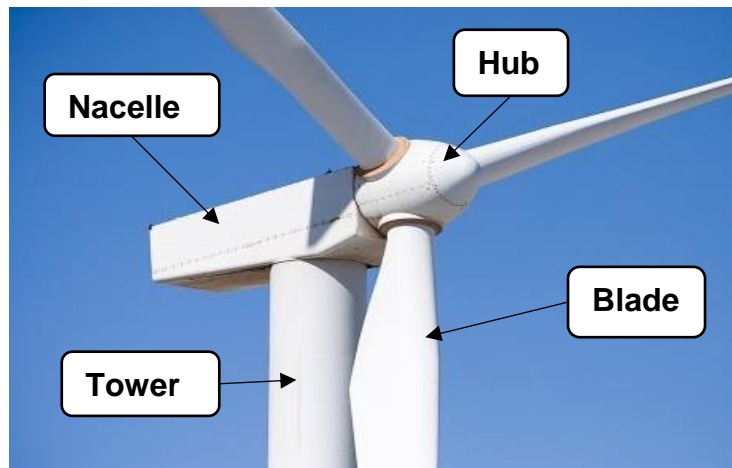


Figure 2.12 Wind turbine description [33].

2.6.1. Blades

Most contemporary blades consist of an upper and lower shell with inner reinforcements ending at a circular section at the blade root. Most often, they are made of composite materials and are very sensitive to damage during transport and installation [34]. Figure 2.13 shows the inside of a blade and its composition.

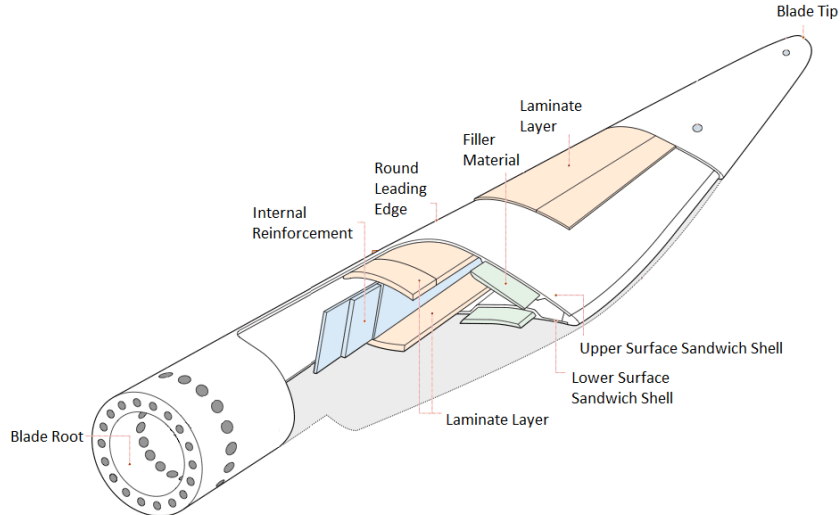


Figure 2.13 Inside look of the constitution of wind turbine's blade. Adapted from [34].

In order to increase the turbine's efficiency, the blades have an aerodynamic profile, which generates lift and rotates the turbine [35]. There are, mainly, two types of forces that command the behaviour of the rotor's blades when acted upon by the wind: lift and drag. Lift is the force that allows for the rotation of the rotor and should be maximized. On the other hand, drag, a resistive force acting against the movement of the blade, ought to be minimized. The aero dynamical principles of the blades are the same as for an aircraft wing's airfoil section, thus such body will be discussed for simplicity. Figure 2.14 shows a typical airfoil section.

When facing a horizontal airstream, this type of body will divide the flow into an upper and a lower flow, relatively to the airfoil. Such division is due to the different geometries used for each side of the airfoil. The upper surface is more curved, which accelerates the air, forcing it to travel further and faster over the wing, contributing to a decrease in pressure at that side. On the opposite side, a flatter geometry is used that will produce a positive pressure. The combination of these effects will promote a lift force. As for the drag, it is to be reduced as much as possible, because a high level of drag will contribute to the creation of eddies, therefore turbulence. To minimize this force, a smooth contour over the body should be designed, causing the flow to stay as close to the wing as possible, consequently remaining in laminar flow conditions [27]. The angle of attack, α , of a blade/wing can be adjusted and this will be discussed at the Control Systems Section.

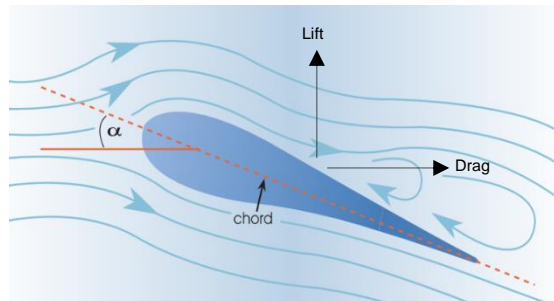


Figure 2.14 Airfoil section. Adapted from [27].

There are different designs where a different number of blades is used per turbine. Figure 2.15 shows a design of a two bladed turbine and other of a one bladed turbine.

The use of three blades was actually a compromise. When the blades swing through the air, they produce turbulence that will affect the air that will flow through the next blade. As the number of blades increase, the airflow through the next blade will be more tumultuous. Hence, the optimal number of blades should be one. The big disadvantage is that the use of just one blade could cause the turbine to become unbalanced and unstable [36,37]. Then, the use of two blades ought to be the right choice. Although they could be cheaper, they are slightly less efficient than three-bladed machines, as they require a higher rotational speed to get the same energy output [38]. Moreover, the yaw alignment operation is very demanding, as with the blades in a horizontal position, the forces required to align the rotor are very high and, in contrast, the forces are very low if the blades are vertical. This imposes cyclic forces much higher than those verified at a three bladed turbine [39,40]. The perfect compromise is using three [41]blades, in order to have better stability, bigger life span and higher energy production [37].



Figure 2.15 Two bladed turbine on the left [39]; one bladed turbine on the right [36].

2.6.2. Dimensions

The rotor's dimension is a direct indicator of the energy production capacity of the turbine. Generally, the bigger the rotor, the more power it will produce. A bigger rotor will also need a bigger structure to successfully support it. The smaller turbines are usually used onshore, due to the difficulty of transporting components of large dimensions on road, with power production ranging from 2 MW to 3 MW and with heights around 100 meters. The offshore turbines are usually much bigger, with power production ranging from 5 MW to 10 MW and with rotor's heights from 100 meters to almost 200 meters [27,42]. Figure 2.16 shows a distribution of the turbine's dimensions according to its power and site of installation. The green side represents onshore turbines, while the blue one represents offshore ones.

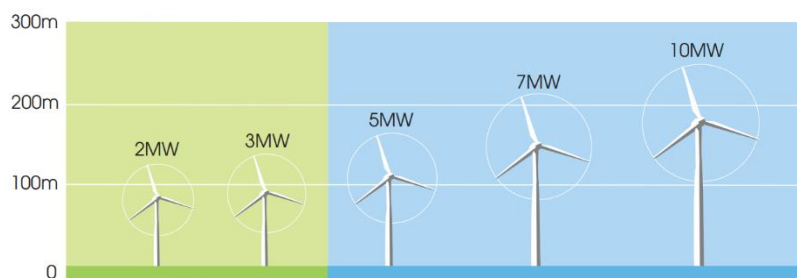


Figure 2.16 Usual power distribution of turbines on onshore and offshore conditions [27].

2.6.3. Control Systems

The wind is not a consistent and uniform phenomenon, it continuously changes its speed and/or direction. As a result, it would be impractical if a turbine and its blades were fixed. In order to solve this problem, several control systems are used, allowing for the optimization of wind capture and also the protection of the turbine from mechanical and electrical overloads.

For these reasons, three types of control systems should be referred:

- **Blade Pitch Control**: this control enables the rotation of the blade itself, allowing for the adjustment of the angle of attack, causing a better harvest of energy. On the other hand, when the wind is too strong, the alignment of the blades with the wind is mandatory, reducing the loads on the blades. The axis of rotation of the blade is represented in Figure 2.17, in black.
- **Yaw Control**: As the direction of the wind changes, the turbine also rotates in order to maximize the energy production in all conditions. Figure 2.17 shows the tower axis of rotation, in green.



Figure 2.17 Wind turbine control axis. Blade pitch control in black and yaw control in green. Adapted from [42]

- **Rotor Speed Control**: for this explanation, 2 MW wind turbine data will be considered, illustrated in Figure 2.18.

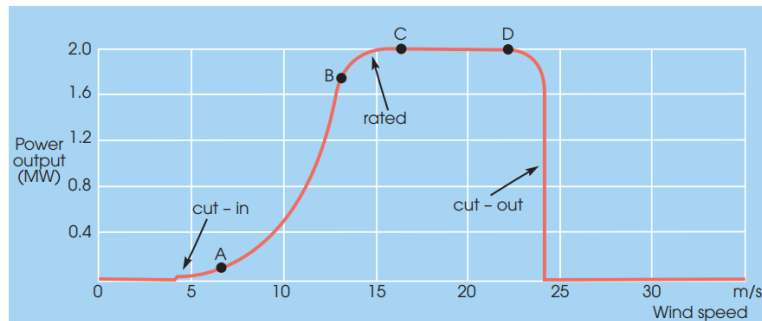


Figure 2.18 Rotor speed control strategy for a 2 MW turbine [27].

A typical control method consists of several regions:

- Cut-in speed: at first, there is the cut-in wind speed, which is the wind speed at which the turbine starts to generate power;
- Region A to B: above the cut-in speed and below the rated power, the turbine's available speed range is used to keep the tip-speed ratio near the optimum value, as the wind speed varies, aiming for a maximization of the overall performance of the turbine. Below point A, there is little power in the wind. At the example shown, this region stands between 7 to 13 m/s;
- Region B to C: close to the turbine maximum speed. A constant-speed mode is used while the power can fluctuate. The rotor torque must be held below its rated value to prevent excessive stress;
- Rated Speed: it is the wind speed at which the turbine starts to produce energy at its nominal power. The nominal power is the value at which the machine is designed to operate for long periods of time;
- Region C to D: the wind carries too much energy but the rated power must not be exceeded. This is accomplished using a constant-power mode. To accomplish this, the Pitch Control is very important, as it allows the production of energy at the same power level with increasing wind speeds;
- Cut-Out Speed: it's the speed at which the turbine stops operating due to the high probability of damaging the components of the structure. As this wind speed is achieved, for this example is around 24 m/s, the rotor is kept facing the wind, the blades are aligned with the flow and a brake is actuated to prevent rotation [27].

It is worth mentioning, the effects of thrust force at the Nacelle. The thrust force is a force acting, more critically, at the top of the turbine and caused by the environmental loads. It is in the same direction of the wind. This force peaks at the rotor's rated speed, as for increasing wind velocities the pitch control will increase the angle of attack and thus reducing the forces taken by the blades [43]. The evolution of this force is shown in Figure 2.19.

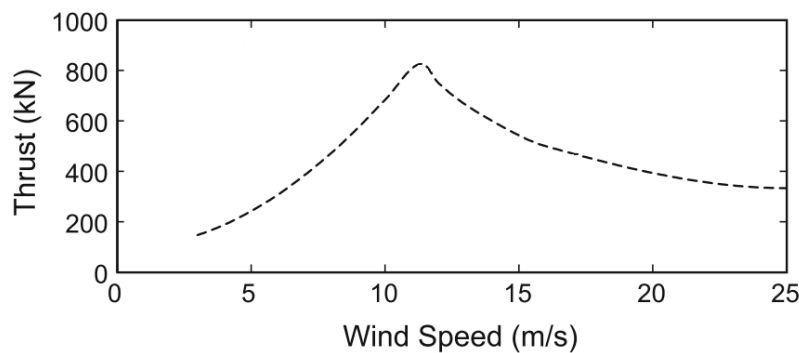


Figure 2.19 Thrust force variation with wind speed [26].

2.7. Offshore Foundations

The world's first offshore wind farm was the *Vindeby Offshore Wind Farm* which was commissioned in 1991. It was built in the south-east of Denmark. It was made up of eleven 450 KW wind turbines, which provided enough power for around 2 200 houses. Currently, it has already endured its lifespan of 25 years and as of 2017, it was being dismantled [44].

Today, the technology has evolved and in September of 2018 the world's largest operational offshore wind farm was officially opened. The *Walney Extension Offshore Wind Farm* is located in the Irish Sea and with 87 turbines, it is capable of powering almost 600 000 homes in the United Kingdom [45].

As stated by the World Economic Forum:

"Offshore wind farms have been the focus of considerable innovation, outpacing development in the onshore wind sector. A major reason for this is that offshore wind farms typically exceed expectations, outperforming their onshore counterparts" [46].

When onshore or offshore wind power are considered, it should be noted the merits and downfalls of each option. On one hand, onshore wind farms are relatively cheap, the installation of the transmission cables to the grid are relatively cheap (compared to the offshore option) and its installation is relatively quick when compared to other power sources. On the other hand, the visual impact on the landscape is one of the biggest concerns, wind conditions are not as uniform as at sea and noise is emitted by the turbines [47].

As for offshore wind power, turbines can be built a lot bigger and taller, allowing for more energy production. Also, if turbines are built far from the coast, it has a smaller visual impact, which means that wind farms can be larger, taking advantage of higher wind speeds and less turbulence at sea, due to the lack of obstacles to the wind flow, like buildings or mountains. In addition, a platform has to be built in order to support the turbine, which is the most expensive part of the project. Long cables also have to be used in order to connect the power generator to the onshore grid, which will need a very expensive installation [47].

The biggest challenge for offshore wind power is to produce a suitable and economically viable platform for the turbine. The platform is the structure that has to be built to support the turbine and its loads. The defining factor for the production of such structures is the sea depth where they will be installed.

2.8. Types of Foundations for Offshore Wind Turbines

As stated, the biggest challenge for offshore wind power is the design of the foundation in a structural and financial viable way [48]. Figure 2.20 shows different designs available for offshore wind power.



Figure 2.20 Types of offshore foundations for wind turbines [48].

The depth of the sea is the most problematic concern, due to the increasing complexity of the structures as the depth also increases. The sea depth, at the continental shelf is generally classified in three categories:

- **Shallow Water:** up to 30 meters;
- **Transitional Water:** from 30 to 60 meters;
- **Deep Water:** deeper than 60 meters [26].

According to the sea depth at the site of installation, there are two major categories in terms of type of foundation:

- **Bottom Fixed Foundations:** foundations that are directly fixed to the sea floor. The most common examples are:
 - Monopile;
 - Jacket;
 - Gravity Based Foundation;
 - Tripod [26].
- **Floating Foundations:** floating platform connected to the sea floor through mooring lines. The most common examples are:
 - Spar-Buoy;
 - Semi-Submersible;
 - Tension Leg Platform (TLP) [26].

2.8.1. Bottom Fixed Foundations

The bottom fixed foundations represent the majority of the solutions implemented. They can be economically viable until 60 meters, depending on the type of structure) [49]. A brief explanation of the most important designs will be made.

2.8.1.1. Monopile Foundation

The monopile is the most used foundation of all. Data of 2018 indicated that, in Europe, they represent 66% of all structures installed, a major decrease when compared to 86% in 2017 [50]. It's a simple construction, which consists mainly of a steel pile driven into the seabed. Its diameter lies typically between 2.5 and 6 meters [51]. It's usually driven, into the seabed, a total length of 10 to 20 meters, but depending on the site conditions a higher length might be required [52]. The monopile is usually selected for depths until 30 meters, although they have been successfully employed until water depths of 41 meters [53]. Its use can be limited by the nature of the seabed [49]. Figure 2.21 shows this type of foundation.



Figure 2.21 Monopile Foundation [52,53].

This giant steel piles are usually transported by boat to the installation site and then are hammered down into the ocean floor. A transition piece is assembled on top, to which the turbine will be bolted. They are relatively easy and quick to fabricate and install. In terms of limitations, the current trend is to use larger turbines and in this case the monopile foundation loses its advantages in manufacturing and cost. It was said, in an interview in 2013, by *Olaf Beeg*, from *Vattenfall's Dan Tysk* field in the German North Sea, that "*traditionally, a 5-6 MW turbine in depths of 25-30 meters would be borderline for the largest monopile*" [51].

2.8.1.2. Jacket Foundation

The jacket is the second most common foundation in commercial use. In 2018, it represented 33% of the total installed capacity in Europe [50]. They can be used in water depths up to around 60 meters [49]. The example of the Scottish *Beatrice Wind Farm* can be used, being the world's largest wind farm that uses jacket foundations. It has a combined power of 588 MW, having 84 turbines, which is expected to power roughly 450 000 homes. At this wind farm, the depths are up to 56 meters and jackets up to 80 meters tall will be used. This wind farm is expected to be fully operational in 2019 [54]. Figure 2.22 shows this type of structure.



Figure 2.22 Jacket Foundation [49,54].

There are several different designs for the Jacket Structure. It can consist of a three or four-legged structure and there are also versions in which the legs are twisted. The twisted jacket design uses less steel and has fewer components [55]. The pillar legs are interconnected with bracings. The structure is attached to the floor by using soil piles, which are driven inside the pile sleeves until the required depth to gain adequate structural stability. Other versions of the Jacket, use Suction Piles instead of the regular ones hammered into the ground. The Suction Piles have the shape of a upturned bucket and they are driven into the marine sediment. This is achieved by pumping water out of the “bucket” to lower the pressure inside the bucket. With the combination of this negative pressure and the weight of the foundations, the suction pile sinks into the sea floor. This type of anchoring has the advantages of being faster and that almost no seabed preparation is needed [56].

2.8.1.3. Gravity Based Foundation

An example of the use of this type of structures is the *Blyth Offshore Demonstrator Wind Farm Project*, in the North of the UK, in 2017. At this wind farm, five structures were installed in water depths of approximately 40 meters. This wind farm is well-known for being the first time that the concept of “float and submerge” has been successfully used and it is expected to power around 34 000 UK homes [57]. It’s also worth mentioning another wind Farm, the *Vindeby Wind Farm*, which also uses this type of foundation and as stated before, was the first offshore wind farm in the world. Figure 2.23 shows this type of foundation.

This type of foundation can typically be used until a depth of 50 meters [49]. This structure is normally made of concrete with a central steel shaft, which constitutes the transition piece to the turbine tower. Due to the majority of the structure being made of concrete, it is more durable in marine environment and reduces the need for maintenance. This structure requires a flat seabed, which needs to be prepared. One great advantage of this type of structure is the “float and submerge” concept. This means that the structure can float, thus tug boats may be used for its transportation, instead of the use of big transport ships that would carry the structure, decreasing the transport and installation costs. The second part of this method is the “submerge” part, which means that when the foundation is at the place of installation, it can be submerged into its final position. This is achieved by pumping water into the

foundation as ballast to lower it to the prepared seabed. Once located at the correct place, the water ballast is replaced by sand, usually, which provides the stability for the structure [58].

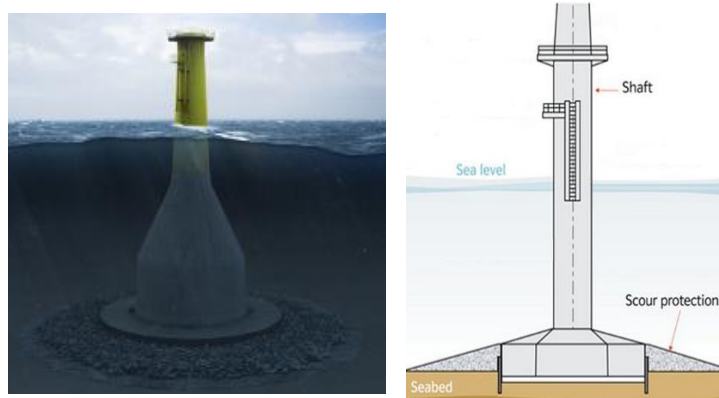


Figure 2.23 Gravity Based Foundation [49,58].

2.8.1.4. Tripod Foundation

This kind of structure was used for example in the *Alpha Ventus Wind Farm*, in Germany, being one the two types of foundations used. It was commissioned in 2010, with a total power production of 60 GW, powering around 40 000 homes. It has 12 turbines installed with water depths around 30 meters [59]. This type of structure is shown in Figure 2.24.

A central steel column is used, which also acts as the connection part to the tower. Under this central column, there is a steel frame that transfers the generated forces into the steel piles. The steel piles, which have relatively small diameters (around 0.9 m), are driven 10 to 20 meters into the ground. This type of structure can be used until 30 to 40 meters deep. This foundation is not suitable to be used at a water depth less than 6 to 7 meters, due to the reduced draught that would exist, not allowing for the appropriate clearance of the frame in order for vessels to approach the foundation [60].

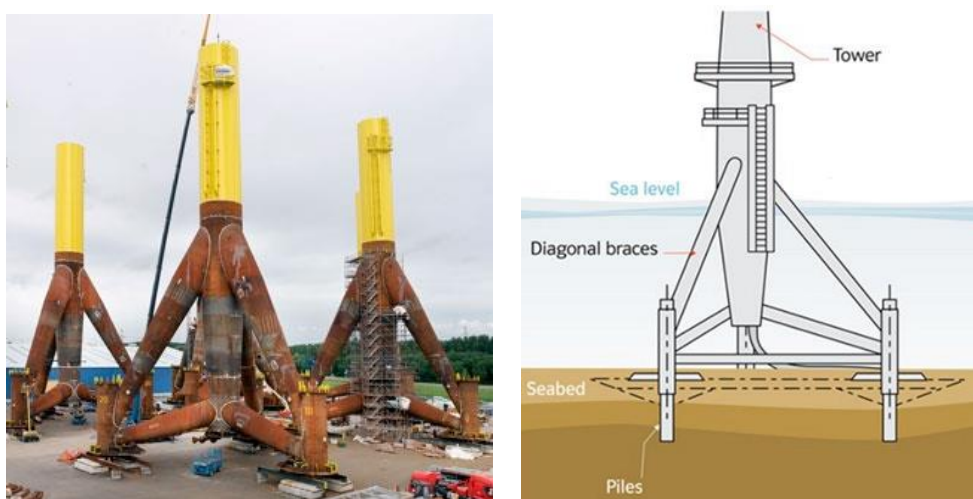


Figure 2.24 Tripod Foundation [49,60].

2.8.2. Floating Structures

In 2012 the average water depth of offshore wind farms was 22 meters and the average distance to shore was 29 km. As of 2014, there were already plans for wind farms located 200 km from shore and in water depths of 215 meters [61]. This shows the trend of moving into deeper waters, with the advantages of less visual impact, less turbulence and higher area of exploration. There are several designs and some models already implemented. Some structures will be presented, being most of them inspired in platforms used in the oil industry.

2.8.2.1. Spar-buoy Foundation

Scotland's *Hywind* was the world's first commercial floating wind farm. It is located northeast of Scotland, nearby Peterhead. The water depths vary from 95 meters to 129 meters. It has a capacity of 30 MW, due to the use of five 6 MW wind turbines, which can power around 22 000 houses. It started producing electricity in October 2017 [62]. Figure 2.25 shows this type of structure.

The spar consists of a large vertical hollow cylinder which is moored by cables, or chains, to the seabed. For better stability, and to guarantee that the structure floats upright, the structure hollow chamber is ballasted [63]. It is usually ballasted with a material with higher density than water, to ensure that the centre of gravity is located below the centre of buoyancy [64]. It has a design draft² between 85 and 90 meters. The diameter of the cylinder at the waterline is around 10 meters and the diameter of the submerged section is about 15 meters [63].



Figure 2.25 Spar-buoy Foundation [64].

² The draft is the vertical distance between the waterline and the bottom of the structure.

2.8.2.2. Semi-Submersible Foundation

The best example of the application of this type of platform is the *WindFloat Project*. The WindFloat project started a demonstration phase in 2011, by installing *WindFloat 1*. *WindFloat 1* was a scale prototype, with a hub height of 70 meters, which was installed off the coast of Portugal, near Póvoa do Varzim. It supported a 2 MW turbine. [65] Figure 2.26 shows the Wind Float platform. Another example of this type of structure is the DeepCWind, which is the structure studied in this project and thus fully explained in later sections. The *WindFloat 1* prototype was later bought to be used in a Scottish wind farm.

Semi-submersibles are, usually, steel structures made out of pontoons³ and hollow columns. This type of structures are build onshore and then towed to the site of installation. For increased stability, water is pumped into the hollow columns, which act as ballast. The use of water as ballast also allows to change the height of the structure above the sea water level, which is useful to adapt to different situations such as transport or operation [66].



Figure 2.26 WindFloat Foundation [65].

2.8.2.3. TLP

The TLP concept is a popular choice to use in oil rigs, such as in the hurricane-prone Gulf of Mexico [67]. Figure 2.27 shows this concept. This design usually consists of a central circular column that connects to the bottom of the turbine and that continues until a certain depth. At the bottom of this main column, there are three or four legs, which can be round or rectangular.

These legs are aligned in a perpendicular direction in relation to the main column. The mooring system, which usually consists of tensioned chains, connects the end of the perpendicular legs to the seabed [41].

³ Name given to the smaller diameter members, which make the connections between large columns.



Figure 2.27 TLP Foundation [41].

2.9. Portugal and the Offshore Wind Power

Data from REN indicates that in March 2018 the production of electricity, through renewable resources, was higher than total consumption of electricity, 4,812 GWh versus 4,647 GWh, respectively, which represents 103.6% of the consumption. This was the first time this happened in 40 years and is an indicator that in the future, the electricity can be fully produced with clean methods [68].

As of 2016, wind power was responsible for 20% of the total production of electricity [69]. Thanks to Portugal's coast line, the use of offshore wind power can be a great solution in adding renewable electricity to the grid. The graphics shown in Figure 2.28 support these claims. On the left, Figure 2.28 shows a simulated map of average wind speeds, in m/s, at an altitude of 80 meters. On the right, it shows a simulated map of average turbulence intensity, in %, at an altitude of 80 meters. As expected, at offshore locations, the relatively high wind speed and the diminished turbulence can have a significant influence in making the offshore wind turbines a great solution for Portugal [70].

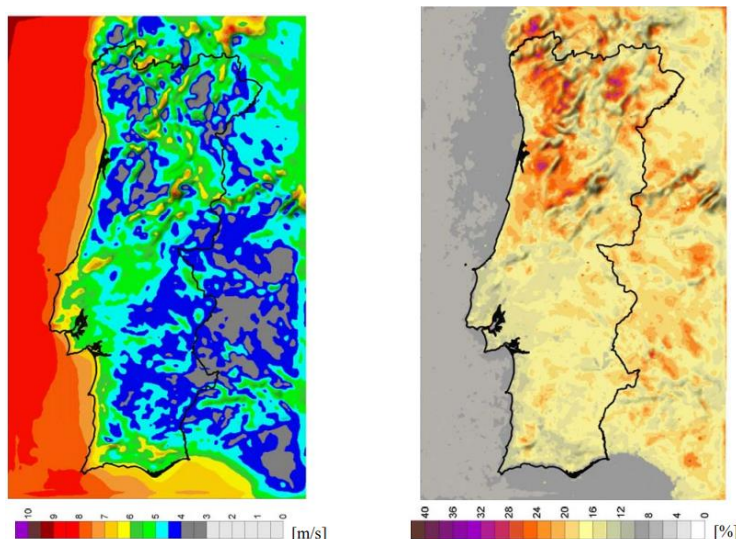


Figure 2.28 At the left, simulated map of average wind speeds at an altitude of 80 m. On the right, simulated map of average turbulence intensity at an altitude of 80 m [70].

In addition, Portugal is trying to increase its already large continental platform to 3 877 480 m², bigger than Brazil's, which may provide a considerable area of exploration for offshore wind power [71]. The Portuguese continental shelf can have depths that go from 25 to 200 meters, which suggests that the most important offshore solutions are of the floating type [72].

The *WindFloat Atlantic* was the first experimental project, tested in Portugal, of offshore floating platforms for wind power. It was installed in 2011, 5 km off the coast of *Aguçadoura, near Póvoa do Varzim*. It used the WindFloat patented design with a 2 MW turbine [65]. As part of the phase 1 of the project, after 5 years of its implementation, it successfully withstood waves of 17 m and wind velocities higher than 100 km/h (27.8 m/s). During this phase, this turbine produced more than 17 GWh [73]. The demonstration phase ended with the successful decommission of the structure. The next step of the project is called the *WindFloat Atlantic* consisting of three platforms with a 8,3 MW turbine each, which will be installed in a 100 meters depth area in the Portuguese coast of *Viana do Castelo* [74]. It is expected that the wind farm will be connected to the grid by 2019. This project is estimated to cost around 115 million euros, being the submersed cable, which connects the wind farm to the onshore grid, the most expensive part [75].

This is one example that shows the potential of floating offshore platforms.

2.10. DeepCWind Foundation

As aforementioned, this project will focus on the DeepCWind foundation design. This structure was developed by the DeepCWind consortium⁴ as an initiative to support the research on floating offshore wind technologies. In 2011, a 1/50 scale model was built and was subjected to a collection of environmental conditions, which included varied wave and wind states [76]. In September 2014, a report called "Definition of the Semisubmersible Floating System for Phase II of OC4" was released by NREL, which documented the specifications of the DeepCWind structure used by OC4. In the cited phase II, the DeepCWind Foundation was modelled and used with the objective of generating test data that would be suitable for the validation of modern floating offshore wind turbine modelling tools. This validation was made by the comparison of results from different modelling tools. The results of the experiment allow for a better understanding of offshore floating wind turbine dynamics and modelling techniques, as well as a better awareness of the validity of various approximations [77,78]. The DeepCWind Foundation was designed to support the NREL 5 MW Reference Turbine. Figure 2.29 displays a computer designed representation of the DeepCWind foundation, in operation, with a turbine installed.

⁴ The DeepCWind consortium is a group of universities, national labs and companies, which are funded by the USA Department of Energy.



Figure 2.29 DeepCWind Foundation [77].

2.10.1. Foundation Members and Dimensions

The DeepCWind foundation is made of cylindrical members connected to each other. The members are arranged in a triangular array with a central column. The members are classified in four groups:

- **Main Column (MC):** it is the central column of the structure and the turbine will be connected on top of it;
- **Upper Column (UC):** it is the upper part of the column that is located at the vertices of the triangle;
- **Bottom Column (BC):** it is the bottom part of the column that is located at the vertices of the triangle, having twice the diameter of the UC and around one fourth of its length;
- **Pontoons:** they are the smaller diameters members that make the connections with the larger diameter members. They are then structured in YU, YL, DU, DL and CB. These different notations are only to distinguish the location of the members and thus their different lengths.

When in operation, the platform is designed to have a depth of 20 m below SWL and an elevation of 12 m above SWL. The platform is connected to the ocean floor by three catenary lines which have a 120° angle between them, to prevent the dislocation of the platform during operation. The mooring lines attach to the platform at a depth of 14 m below the SWL and at a radius of 40.87 m from the platform centreline. The other end of the mooring line is secure to the ocean floor at a water depth of 200 m below the SWL and at a radius of 837.6 m from the platform centreline. Each mooring line has 835.5 m in length when not stretched.

Figure 2.30 shows the general dimensions of the structure and the identification of the structure larger diameter members. Table 2.1 presents the dimensions of each member.

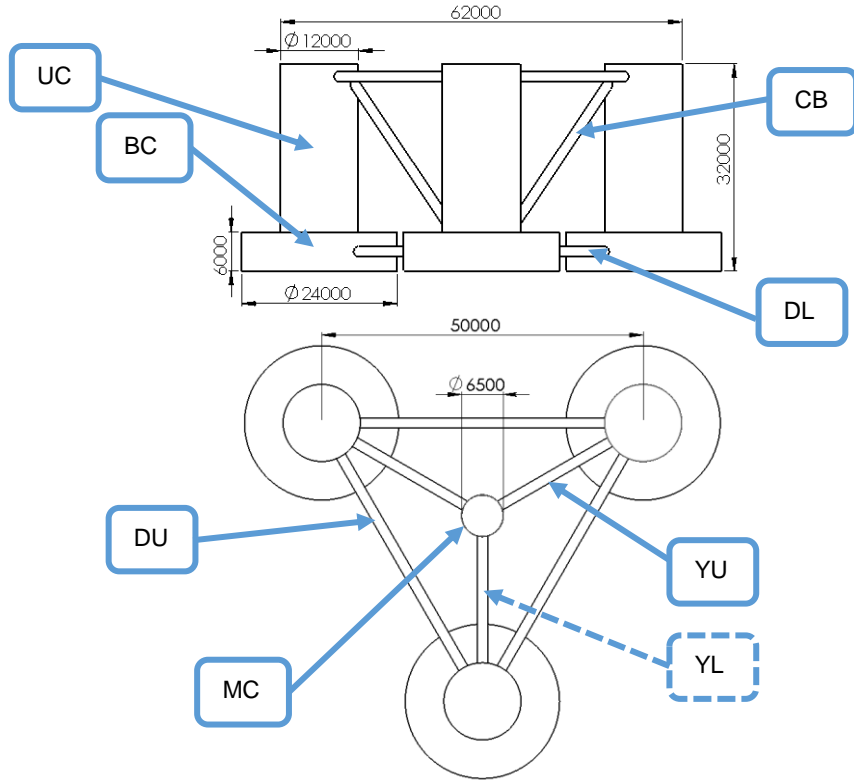


Figure 2.30 General dimensions of the structure and identification of the larger members [78]. YL member is hidden, connecting the bottom of the MC and the BC.

Table 2.1 Members dimensions [78].

Member Identification	Diameter [m]	Length [m]	Wall Thickness [mm]
MC	6.5	32	30
UC	12	26	60
BC	24	6	60
DU	1.6	38	17.5
DL	1.6	26	17.5
YU	1.6	19.6	17.5
YL	1.6	13.6	17.5
CB	1.6	32	17.5

2.10.2. Platform Properties

The DeepCWind platform has a total mass of 13 473 tonnes, which includes the total mass of steel and the added water used as ballast. The platform total mass, including the steel structure and the water ballast, was projected to ensure that the combined weight of the tower (including the rotor-nacelle assembly) and of the floating platform, will balance with buoyancy force of the undisplaced platform in still water. The floating platform (not including the tower, rotor+nacelle and moorings) possess a centre of mass(CM), that is located 13.46 m below SWL [78]. As such, the total mass of the structure should be maintained as 13 473 tonnes and if there is an increase in the weight of the steel used, a decrease in the weight of water used as ballast should also be made. The current design of the platform has 3 852 tonnes of steel and 9 621 tonnes of water. These weights were calculated considering a steel density of 7850 kg/m³ and a water density of 1025 kg/m³ [78].Table 2.2 shows information on the inertia properties of the structure.

Table 2.2 Inertia properties of the structure [78].

Platform roll inertia about CM	6.827E+9 kg m ²
Platform pitch inertia about CM	6.827E+9 kg m ²
Platform yaw inertia about CM	1.226E+10 kg m ²

2.10.3. Previous Structural Improvements to Original Structure

A master thesis called “*Análise da Integridade Estrutural de uma Fundação Flutuante para Energia Eólica Offshore*” [79] (Structural Integrity Analyses of an Offshore Floating Platform for Wind Power) evaluated the original DeepCWind foundation and improved the structure for better performance in the required conditions of operation. Internal Reinforcements were added to the BC and MC columns. Figure 2.31 shows the referred reinforcements, respectively. Additionally, the wall thicknesses of the foundation’s members were also increased. The original and final thicknesses are shown in Table 2.3. The steel mass of the original structure was 3 852 Tonnes and after the improvement process it went up to 9 188 Tonnes. Three analyses were performed, at different wind speeds, and the achieved security coefficients were: 1.57 for 11.4 m s⁻¹, 1.035 for 18 m s⁻¹ and 0.94 for 24 m s⁻¹. For more information on this analysis consult [79].

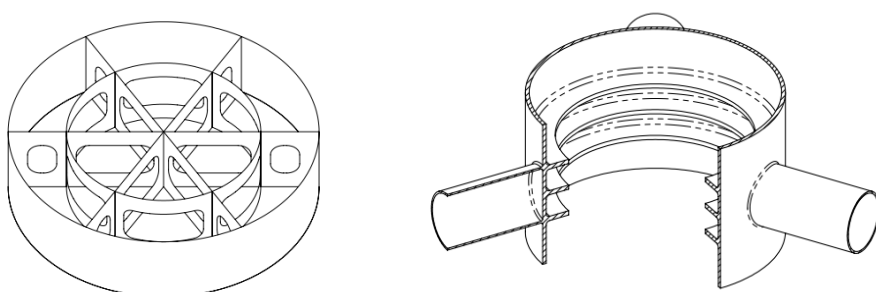


Figure 2.31 Reinforcements used in previous improvement process [79].

Table 2.3 Members dimensions [79].

	Original Thickness [mm]	Final Thickness [mm]
MC	30	100
UC	60	120
BC	60	120
Pontoons	17.5	50

2.11. Finite Element Analysis and the Aliasing Problem

2.11.1. Finite Element Method

The Finite Element Method (FEM) is a numerical technique, used in Finite Element Analysis (FEA), which simulates physical phenomena. It is widely used to reduce the amount of physical prototypes and to optimize components in their design phase, allowing for a faster and cheaper way of developing new products [80].

A transient analysis should be made if the simulation involves loads that vary with time and/or if the inertia effects are important. The applied loads vary in a certain time interval. This time interval is called a *Time Step*, which means that the loads are updated every amount of time defined as the Time Step itself [81].

In the real world, all phenomena occur in a continuum way. When trying to reproduce these phenomena in a computational simulation, there has to be a discretization of the events. It is in this discretization that the Time Step is applied, being the frequency at which the data is reproduced.

The discretization of data might produce an error, which is known as *aliasing* [82]. Aliasing can be described as misinterpretation of the data, producing a structural effect that might differ from the phenomena that the data refers to. Figure 2.32 shows this effect.

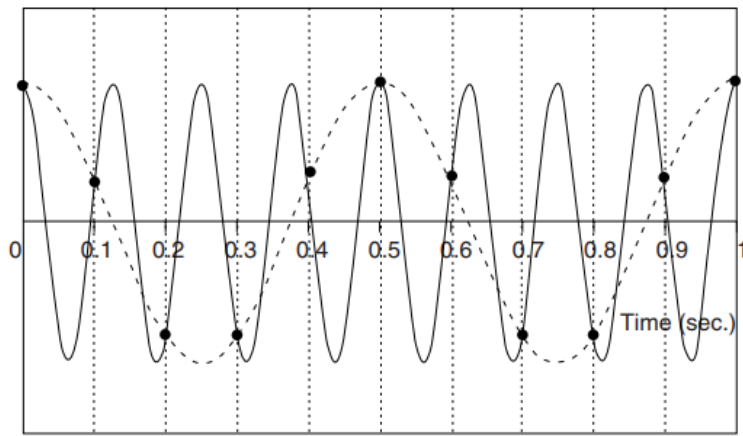


Figure 2.32 Aliasing effect [82].

Figure 2.32 exemplifies two different signals. The signal in solid line represents the real world phenomenon, which is a 8 Hz cosine wave. Being discretized in a time interval of 0.1 seconds, it results

in the data represented by the dashed line. When interpreting the data, the computational software can interpret the data as a 2 Hz cosine wave, which is represented by the dashed line. This would result in a wrong reproduction of the real world and probably a loss of information.

Chapter 3

3. Methods

3.1. Tower and Turbine Properties

This research considered the NREL 5 MW Reference Turbine. It is an upwind 3-bladed turbine. Due to the high costs of the support structures of an offshore wind system, a wind turbine should be rated, at least, at 5 MW in order for the system to be cost effective [83]. This type of turbine is often used in conceptual design calculations for Offshore Wind Turbines [83]. Table 3.1 displays information on the referred turbine.

Table 3.1 NREL 5 MW wind turbine information [83].

Cut-in Wind Speed	3 m/s
Rated Wind Speed	11,4 m/s
Cut-Out Wind Speed	25 m/s
Rotor Diameter	126 m
Hub Height	90 m
Tower Height above Ground	87.6 m
Tower Mass	347 460 kg
Tower Base Thickness	27 mm
Tower Top Thickness	19 mm
Blade Length	61.5 m
Blade Overall Mass	17 740 kg
Cut-In Rotor Speed	6.9 rpm
Rated Rotor Speed	12.1 rpm
Rotor Mass	110 000 kg
Nacelle Mass	240 000 kg
Electrical Generator Efficiency	94.4 %

3.2. Material Properties

The platform material is steel, namely S355 steel. This material has a Young modulus of 210 GPa and a shear modulus of 80.8 GPa. Steel's density is $7\ 850\ \text{kg/m}^3$, but it was considered a density of $8\ 500\ \text{kg/m}^3$, in order to account for paint, bolts, welds and flanges [84]. The S355 steel yield strength is considered to be 355 MPa [85]. For the analyses, the density of water was also needed, thus it was defined as $1025\ \text{kg/m}^3$ [78].

3.3. FAST Software

Offshore structures are subjected to hydrostatic, hydrodynamic and aerodynamic loadings, usually due to the wind, waves and tides. In order to produce the correct inputs to use as loads on the Finite Element Analysis, the FAST code from NREL was used.

FAST stands for *Fatigue, Aerodynamics, Structures and Turbulence*. This software is an aeroelastic simulator capable of calculating loads on two or three bladed horizontal-axis wind turbines [86]. The structure being analysed is specified within the program, as well as the sea and weather conditions that are desired. Figure 3.1 shows the real world phenomena simulated by FAST.

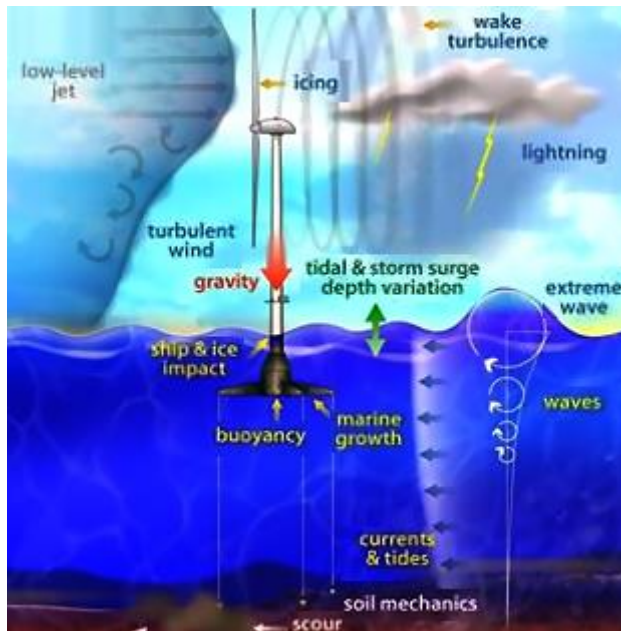


Figure 3.1 FAST environmental conditions [77].

FAST is composed of several modules, each one responsible for the simulation of a specific part of the effects that interact with the structure. The modules used for this research were:

- **ElastoDyn:** responsible for the simulation of the physical properties of the structure and the turbine initial working settings [26];
- **ServoDyn:** responsible for the settings of the control systems of the turbine [26];
- **Inflow:** processes wind-inflow data enabling the simulation of aero-elastic effects acting on horizontal-axis wind turbines [87];

- **AeroDyn:** time-domain wind turbine aerodynamics module that enables the simulation of aero-elastic effects acting on horizontal-axis wind turbines [88];
- **HydroDyn:** responsible for computing the hydrodynamic loads [89];
- **MoorDyn:** lumped-mass mooring line model that enables the prediction of the dynamics of typical mooring systems [90].

The DeepCWind is one of the several *Certification Tests* that comes integrated with the software. As such, the Fast simulation was developed using the 25th *Certification Test* as a basis and making changes according to the existing needs.

3.4. Coordinate Systems for the Analysis

The motions assessed are relative to a coordinates system that is pre-defined. The most usual type of coordinate system is shown in Figure 3.2. The rotation movement around each axis are also shown and are named as *Yaw*, *Pitch* and *Roll*. *Yaw* is the rotation around the Z axis, *Pitch* is around Y and *Roll* is around X [89].

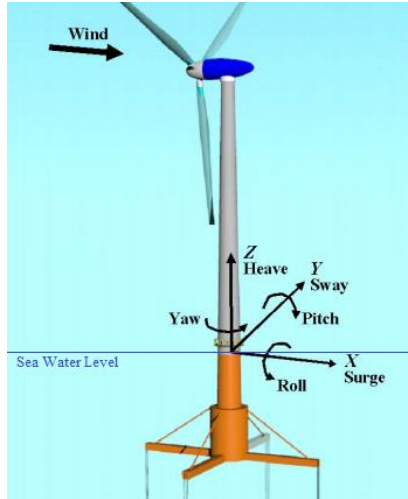


Figure 3.2 Structure coordinate system [89].

3.5. Simulation Parameters

One of the most important aspects of the simulation is the behaviour of the sea, as it is responsible for the most destructive loads that act on the structure. Hydrodynamic effects are modelled using a combination of incident-wave kinematics and hydrodynamic loading models. Hydrodynamic loads, which come from the integration of the dynamic pressure of the water over the wetted surface of the considered floating platform, include inertia, linear drag, buoyancy, incident-wave scattering⁵, sea current and nonlinear effects [84].

⁵ Corresponds to the change in the direction of motion of the waves particles due to the “collision” with the platform structure.

The sea waves can be simplified by assuming that their behaviour is similar to a sinusoidal wave, as seen in Figure 3.3.

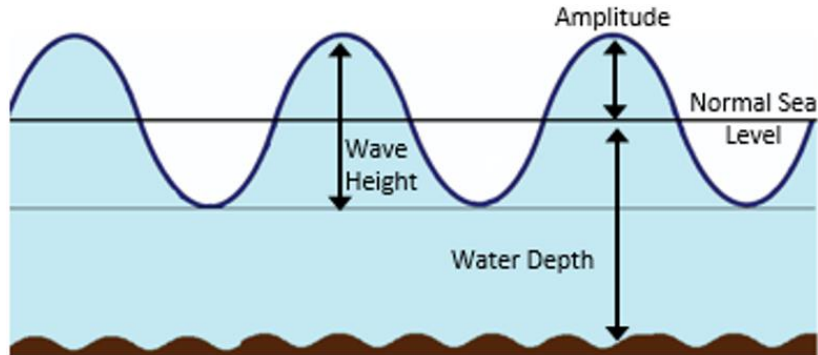


Figure 3.3 Mathematical wave simplification.

The waves usually have a random behaviour, varying in their heights, wave lengths and periods. For this reason, a probabilistic approach is used, describing an idealized sea state. . For this reason, its behaviour has to be described in a probabilistic way. Several quantities may be used to describe it stochastically, being the most important the *Significant Wave Height* and the *Peak Wave Period*. The Significant Wave Height, H_s , is the mean of the highest third of the waves in a time-series that represents a certain sea state. The Peak Wave Period, T_p , is the wave period with the highest energy [26].

In order to use accurate data of weather and sea conditions, a real specific location had to be chosen. For the NREL's study, the location used was $61^{\circ} 20' \text{ N}$ latitude and $0^{\circ} 0' \text{ E}$ longitude, thus the same choice was made. This location is at the northeast of the Scottish Shetland Islands and it was chosen due to its extreme wind and wave conditions, which would allow the structure to be used at locations that combine extreme weather conditions and high sea depths. This location is shown in Figure 3.4.



Figure 3.4 Location specified for this project.

Two wind speeds were selected, in order to cover the spectrum demanded by DLC 1.1 (detailed in later sections), which were the rated wind speed, 11.4 m s^{-1} , and the cut-out wind speed, 25 m s^{-1} . After a review of the environment at this site, the following external conditions were considered [79]:

- 11.4 m s^{-1} :
 - $H_s: 2.466 \text{ m}$;
 - $T_p: 13.159 \text{ s}$;
- 25 m s^{-1} :
 - $H_s: 5.896 \text{ m}$;
 - $T_p: 19.266 \text{ s}$.

With the intention of calculating the hydrodynamic loads on the structure, three options can be used: potential-flow theory, strip-theory or a combination of both.

The *potential-flow* theory can be used to substructures or members of substructures that are large relatively to a typical wavelength. It includes linear hydrostatic restoring, the added mass and damping contributions from linear wave radiation⁶ and incident-wave excitation [89].

The *strip-theory* is better for substructures or members of substructures that are small in diameter, relatively to a typical wavelength. This theory's hydrodynamic loads can be applied to multiple interconnected members, inclined or tapered, and are derived directly from the undisturbed wave and current kinematics at the undisplaced position of the structure. Its loads include the relative form of *Morison's Equation* for the distributed fluid-inertia, added-mass and viscous-drag components. Strip-theory allows for the use of ballasting members, as well as the effects of marine growth [89].

A combination of the *potential-flow* with the *strip-theory* can also be chosen. This is advisable when the hydrodynamic loads from the *potential-flow* theory have to be increased with the loads that come from flow separation. This is accomplished by including the viscous-drag component of the *strip-theory* into the *potential-flow* theory solution [89].

When there is flow separation, viscous-drag forces become dominant and the *strip-theory* formulation is preferable. In addition, *Morison's equation* is preferential for severe wave conditions. For these reasons, as the most critical conditions are to be evaluated, the Morison's equation was used [79].

The hydrodynamic model, as defined in linear hydrodynamics, is described by Equation 3.1. Three different phenomena are present in this equation: diffraction, radiation and hydrostatics.

$$F_i^{Hydro} = F_i^{Waves} + \rho g V_0 \delta_{13} - C_{ij}^{Hydrostatic} q_j - \int_0^t K_{ij}(t-\tau) q_j(\tau) d\tau \quad (3.1)$$

Diffraction consists on the scattering of incident waves. The first term of Equation 3.1 represents the total excitation load from incident waves, being highly associated with the wave elevation, ζ . The *Airy wave theory* describes the kinematics of regular waves (simplified as sinusoidal waves). Irregular or random waves, representing various stochastic sea states, are modelled as the summation or superposition of multiple wave components, which are regulated by an appropriate wave spectrum [84]. Two different wave spectra may be used: the *Pierson-Moskowitz* and the *JONSWAP* (Joint North Sea

⁶ Wave radiation correspond to the wave making when the body pushes fluid "out of the way" when moving relatively to still water [117].

Wave Project) spectrum. On one hand, the *Pierson-Moskowitz* is based on a fully developed sea state. Fully developed sea state concept states that a balance has been achieved between the energy that is exchanged between the wind and the sea, thus the energy of the wave remains constant. On the other hand, the *JONSWAP* spectra considers that the fully developed state is never achieved, consequently the waves continue to grow as they travel. The *Pierson-Moskowitz* spectrum was used, as it was the one also considered for the data analysis of the sea and wind conditions [79].

The second and third terms of Equation 3.1 correspond to the *hydrostatic contribution*. In the second term, ρ corresponds to water density, g is the gravitational acceleration constant, V_0 is the dislocated volume of fluid for the platform undisplaced position and δ_{i3} is the (i,3) component of the *Kronecker-Delta* function. This term represents the buoyancy force. The third term represents the variation in the hydrostatic force and moment, which is caused by the effects of the displacement of the platform and changes in the water-plane area. $C_{ij}^{Hydrostatic}$ corresponds to the linear hydrostatic-restoring matrix and q_j corresponds to the platform displacement [84]. The FAST's module, HydroDyn, does not recompute the structure buoyancy, in the strip-theory, according to the displaced positions of the structure. For floating platforms, this change in buoyancy, due to structure movement, is considered important. As such, a linear hydrostatic restoring matrix should be manually calculated and inserted in HydroDyn as an additional linear restoring stiffness matrix [89]. This matrix is shown in Figure 3.5. The considered structure has a X-Z plane of symmetry, directly putting some elements equal to zero.

$$\begin{bmatrix} 0 & 0 & 0 & 0 & 0 \\ 0 & 0 & 0 & 0 & 0 \\ 0 & 0 & \rho g A_0 & \cancel{\rho g \iint_A y dA} & -\rho g \iint_A x dA \\ 0 & 0 & \cancel{\rho g \iint_A x dA} & \rho g \iint_A y^2 dA + \rho g V_0 z_b - m_{mg} g z_{mg} - m_f g z_f & -\rho g \iint_A y dA \\ 0 & 0 & -\rho g \iint_A x dA & -\rho g \iint_A y dA & \rho g \iint_A x^2 dA + \rho g V_0 z_b - m_{mg} g z_{mg} - m_f g z_f \\ 0 & 0 & 0 & 0 & 0 \end{bmatrix}$$

Figure 3.5 HydroDyn additional linear restoring stiffness matrix [89].

The terms used are defined as:

- ρ : water density, 1025 kg/m^3 ;
- g : gravity, 9.81 m/s^2 ;
- A_0 : undisplaced waterplane area of platform, m^2 ;
- V_0 : undisplaced volume of platform, m^3 ;
- (x_b, y_b, z_b) : coordinates of the centre of buoyancy of the undisplaced platform, m ;
- (x_{mg}, y_{mg}, z_{mg}) : coordinates of the centre of mass of the undisplaced marine growth mass, m ;
- (x_f, y_f, z_f) : coordinates of the centre of mass of the undisplaced filled fluid (ballast) mass, m ;
- m_{mg} : total mass of marine growth, kg ;
- m_f : total mass of ballast, kg [89].

After also discarding other entries due to the alignment of some of the coordinates the centres of mass with the structure's coordinate system, the considered structure possess only three non-zero entries in the matrix. Their values, for the original structure, are [78]:

- $C_{3,3}^{\text{hidr}} = 3.836 \times 10^6 \text{ N m}^{-1}$;
- $C_{4,4}^{\text{hidr}} = 1.074 \times 10^9 \text{ N m}^{-1}$;
- $C_{5,5}^{\text{hidr}} = 1.074 \times 10^9 \text{ N m}^{-1}$.

The final term in Equation 3.1 is a convolution integral, which comprises the contributions from *wave-radiation*, including a combination of hydrodynamic added mass and damping. The wave-radiation effects depend on the history of motion of the support platform. In the expression, τ is a dummy variable with the same units as the simulation time, t . K_{ij} is the (i,j) component of the wave-radiation-retardation kernel matrix. This matrix's component, represents the hydrodynamic force at a time t in the direction of DOF i that results from a unit impulse in velocity at time zero of DOF j [84]. For further explanation on this topic, [84] should be consulted.

3.6. Sea Currents

Sea current models contemplate the profile shapes created by water velocity, as a function of water depth. In general, three models are considered: *sub-surface current model*, *near-surface current model* and *depth-independent current model*. These models are illustrated in Figure 3.6.

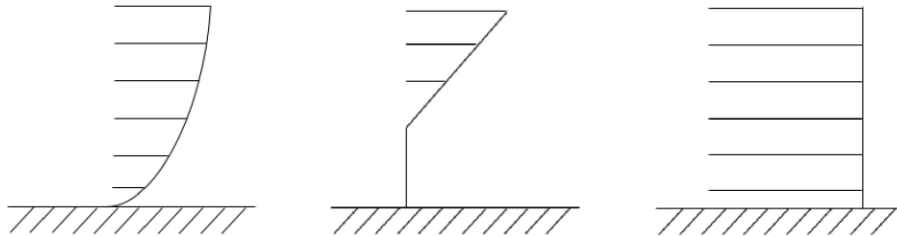


Figure 3.6 Water velocity profiles as a function of water depth [26].

The *sub-surface (SS) current model* respects a power law, as shown in Equation 3.2.

$$U_{SS}(Z) = U_{0SS} \left(\frac{Z + d}{d} \right)^{1/7} \quad (3.2)$$

The variables used correspond to:

- Z is the local depth of a certain point, below the SWL (negative downward);
- d is the water depth;
- U_{0SS} is the current velocity at SWL [89].

The *near-surface (NS) current model* relates to a linear relation down to a certain depth, as shown in Equation 3.3.

$$\begin{cases} U_{NS}(Z) = U_{0NS} \left(\frac{Z + h_{ref}}{h_{ref}} \right), & -h_{ref} < Z < 0 \\ U_{NS}(Z) = 0, & \text{otherwise} \end{cases} \quad (3.3)$$

The variables used correspond to:

- h_{ref} is the reference depth;
- U_{0NS} is the current velocity at SWL [89].

The *depth independent current model* represents the real-life currents as always having the same velocity, independently of the water depth [89].

3.7. Marine Growth

Marine structures will eventually serve as support for the proliferation of marine wild life (phenomenon known as Marine Growth). Despite being a predictable occurrence, it can have significant effects in the structure behaviour, being even more damaging for floating structures. Marine Growth increases the diameters of the affected members, which in turn increases the area of the plane of water at SWL, for the undisturbed structure. There are also increments on the surface roughness, on the total weight of the structure and on the amount of displaced fluid, which has implications in several hydrodynamic properties of the structure and its response to exterior conditions [79].

As indicated by the Germanischer Lloyd (GL) “*Guideline for the Certification of Offshore Wind Turbines*” [91], the effects of Marine Growth are to be considered according to data from the site of installation. In cases where substantial data is not available for the considered location, the approximations presented in Table 3.2 should be used. This information was used for this project.

Table 3.2 Marine Growth Data [83].

Sea depth [m]	Marine Growth Thickness [mm]	Density [kg/m ³]
> + 1.5	0	
[+ 1.5; -4]	160	1400
[-4; -15]	100	
< -15	50	

3.8. Finite Element Method

The examination of physical phenomena, such as structural or fluid behaviour, can be made using Partial Differential Equations. These type of equations can be very complex to solve and a great amount of them must be solved in order to solve problems at a real world scale. FEA is a numerical approach to get the result of these partial differential equations and thus a prediction on how a part or assembly will comply under given conditions. The results are usually expressed with a colour scale, which typically goes from blue to red (blue for the more favourable results and red to the least favourable), as can be seen in Figure 3.7 [80].

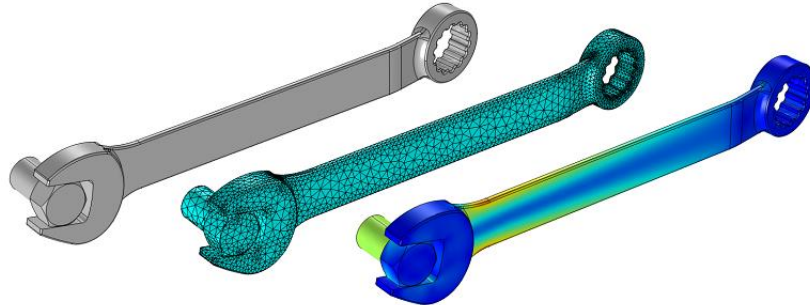


Figure 3.7 FEA procedure example [80].

This method can be applied to many fields of interest, such as structural, mechanical or fluid problems. For this project, only structural and mechanical analysis are of interest.

Structural Analysis is in itself a large field of study, with many types of analyses such as strength analysis, vibrations, motion, between many others. This study will use three types: *Static Structural Analysis*, *Transient Structural Analysis* and *Modal Analysis*.

3.8.1. Static Structural Analysis

A static structural analysis is used to determine displacements, stresses, strains and other effects as a result of applied conditions. In this type of analysis, loads do not produce significant inertia and damping effect. The name “static” is due to the assumption that the loads and structure’s responses are expected to vary very slowly in time [92]. This type of simulation is usually relatively quick, therefore is very useful for comparing simulations with small changes.

3.8.2. Transient Structural Analysis

In the real world, all loads vary with time and so do the structures’ responses [93]. A transient analysis is used to evaluate the time-varying displacements, stresses and other effects of the applied loads. Inertia and/or Damping effects are considered important [81]. This kind of analysis takes much more time than an “equivalent” static one.

3.8.3. Modal Analysis

A modal analysis is a type of dynamic simulation that focus on free vibrations. From the analysis of free vibrations, the natural frequencies can be studied and their corresponding vibration mode shapes [93]. This type of analysis is important when loads are applied rapidly and the dynamic affects should not be ignored [94].

A natural frequency is a frequency at which the structure will vibrate, due to the applied external forces. All physical structures possess infinite natural frequencies and they are determined by the way mass and stiffness are distributed in the structure. When dynamic forces cause a structure to vibrate at its natural frequencies, resonance happens. When in resonance, a small force might produce a large vibration response. These amplified vibrations can be catastrophic if they occur naturally for the structure operation conditions [95].

When vibrating at a certain natural frequency, the structure will vibrate differently at each frequency. The way that it deforms at a particular frequency is called a mode shape. The way that the structure deforms is very important as it shows as a structure should be reinforced if it is to endure a natural frequency during operation [95].

A way of understanding the natural frequencies and the resonant behaviour in real world objects is through a simplified mass-spring system, as shown in Figure 3.8.

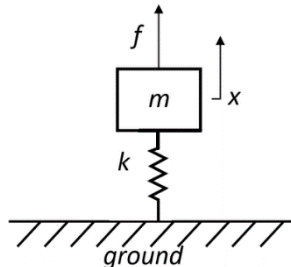


Figure 3.8 Simplified mass-spring system [95].

This simplified system permits the use of an equation which relates the mass (m) and stiffness(k) of the system to its natural frequency (w_n), as shown in Equation 3.4.

$$w_n = \sqrt{\frac{k}{m}} \quad (3.4)$$

As shown in Equation 3.4, a natural frequency is directly dependent on the stiffness to mass ratio. On one hand, the rise in stiffness will increase the value of the natural frequencies. On the other hand, an increment in mass will decrease the value of the natural frequencies [95].

3.8.3.1. Real World Effects for the Modal Analysis

Slim and tall structures, such as, offshore wind turbines are sensitive to dynamic excitations, which is enhanced by the presence of a large mass on top of it. This sensitivity is due to the natural frequencies of the structure being close to its working conditions [79].

For the present structure, there are four sources of excitation that are of major importance:

- Loads due to wind turbulence;
- Loads due to waves, which depend on the wave height and wave period;
- Loads caused by the vibration effects at the hub level due to aerodynamic imbalances on the rotor as well as the mass at the top of the tower;
- Loads caused by the vibration due to blade shadowing, i.e., the passage of the blades in front of the tower cause a shadowing effect, producing a loss of wind load on the tower [96].

At the considered site of installation, typically the waves present a range of frequencies that goes from 0.05 Hz to 0.167 Hz [79].

When it comes to the vibrations from the rotor, the induced frequency is equal to the rotational frequency of the rotor, also known as the 1P frequency. Most turbines work within a range of velocities, and the NREL 5 MW Turbine has a working range that goes from 6.9 rpm to 12.1 rpm. This will translate into a range of frequencies going from $f_{1P,\min} = 0.115$ Hz to $f_{1P,\max} = 0.202$ Hz [79].

The blade shadowing effect is intimately connected do the rotational frequency of the rotor, therefore the produced frequency is calculated by the multiplication of the 1P frequency range for the number of blades [96]. This frequency, known as 3P, is thus $f_{3P,\min} = 0.345$ Hz and $f_{3P,\max} = 0.605$ Hz.

The DNV states that a 10% security factor should be used for the 1P and 3P frequencies [97]. Figure 3.9 shows the combination of the described ranges.

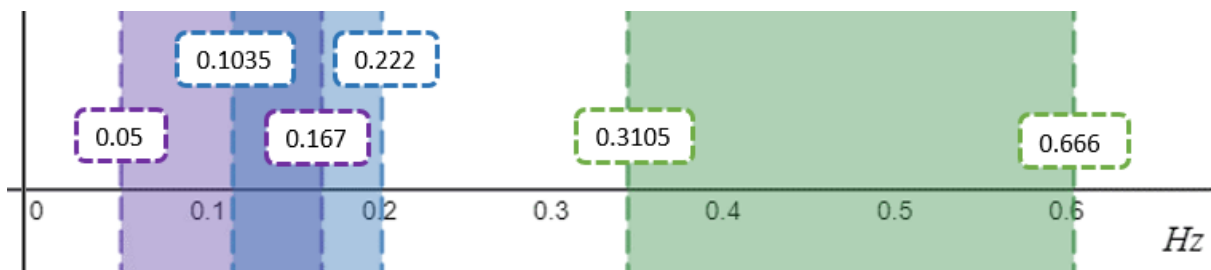


Figure 3.9 Interval ranges for resonance, already including safety coefficient of 10%.

Depending on where the fundamental frequency (the first bending natural frequency), f_0 , is located, the structure can be classified as:

- Soft-Soft: if the fundamental frequency is lower than the 1P frequency;
- Soft-Stiff: if the fundamental frequency is higher than the 1P frequency but lower than the 3P frequency;
- Stiff-Stiff: if the fundamental frequency is higher than the 3P frequency [96].

3.9. Modelling Techniques

There are several techniques available to produce a geometry to analyse. The techniques should be chosen according to the requirements and resources available for the analysis. The techniques used for this project were: Shell Analysis, Shell+Solid Submodel Analysis and Shell-Solid Hybrid Model Analysis.

3.9.1. Shell Analysis

Shell elements are a mathematical simplification of solids and are used to model relatively thin structures, i.e., structures where one dimension is much smaller than the other two dimensions [98]. This type of elements, if correctly used, can produce effective results, while saving huge computational times. This type of simulation is much faster, than one using a solid model, because fewer mesh elements are used to model thin features and shell elements are easier to mesh, also having less tendency to negative Jacobian errors that might occur when using extremely thin solid models [99].

This type of analysis is most appropriate when the t/L coefficient is low (lower than 0.2), where t is the thickness of the member and L is its length [99]. The maximum coefficient for the present structure is 0.01, which more than satisfies the limit.

3.9.2. Shell + Solid Submodel Analysis

The use of submodels is highly beneficial when using a relatively large model and there is a need to obtain more accurate results in a particular region of the model [100].

For this analysis, a complete model is analysed using a shell formulation, which, as previously discussed, will yield overall accurate results. Afterwards, a solid submodel is analysed, allowing for more accurate results at stress concentration areas.

3.9.3. Shell – Solid Hybrid Model Analysis

A shell-solid model is useful when certain areas of the model are not fit to be modelled using shell elements and should use solid elements. Whereas, other parts of the structure can be represented by shell elements. The use of this technique can produce accurate results at stress concentration areas, while using a faster and easier formulation for simpler and thin areas [101]. The use of this modelling techniques avoids possible errors at the submodel analysis due to the information passed by the previous shell analysis, where fillets are not used at stress concentration areas.

3.10. Boundary Conditions

Boundary conditions are applied as constraints and loads to the analysed model. Generally, loads represent inputs to the model, such as forces, moments, pressures or temperatures. Constraints act as reactions to the applied loads, for instance imposing a fixed behaviour to a face of the model [102].

The definition of these conditions is of great importance. Small errors in modelling, data input and boundary conditions may result in very large errors in the results. In addition, in some cases the errors might be small and easily missed [103]. The loads applied to the present model include: hydrostatic pressure, forces (caused by the mooring lines), buoyancy forces, ballast pressure, earth gravity, ballast inertia and dynamic pressures. Further information on these loads can be consulted in [79].

The DeepCWind platform is, as previously discussed, connected to the sea floor through mooring lines in catenary form. At the equilibrium position, the mooring lines are not under tension, which means that under the applied loads the structure will undergo a dynamic offset [43]. An example of this kind of offset is presented in Figure 3.10.

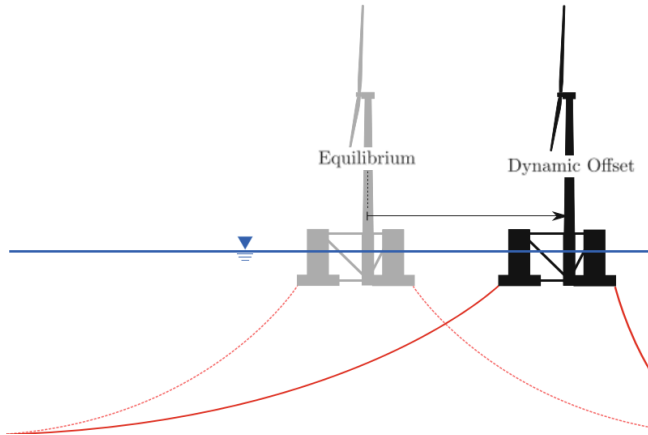


Figure 3.10 Platform dynamic offset representation [43].

In order to guarantee the validity of the results, two approaches were used, concerning the constraints:

- **Displacements Formulation** – the use of displacements as boundary conditions, also called essential boundary conditions, is one of the most used type of constraints. In these boundary conditions, the exact value of the displacement of a certain point (or edge or face) is specified. From the FAST software it is possible to obtain the displacements of the tower, which are considered the real displacements. The use of displacements led to a maximization of the stresses near the connection of the tower to the platform and at the joints at the MC supporting members. Therefore, this approach was considered more valuable to analyse members which were not in the vicinities of the applied essential boundary conditions. Figure 3.11 shows where the displacements are applied.
- **Springs Formulation** – This approach is based on the dynamic offset of the floating platform, as a response to the applied loads. To simulate the behaviour of mooring lines, the ANSYS software allows the use of springs, even though this modelling technique has some limitations for reproducing the catenary behaviour [104]. Typical chain mooring lines, can have an axial stiffness of around 7.1×10^8 N, when divided in 8

segments with a combined length of, approximately, 500 m [105]. As previously presented, the FAST software already had an implementation of the DeepCWind structure as a certification test, having the mooring lines described as 20 segments, each with an axial stiffness of 7.54×10^8 N. The stiffness of the combined mooring line will be lower than that of the individual segments, as they are assembled in series, thus the global axial stiffness should be lower. Despite this, to yield reliable results, when using linear springs, vessel displacements should be kept small [43], as this will also prevent rigid body motions [102]. Due to this, and also to guarantee that the applied forces are at least higher than the real ones, an axial stiffness of 1×10^8 N was used for the computational spring. Figure 3.12 shows how the springs were used. Although, this formulation simulates the real conditions more accurately, it shows a big disadvantage. In order to simulate the floating dynamics, 8 springs needed to be used, in different locations of the BC members, otherwise the small displacements of the vessel could not be satisfied. This led to virtual stresses created by the anchoring points of the springs.



Figure 3.11 Displacement Formulation input.

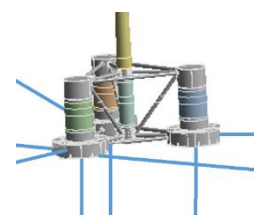


Figure 3.12 Springs Formulation input.

It was decided to use both formulations in a complementary approach. The most reliable and more accurate formulation is the one with the springs, thus being the formulation of reference for this project. Due to the virtual stresses created by the springs, this formulation can not truthfully evaluate the BC members. Therefore, the BC members were evaluated using the displacements formulation, as these formulation is appropriate for members distant from the connection tower-platform.

3.11. Linear Analysis

When projecting a structure, it is generally desired that it does not undergo plastic deformations, in other words, all the stresses verified should be confined to the elastic dominion. The objective of this research is to have a structure that is capable of enduring the applied loads, thus remaining in the linear region. This can be examined using a Linear Analysis, which can have two conclusions:

- **The structure can withstand the applied loads, while remaining in the elastic region** – this means that the structure may be suitable for its intended use. The linear analysis is valid, as only the linear region is analysed, and its results can be taken into account;

- **The structure cannot withstand the applied loads, thus entering the plastic region** – this indicates that the structure does not present evidence of being able to be used for its intended use. Using a linear analysis, which yields results showing plastic deformation, may only be used to check that it enters the plastic regimen. If it is intended to analyse the real behaviour of the structure under plastic deformation, a non-linear analysis should be performed.

When performing a linear analysis, it is assumed that occurs no large deformation. If large unrealistic deformations are present, it usually means that a non-linear analysis ought to be performed.. However, for this research, the plastic behaviour of the structure is not under examination, thus the only interest is to check if the structure endures only elastic deformations and to analyse its behaviour inside the elastic region. As such, linear analysis are considered suitable, which will also save computational resources. If plastic deformation occurs, the results should be carefully examined, as the stress magnitudes should only be considered as an approximation and the deformations should not be considered.

3.12. Design Load Case

A Design Load Case (DLC) is a test that should be made to the structure, to access its suitability to endure the loads it is intended for. These tests are usually part of norms for the certification of structures. In order to access its full suitability, a series of DLCs have to be passed, which test the various scenarios that the structure will be subjected to, such as: normal power production, start-up, emergency shut-down, storms, etc.

This project will evaluate the DLC 1.1, which is presented by GL standard [91], nonetheless producing only ultimate stress analysis. This test states that the turbine is producing energy while connected to the grid. The wind velocity should be between the cut-in wind speed and the cut-out wind speed. The cut-in speed is 3m/s and the cut-out speed is 25 m/s. As previously stated, the chosen wind speeds were of 11.4 m s^{-1} and 25 m s^{-1} .

According to the GL standard, the time of the simulation ought to be of 10 minutes (600 seconds). For this type of analysis, 10 minutes are seen as representative, due to the fact that they can represent what is called an environmental state. An environmental state is a set of brief environmental conditions of approximately constant intensity parameters, with an usual duration of 10 minutes or one hour.

To accurately represent these 10 minutes (600 seconds), a simulation of 1000 seconds was made with FAST. During the treatment of the FAST data, the first 200 seconds were ignored, as the initial conditions are not correct, as they reflect a computational transitory response to the imposed conditions. Then, 800 seconds are inserted into ANSYS, from which the first 200 seconds of the simulation will be ignored, due to the same referred reasons. As a result, the analysis will have the required 600 seconds.

The DLC 1.1 states that it should be evaluated as “Normal Conditions”, which according to the 2010’s GL standard requires a 1.35 safety factor [105]. However, it should be noted that at the 2012’s GL standard, a safety factor of 1.2 is appointed [91]. Therefore, a safety factor of 1.2 is allowed but it was pursued a safety factor of 1.35.

3.13. The Rainflow Counting Method

When studying the behaviour of structures under fatigue conditions, the loading sequence and number of cycles is of the utmost importance. The *Rainflow Counting Method* is a cycle-counting procedure that examines a series of measurements in a suitable way for structures’ fatigue analysis [106]. Fatigue failure corresponds to the breakdown of a material when subjected to the action of repeated and/or fluctuating stresses, even if these stress are below the yield strength of the material [107]. This method analyses a load time series, as seen in Figure 3.13.

The version of this method, which will be succinctly explained, is the one indicated by the *ASTM Standard Practices for Cycle Counting in Fatigue Analysis* [108].

This version contains some designations that should be clarified:

- It considers a moving reference point, **Z**;
- The first and second points analysed are, together, called **X**;
- The second and third points analysed are, together, called **Y**;
- $r(x)$, or $r(y)$, denotes, respectively, the range of X, or Y. The range is the absolute value of the difference between the amplitude of the analysed points [109].

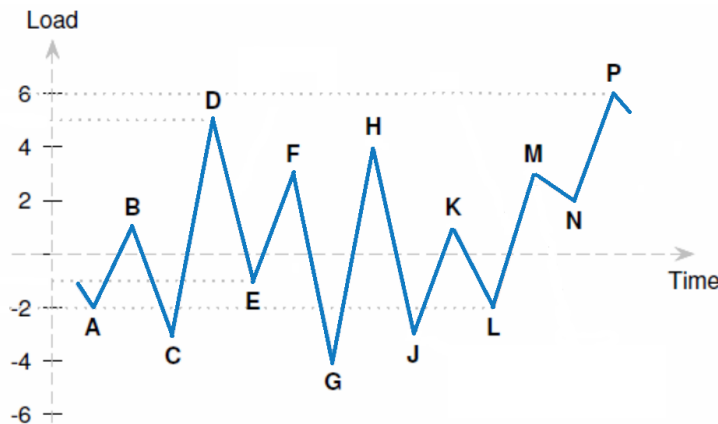


Figure 3.13 Load time series. Adapted from [110].

Figure 3.14 shows the algorithm used for this cycle counting. Further reading on this method can be found at [109,110].

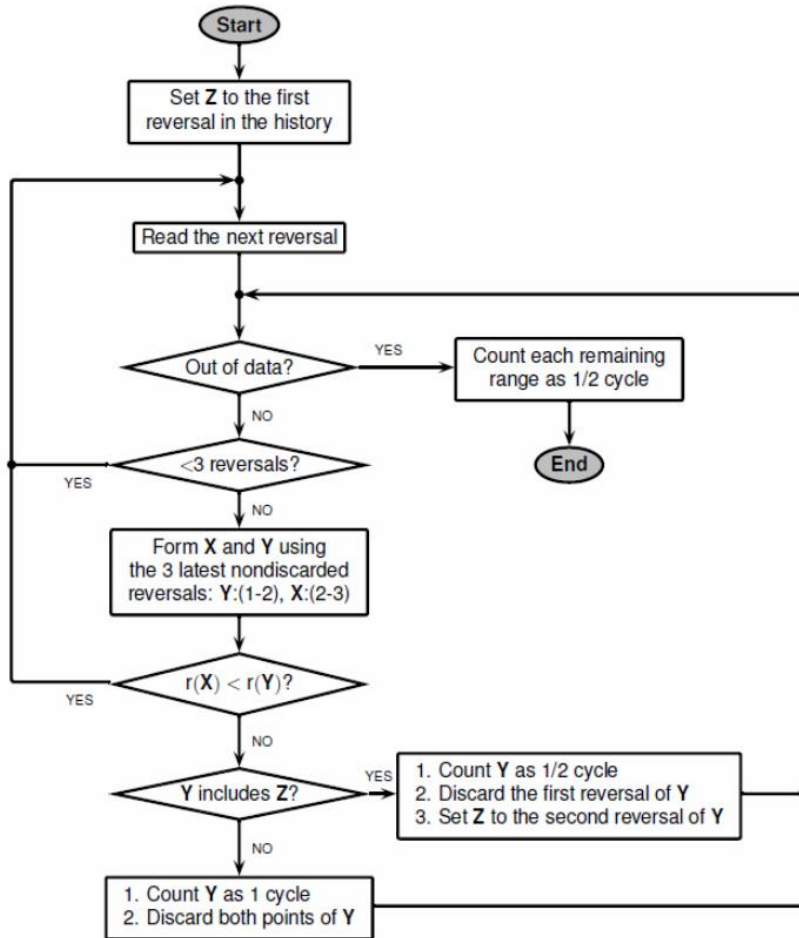


Figure 3.14 Rainflow Algorithm [110].

Chapter 4

4. Results

4.1. Time Step Study and Aliasing

As discussed in Chapter 2, the definition of the time step can have great influence on the results yielded by computer simulations. FAST software produces results every 0.05 seconds. As referred, 800 seconds are analysed by ANSYS, which would result in 16 000 time steps on each analysis. Additionally, these inputs would vary between each region of the structure, according to the number of inputs used. This would result in a massive amount of data, which cannot be solved using a normal home computer in a reasonable amount of time.

In order to correctly choose a time step that will yield acceptable results while having a practical computational time, a time step study was performed. This study consisted on the variation of the time step used while comparing the ultimate stresses verified and the amount of load cycles that the structure was subjected to. The original DeepCWind platform was analysed for 600 valid seconds with a transient structural analysis. This analysis is performed using a shell model, as it would be highly computationally expensive to perform a solid model analysis with low time steps. Furthermore, the objective is to analyse the obtained results and as each analysis has the same model and the same loads, a direct comparison may be executed. Quadrilateral elements were selected, *SHELL181*, for showing a good relation on computational time with the accuracy of the results [111].

4.1.1. Experiment Method

In order to evaluate the time step variation effects, four different time steps were used: 0.5 seconds, 1 second, 2 seconds, 3 seconds and 10 seconds. The lowest time step that could be successfully examined, due to computational limitations, was 0.5 seconds. As such, it will be the time step of reference. For these analyses, the displacement formulation was used.

For the analysis of the ultimate stress verified in each simulation, the maximum stress verified at the structure was searched from the entire time domain. The von Mises Stress were examined.

As for the cycle count, a point of reference was chosen, in order to always compare the results inside the same mesh element (there is no mesh variation). This point of reference was selected to be in an area of high stresses, while not being too close to stress concentration areas. Figure 4.1 shows where the selected point is located. To analyse the amount of cycles that the selected element was subjected to, the Rainflow Counting Method was used, considering the variation of the maximum stresses.

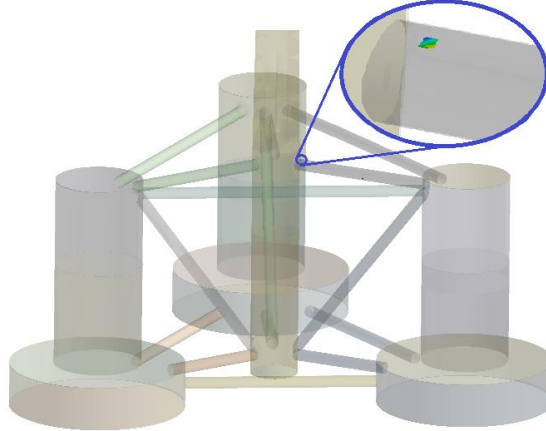


Figure 4.1 Location of selected point.

The simulations duration and computer's disk size occupied was also retrieved. This experiment was performed using ANSYS [112]. As a benchmark, some of the most important computer specifications are presented:

- 32 GB RAM Memory;
- Intel® Core™ i7-6820HK CPU @ 2.7 GHz, turbo up to 3.6 GHz;
- SSD 2.5" SanDisk Ultra 3D 2TB NAND SATA.

4.1.2. Results and Discussion

Figure 4.2 and Figure 4.3 show the results for the performed simulations. Figure 4.2 displays the maximum stresses verified at the global model, for the various simulations. Figure 4.3 shows the number of cycles that the selected element was subjected to. At this chart, the fluctuation of the maximum stresses is displayed. Subsequently, Figure 4.4 presents the error verified as the time-step varies, using the 0.5 time-step magnitudes as a reference. (It is worth mentioning that the maximum stress at the global model for the 10 second time-step was not registered) Table 4.1 shows the simulation's duration, as well as the disk's space used, for two selected simulations.

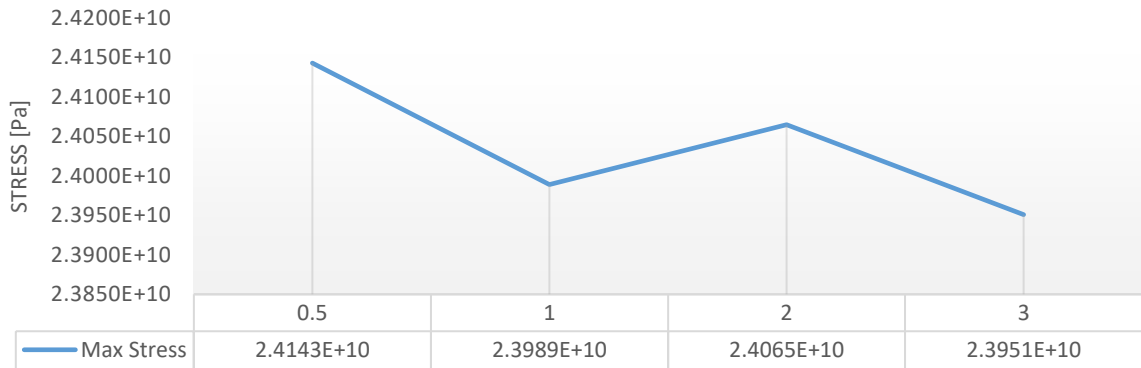


Figure 4.2 Stresses verified.

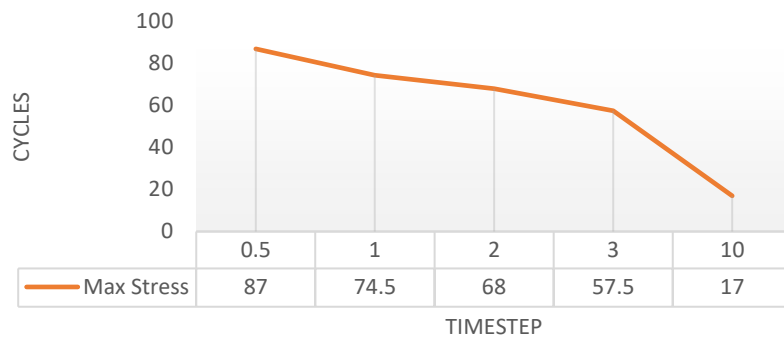


Figure 4.3 Amount of cycles verified at the selected element.

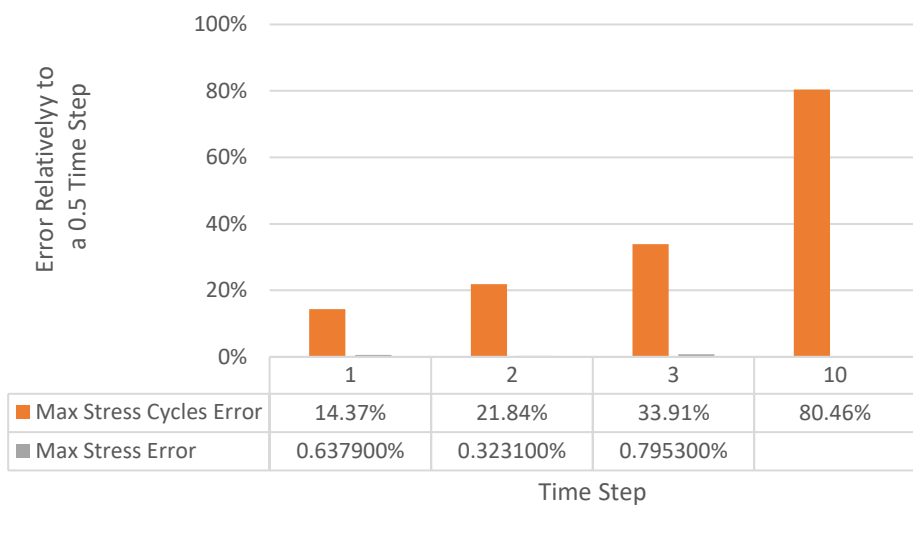


Figure 4.4 Relative error of using different time steps.

Table 4.1 Computational data.

Time Step	Simulation	Simulation
	Duration	Size on Disk
0.5	95 hours	600 GB
2	28 hours	141 GB

From the examination of the previous information, several conclusion were attained:

- **Maximum Stress at the global model** – it could be established that the variation of the time step presents no apparent relation to a possible miscalculation of the highest stress verified by the model. The biggest relative error verified was of 0.8 %, still verifying a good correspondence with the reference value.
- **Number of Cycles the element was subjected to** – the number of cycles considered the fluctuation of the maximum stresses at the selected element. As expected, there is an important loss of information as the time step increases. The error goes up to 80% at the time step of 10 seconds. In spite of lowering to around 35% for a 3 seconds time step, it still shows a big disparity. Consequently, for a fatigue analyses the time step should be as low as possible, according to the existent computational limitations.

This project aims to study the maximum stresses verified by the structure. As such, a 3 seconds time step was considered adequate and less computationally expensive. Thus, this was the selected time step for the transient analysis.

4.2. Structural Analysis

This section starts with an analysis of the original platform. Afterwards, it was recommended that the reinforcements suggested in [79] were changed, thus an improvement study to the original structure was made. Lastly, an analysis of the final solution was made and compared to previous versions. The stress analyses all share the Pa unit, being the von Mises stress the magnitude considered.

4.2.1. Original DeepCWind Platform Analysis

Modal and Static Structural Analysis were performed. Furthermore, the presence of ballasts in the structure was simulated with the use of point masses at their respective centres of mass. Quadrilateral elements were used for the shell analysis, *SHELL181*, while tetrahedral, *SOLID187*, were used for the solid submodels. Further details on the following analyses may be consulted in Appendix A.

4.2.1.1. Static Shell Simulation – Displacement Formulation

Figure 4.5 shows the overall result of the shell analysis, using the displacement formulation.

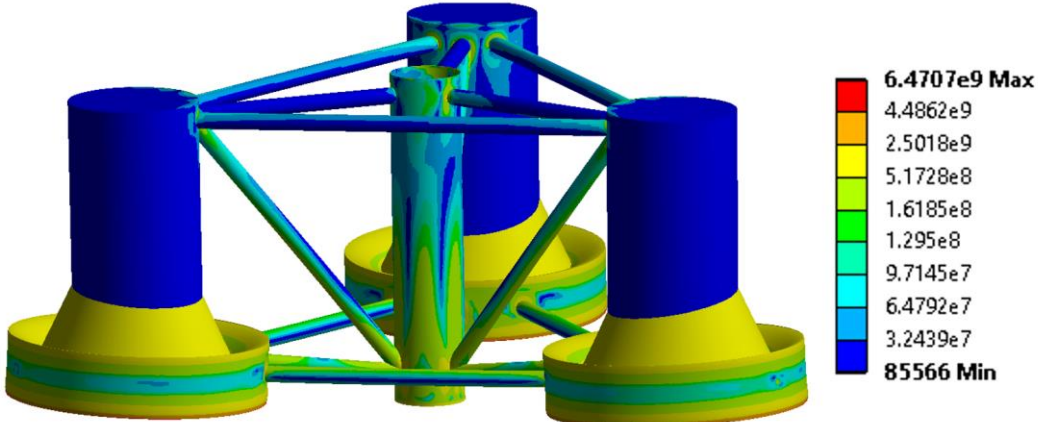


Figure 4.5 Global model analysis with the displacement formulation. Units in Pascal.

From the observation of Figure 4.5, three regions are noticeably more critical:

- The joints where the *Pontoons* connect to the larger diameter elements;
- The Bottom Columns;
- The Main Columns.

As previously discussed, the analyses using the displacements formulation should be considered to analyse the BC members. The BC column could not endure the normal stresses on its top and bottom faces, thus causing them to deform as represented. From this simulation, it is already possible to acknowledge that the structure is not suitable for operation as it is dimensioned. Despite this conclusion, a Submodel analysis was performed afterwards, in order to get a more reliable simulation at the stress concentration areas.

4.2.1.2. Submodel Analysis – Displacement Formulation

The use of a submodel analysis allows having solid elements at stress concentration areas, while still consuming much less computational resources than a full solid model simulation. For this simulation, the joints between *Pontoons* and larger diameter members were examined. Figure 4.6 shows a part of a submodel of one of the BC members.

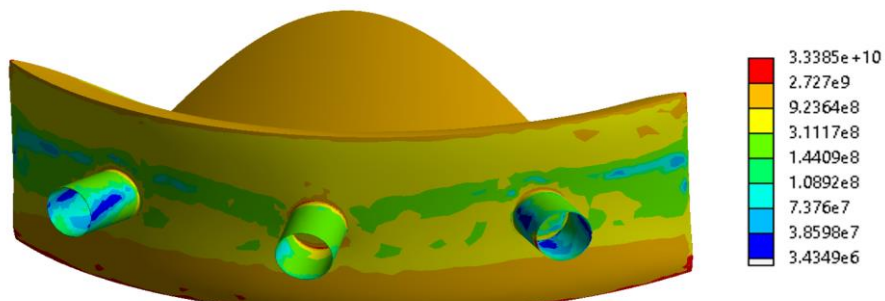


Figure 4.6 BC submodel with the displacements formulation. Units in Pascal.

Both solid submodel and shell model show similar stresses and deformations. The highest stress is in the order of 10^{10} but this is due to the presence of singularities. A singularity is a point where some results of the solution do not converge. This happens when a certain load is applied to a corner or edge that is perfectly sharp (in the real world, there are seldom perfectly sharp edges). The imported displacements from the Shell analysis are directly applied as boundary conditions, in the Submodel analysis, on faces that in the real world possess no discontinuities [102]. Hence, these fictional high stress areas should not be considered. The high concentration areas taken into account are located at the joints of the elements. The results of a solid model are considered to describe reality more truthfully than a shell model, thus its results ought to be more accurate [110]. The BC members are shown to be structurally unable to cope with the considered conditions.

4.2.1.3. Static Shell Simulation – Springs Formulation

As aforementioned, a spring formulation was also used. The objective of this analysis is to ensure that the structure is correctly constrained, by using two different methods, as well as having a constraint situation that describes the reality more accurately. It is worth reminding that the springs used, create fictitious stresses at the BC members and thus these members were previously examined. Figure 4.7 shows the result of this analysis, with a shell model. Using a different formulation also allows checking if there are fictitious stresses due to the previous constraints.

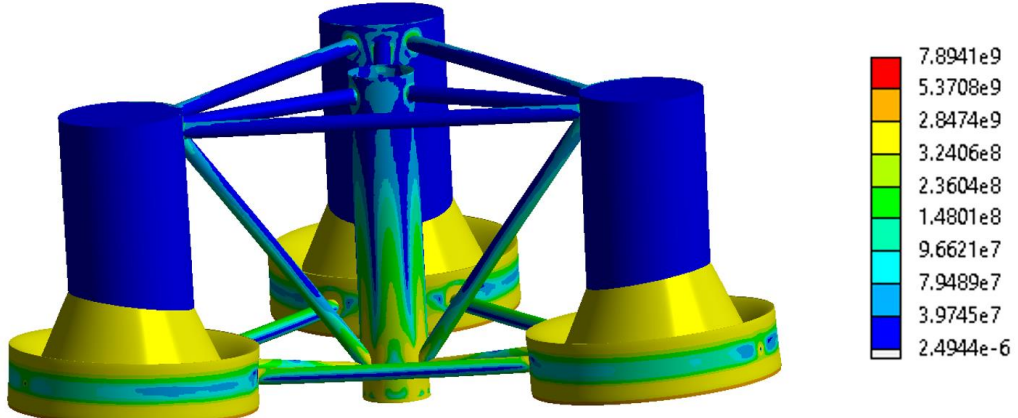


Figure 4.7 Global model analysis with the springs formulation. Units in Pascal.

After consideration of Figure 4.7, it can be stated that both analyses formulations give equivalent stresses and deformations. Figure 4.8 shows two details of this analysis. On the left corner of this Figure, both details are located in the global model.

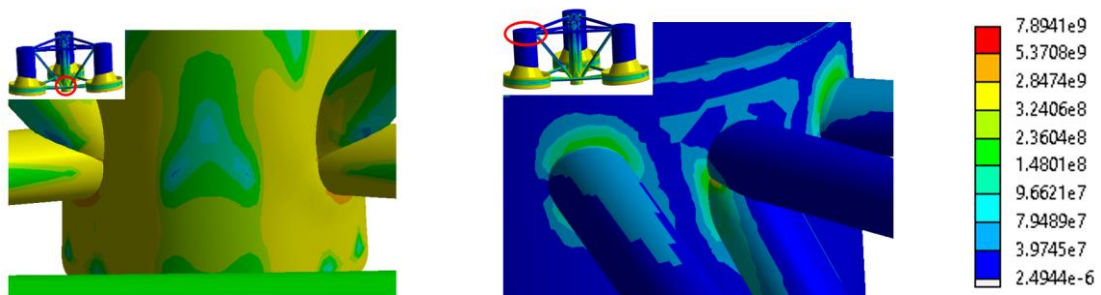


Figure 4.8 Details of the global model analysis with springs formulation. Units in Pascal.

4.2.1.4. Submodel Analysis – Springs Formulation

The submodel analysis, once again, confirmed the shell results by using reduced solid models of the areas with higher stress concentrations. The UC members, MC members, pontoons and joints were of concern for this analysis. Figure 4.9 and Figure 4.10 show the submodels with the greatest importance.

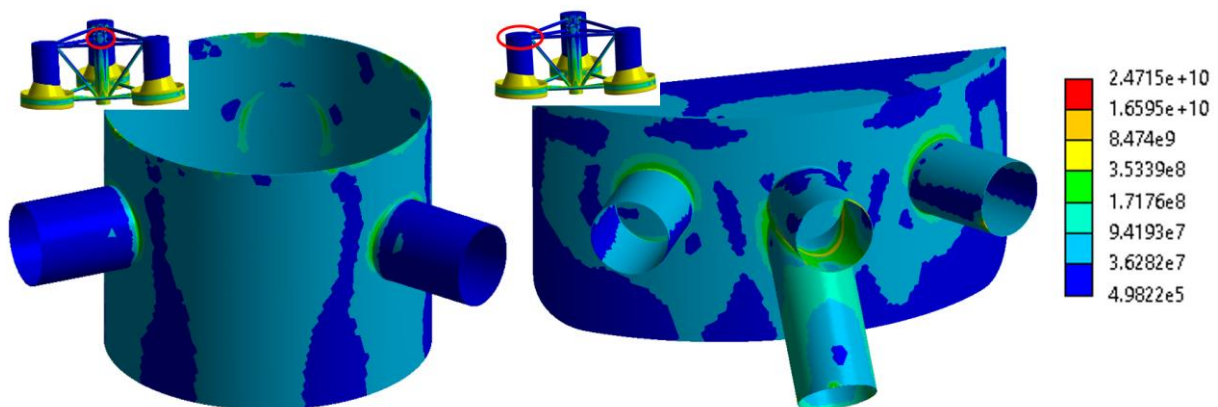


Figure 4.9 Details of the global model analysis with the displacements formulation. Units in Pascal.

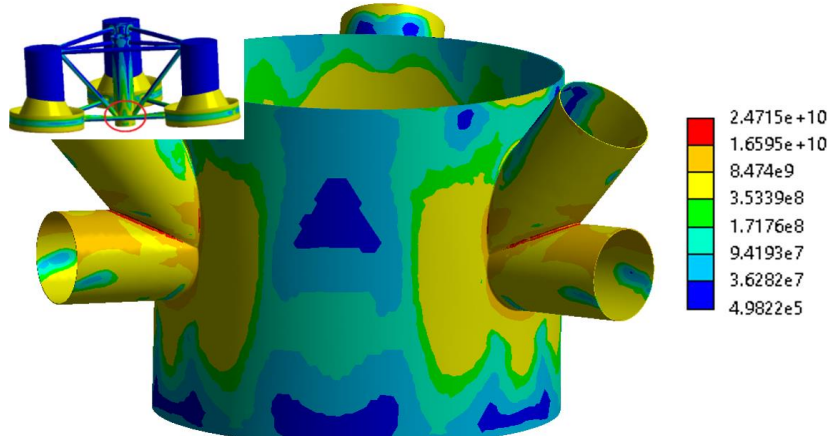


Figure 4.10 Details of the global model analysis with the displacements formulation. Units in Pascal.

These figures confirm that the higher stresses are located at the bottom of the MC column. After consideration of the presented results, transient analyses were found unnecessary for the current structure. It was verified that the original structure could not endure the loads it was supposed to. Therefore, a structural improvement was needed.

4.2.1.5. Modal Analysis Results

The natural frequencies of the turbines' blades are of no interest during this research, as it only focuses on the structural behaviour of the supporting structures (tower and foundation). For simplification, the blades and the nacelle, are not represented, instead they are idealized as point masses

Figure 4.11 shows the results of the modal analysis performed and the deformation shapes for Mode 1 (Side-to-Side and Fore-Aft) and Mode 2 (Side-to-Side, Fore-Aft and Torsion). Table 4.2 shows the values of the pertinent natural frequencies of the structure.

Table 4.2 Considered Natural frequencies of the structure.

Mode Description	Frequency [Hz]
Mode 1 – Side-to-Side	0.278
Mode 1 – Fore-Aft	0.279
Mode 2 – Side-to-Side	0.535
Mode 2 – Fore-Aft	0.537
Mode 2 - Torsion	0.546

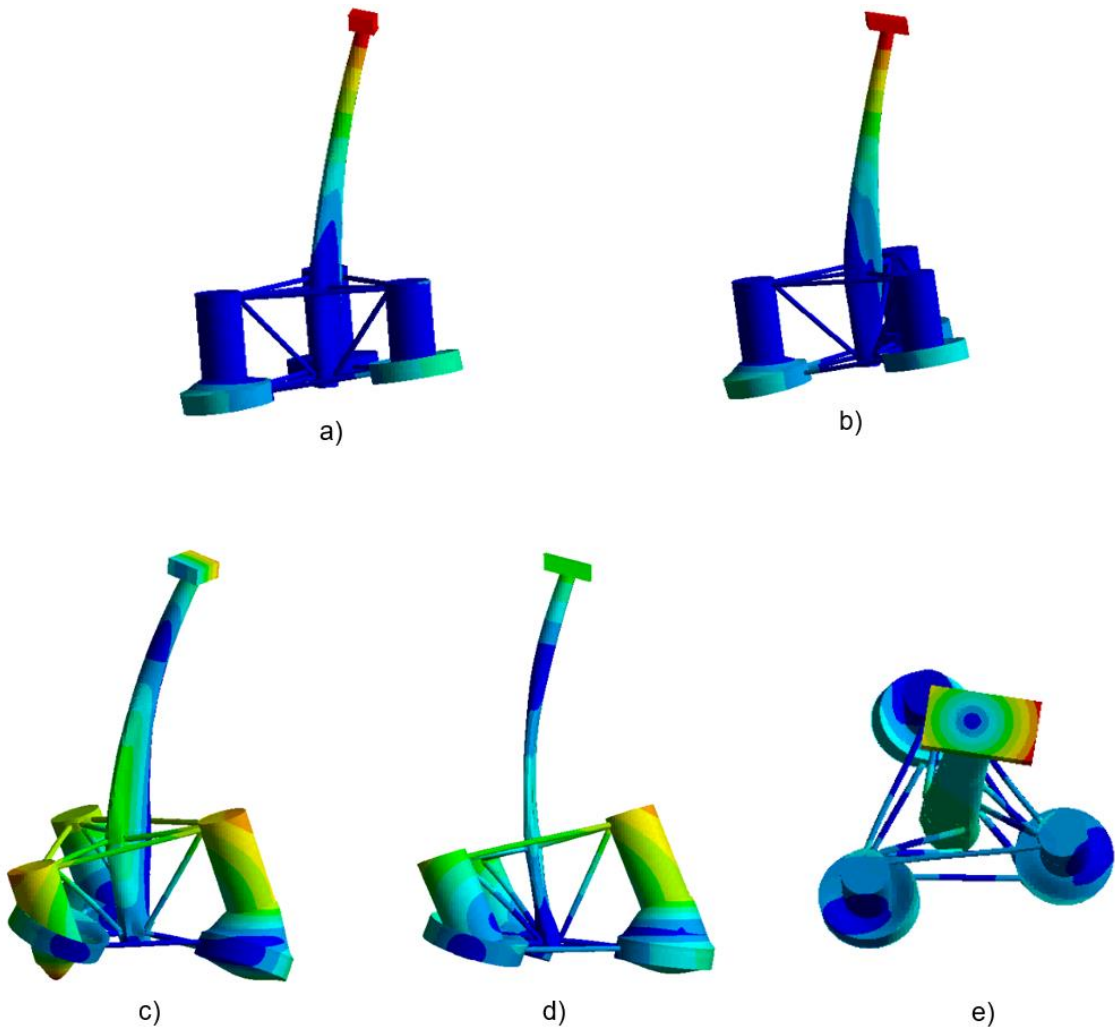


Figure 4.11 Deformation Shapes: a) Mode 1 – Side to Side; b) Mode 1 - Fore-Aft; c) Mode 2 - Side-to-Side; d) Mode 2 - Fore-Aft; e) Mode 2 – Torsion.

The structure's fundamental frequency is 0.278 Hz. It is of good practise to ensure that this fundamental frequency does not coincide with the real world working frequencies, in order to avoid resonance. This structure can be classified as Soft-Stiff, as the structure's fundamental frequency is between the interval that goes from 0.22 Hz to 0.31 Hz.

4.2.2. Structural Improvement

The DeepCWind was subjected to a partial improvement process in a master thesis, which can be consulted in [79]. However, those results could not be reproduced. Moreover, it was recommended, by the project supervisors, to redesign the supports used for structural reinforcement. For this improvement process, several assumptions were considered:

- The general dimensions, as well as the outside diameters of the constitutive members, should not be modified. Minor changes in the layout could be allowed, if advantageous;
- The main objective is to create a structure that would endure the simulated outside environment, while remaining in the elastic region with a required coefficient of safety;

- In spite of the results of the previous improvement process not being verified, it only passed the analysis at 11.4 m s^{-1} . This research should produce valuable results at 11.4 m s^{-1} and 24 m s^{-1} ;
- The mass obtained in the previous process, 9 188 Tonnes, should not be significantly increased, if possible it should be decreased;
- The reinforcements used should be considered for their suitability for manufacturing.

It should be noted that the improvement process was a gradual process, in which several parts of the structure were improved at the same time. However, for the sake of clarification, this document details this process by regions, for example, the UC improvement process will be dealt with separately from the BC process. Consequently, some analyses' figures may show improved members, which are only referred to in later sections. Therefore, it is advisable not to pay attention to structural members aside from the ones that the section refers to.

Further details on the following analyses may be consulted in Appendix B.

4.2.2.1. UC and BC Joint Improvement

The first improvement was to change the connection of the UC+BC members. At first, the UC member finished on top of the BC member, being welded there, as shown on the left in Figure 4.12. In order to enhance the structure's performance, the UC member was extended until the base of the BC member, thus welded there, as shown on the right in Figure 4.12. This reduced the forces/weight being applied on top of the BC and gave better stability to these members.

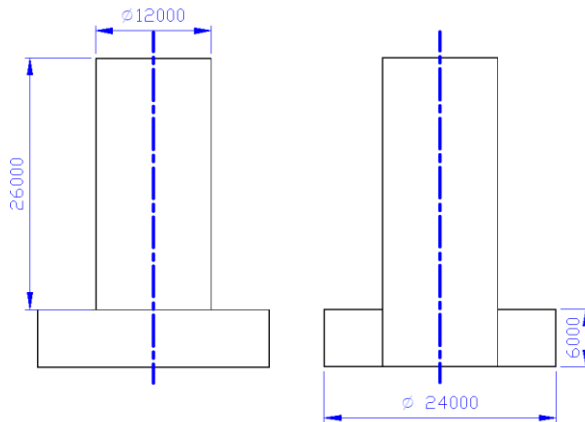


Figure 4.12 UC and BC joint cut view. Original on the left; Improved on the right.

4.2.2.2. BC Improvement

Inner reinforcements were used at the BC member. The main objective was for these reinforcements to be as strong as possible, while adding as less weight as possible. The manufacturability was also of great concern, therefore it was decided to use reinforcements that could be cut in CNC machines, which would accelerate the process of production, while also improving its reproducibility. The primary reinforcement consisted of a sheet metal with 5800 mm x 5890 mm (these values are the maximum verified at the final project, however they are altered if the thickness of the BC member itself is changed). This sheet metal is shown in Figure 4.13. This reinforcement was designed

with patterned holes, in order to decrease the weight by removing material that was not necessary. The round shapes could be further optimized to reduce the weight, or in contrast to gain further stress resistance if needed. These reinforcements were assembled in a circular pattern arrangement around the UC column, inside the BC column, as shown in Figure 4.14 (this figure shows a section cut of BC).

For all the connections of this research, it was considered a fillet at the edge joint. These fillet possessed the maximum allowable radius of concordance, which is equal to the thickness of the thinnest plate, according to the GL guideline [91].

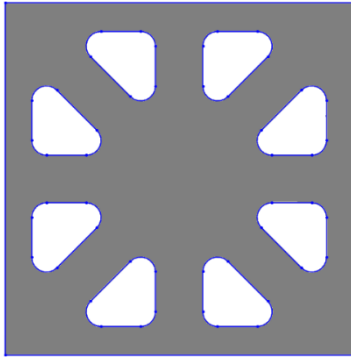


Figure 4.13 Reinforcement used at BC.

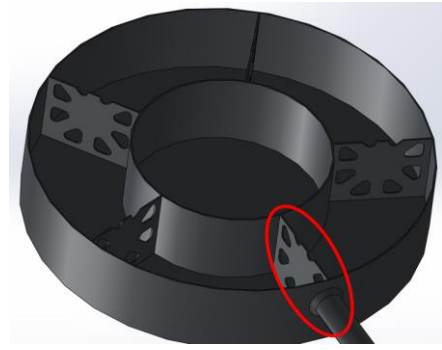


Figure 4.14 Reinforcements assembled.

Several analysis were made, modifying the number of reinforcements used, ranging from 5 to 8, while also changing the thickness of the reinforcements, from 50 mm to 180 mm. These thicknesses are considered high for common machines. One possibility for the use of CNC machines is to use water jet machines. In order to get information of an example of a machine able to make this type of cut, the *Water Jet Sweden* website was consulted. This company sells water jet machines that cut steel up to 300 mm [111]. These machine can also deal with the large dimensions of the reinforcements [112].

In one of the first designs, it was decided to use 5 reinforcements of 90 mm. The thickness of the BC member itself was insufficient, thus a thickness of 120 mm was used. The thickness of the bottom of the BC was also increased to 120. These improvements were not enough, as it is shown in Figure 4.15, in an analysis at 11.4 m s^{-1} . The centre of the bottom of the BC presented high stresses, as well as the zones between the reinforcements. These led to the necessity of using further reinforcements.

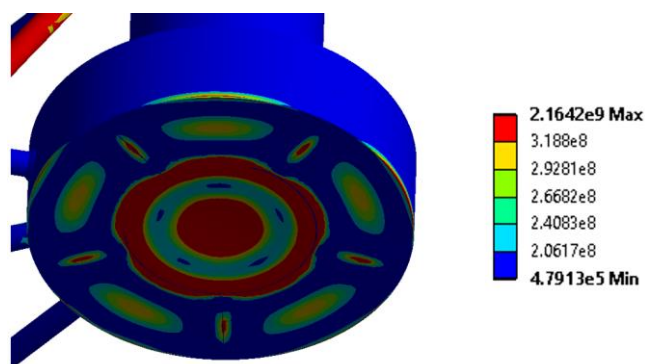


Figure 4.15 Model analysis at 11.4 m s^{-1} , with the displacement formulation. Units in Pascal.

To strengthen the centre of the BC, the type of reinforcements used are shown in Figure 4.16. These reinforcements have 100 mm in thickness and were assembled in a circular pattern as shown in Figure 4.16 b). Two circular reinforcements were also used, one next to the previously discussed reinforcements and other at the level of the top of the BC, as also shown in Figure 4.16 b) pointed by arrows.

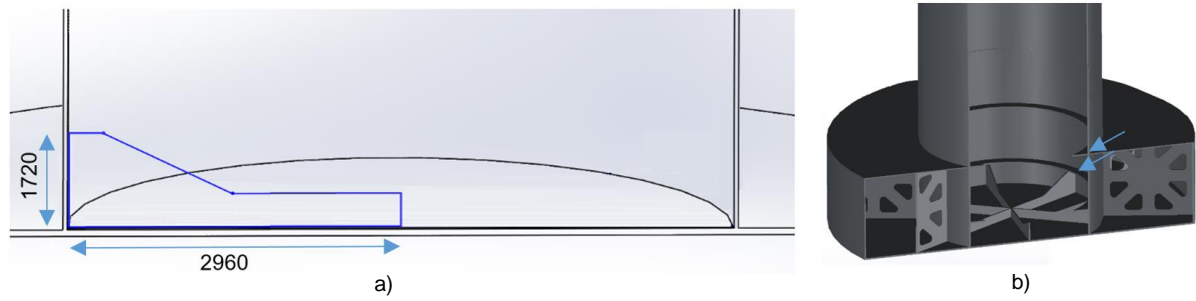


Figure 4.16 Central reinforcements at the BC. a) Dimensions; b) Location.

Similar reinforcements were used at the non-central zone. These are shown in Figure 4.17 and Figure 4.18. On the left in Figure 4.17, one reinforcement is at the bottom, while other is at the top. Both have 80 mm in thickness. A similar reinforcement is shown on the right in Figure 4.17, which is assembled at the bottom, perpendicularly to the previously ones that are on the left, having a thickness of 120 mm. Figure 4.18 shows the resulting assembly.

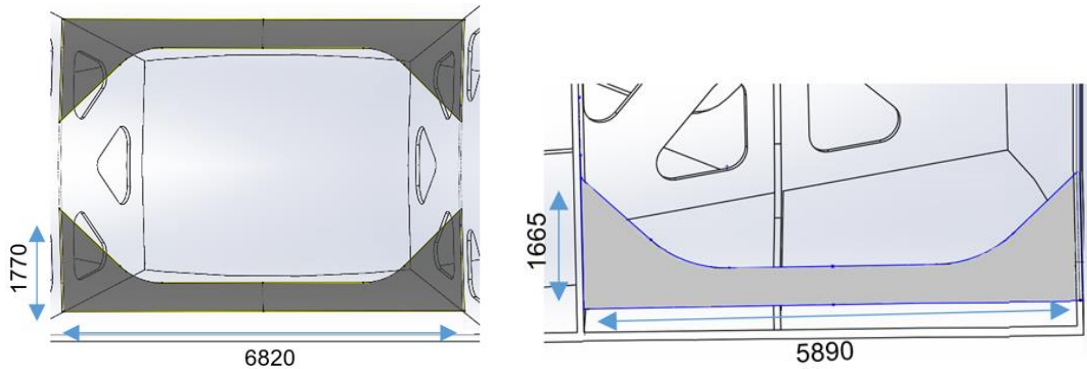


Figure 4.17 Reinforcements' Geometries and Dimensions.

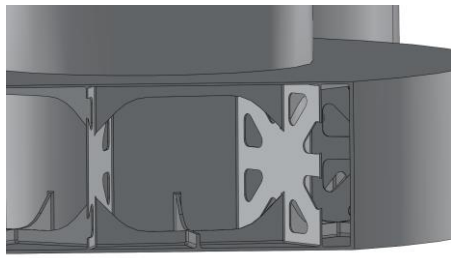


Figure 4.18 Reinforcements Layout.

After examination of the results, it was decided to use 8 reinforcements, of the type shown in Figure 4.13, with thicknesses of 60 mm each. However, the reinforcement that is in alignment with the connection of the BC to the pontoon YL (circled in Figure 4.14) showed stresses much higher than those verified at the other reinforcements. This is shown in Figure 4.19, in an analysis at a wind speed of 11.4 m s⁻¹.

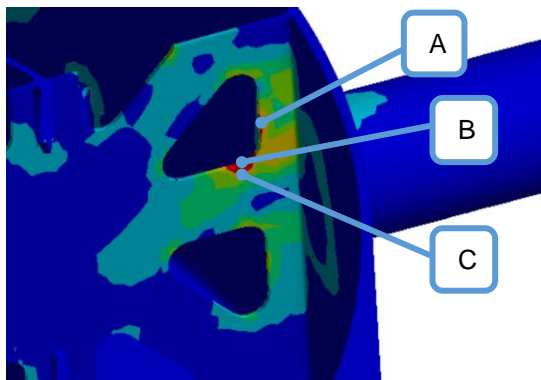


Figure 4.19 BC reinforcement analysis at 11.4 m s⁻¹, with the displacements formulation.

The selected points have the following magnitudes: **A** is 340 MPa, **B** is 452 MPa and **C** is 369 MPa. This led to the necessity of increasing the thickness of this reinforcement alone. The thickness was increased to 180 mm. The results of this analysis are shown in Figure 4.20.

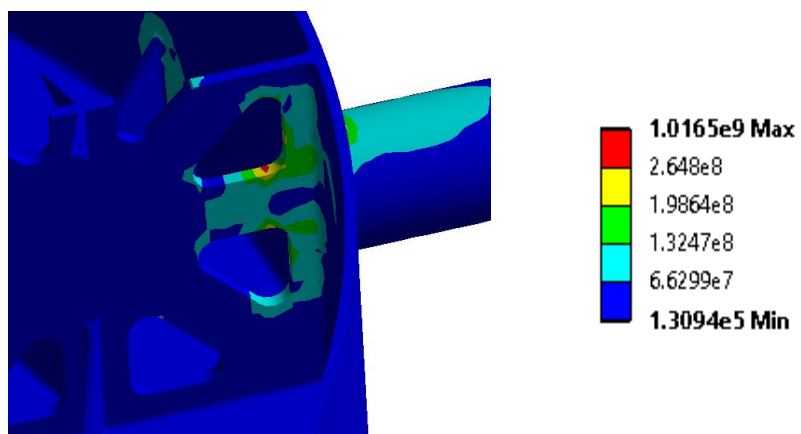


Figure 4.20 Reinforcement improvement. Analysis at 24 m s⁻¹, with the displacements formulation. Units in Pascal.

This analysis shows that the increment in thickness was not enough. Moreover, the analysis was at 11.4 m s^{-1} and it should endure 24 m s^{-1} . As the stresses were still above the safety criteria, it was opted to change the sheet metal design, which led to the reduction of number of holes, resulting in the reinforcement shown in Figure 4.21. The resulting reinforcement used the thickness of 160 mm.

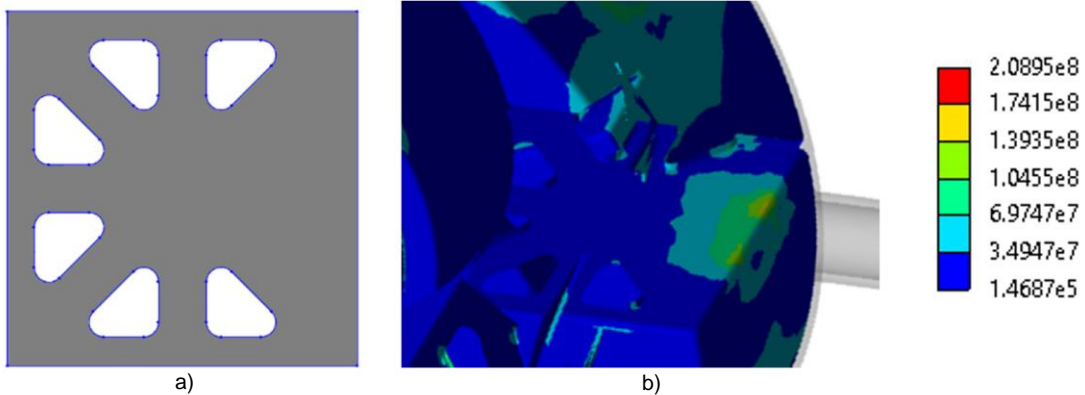


Figure 4.21 Improved Reinforcement. a) Reinforcement geometry; b) Analysis of this reinforcement. Analysis at 24 m s^{-1} , with the displacements formulation. Units in Pascal.

Finally, in order to decrease the weight of the BC member, the thickness of the BC itself was segmented. This means that the thicknesses would remain high at zones of relatively large stresses, while being decreased at zones of lower influence. The GL's guideline [91], states that for the alignment of plates of different thicknesses, the neutral fibre should be used as guide. The misalignment of this fibre of both plates should not be higher than 3 mm. Due to the high thicknesses involved in the present structure, it was decided to perfectly align the fibres, thus being collinear. The thickness were defined as shown in Figure 4.22. The sheet metal used for the red zone had a thickness of 120 mm while at the green area the thickness was 80 mm.

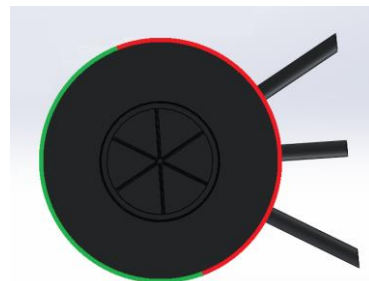


Figure 4.22 BC thickness segmentation.

The final analyses will show in detail the results of these final improvements.

4.2.2.3. UC Improvement

From the analysis of the original structure, it can be stated that the UC members possesses a vast gradients in terms of the applied stresses. It presents high stresses at connection areas while showing other regions of relatively low stresses. Due to this, it was established that thickness segmentation should also be used there. Figure 4.23 a) shows the first design used and the thickness variation, assigned by colours. The rounded plates marked by blue had a thickness of 80 mm, red of 95 mm and yellow of 120 mm. Figure 4.23 b) shows one analysis of this design.

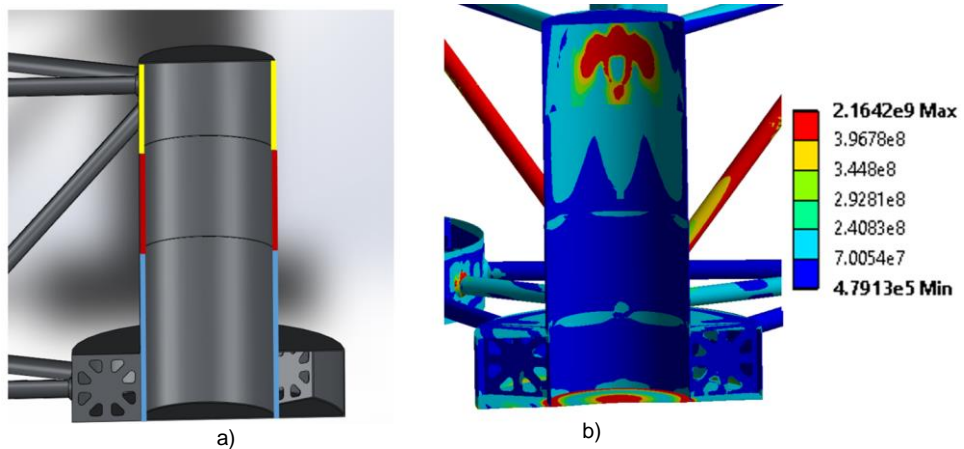


Figure 4.23 MC. a) Thickness segmentation. b) Analysis' results. Analysis at 11.4 m s^{-1} , with the displacements formulation. Units in Pascal.

In order to strengthen the structure, circular reinforcements were used at the top of the UC. Worth noting that the reinforcements used on the lower part of the UC were discussed in the previous section. Various simulations were made, changing the number of reinforcements as well as their thicknesses. Figure 4.24 a) shows a design with 4 reinforcements, which was the maximum used. Figure 4.24 b) shows an analysis of this design.

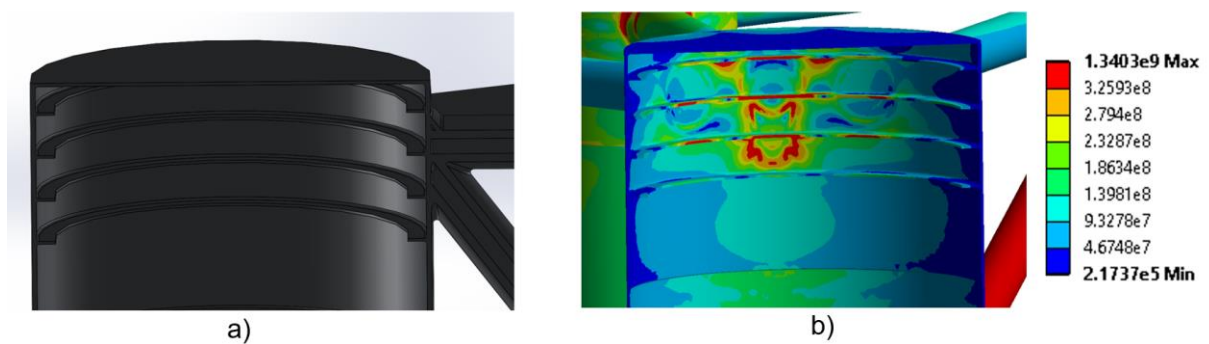


Figure 4.24 UC. a) UC reinforcements; b) UC analysis. Analysis at 11.4 m s^{-1} , with the displacements formulation. Units in Pascal.

The supports showed difficulty enduring the stresses. Furthermore, there were zones where the stresses were very low. It was decided to make another thickness segmentation. This variation is shown in Figure 4.25, being a) and b), a top view and a cut side view, respectively. At the top segment, it is

divided in two, with the yellow portion having 140 mm and the red half having 60 mm. The red medium section also presents 60 mm and the green lower section has 80 mm. The previous circular reinforcements were found unnecessary with this design, instead using a single circular reinforcement at the horizontal section of transition from the 140 mm to 60 mm, as assign by an arrow in Figure 4.25 b). All the reinforcements may be produced using CNC machines, as previously discussed, though some of them might need to be cut by subdivisions, such as the circular reinforcements that have a large diameter.

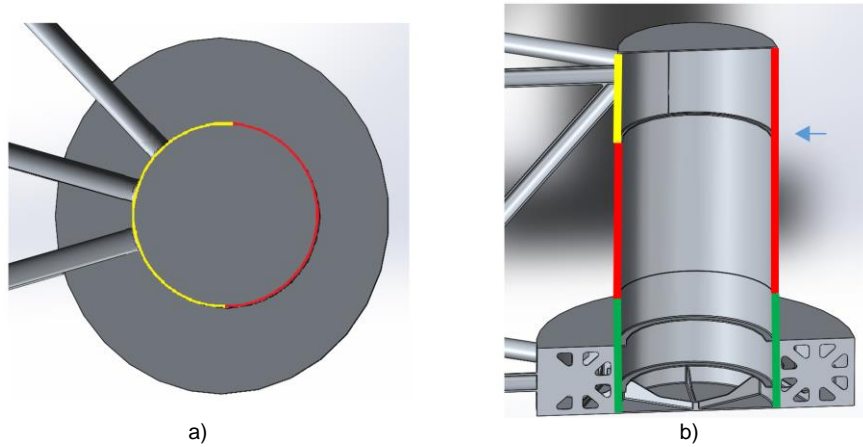


Figure 4.25 UC. a) UC top view; b) UC side cut view.

The final analyses will show in detail the results of these final improvements.

4.2.2.4. MC Improvement

The MC member is one of the most critical regions of the structure. The tower is supported by it. At first, the global thickness was increased to 100 mm. Circular reinforcements were also added at the zones of stress concentration. Some simulations were performed with different number of reinforcements and different thicknesses. Figure 4.26 a) shows one of the earliest designs and Figure 4.26 b) shows this design under analysis, with reinforcements presenting 80 mm in thickness.

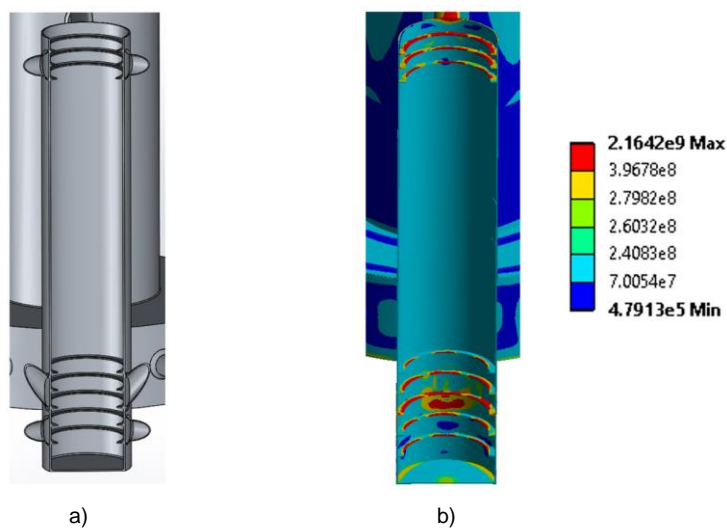


Figure 4.26 MC. a) Reinforcements design; b) Reinforcements analysis. Analysis at 11.4 m s^{-1} , with the displacements formulation. Units in Pascal.

At the bottom of the MC, it was found necessary to use reinforcements similar to those used at the BC column, with thicknesses of 100 mm. It was examined the use of 4 to 6 supports. Figure 4.27 a) shows the dimensions of these supports, b) shows the use of these supports and c) shows an analysis of an initial design.

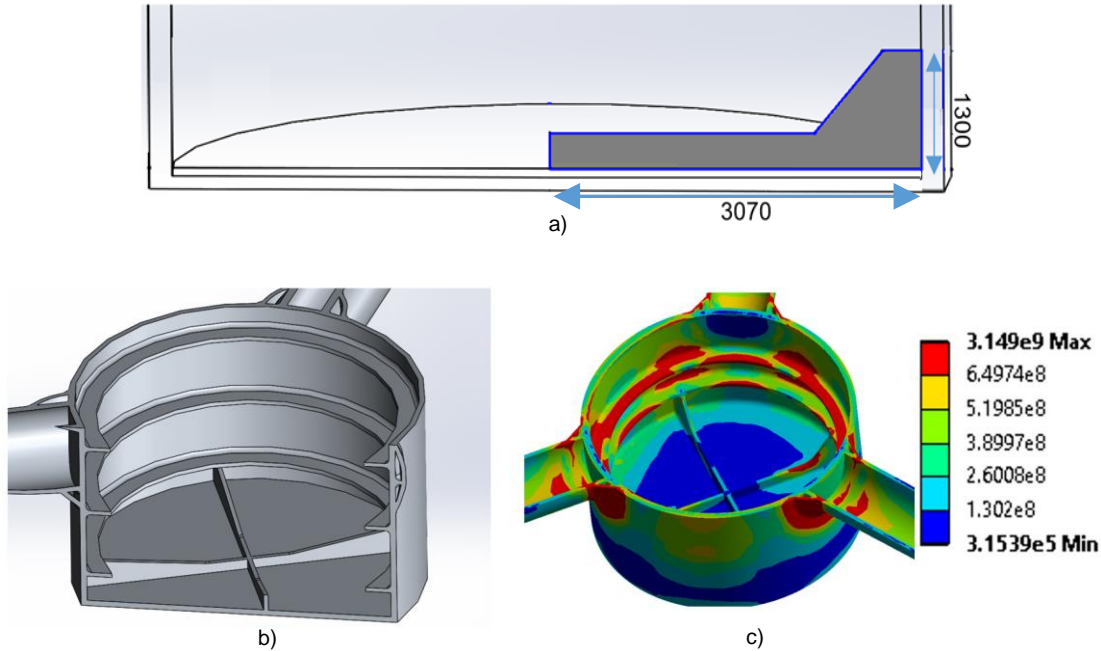


Figure 4.27 MC's bottom. a) Dimensions; b) Design; c) Analysis. Analysis at 11.4 m s^{-1} , with the displacements formulation. Units in Pascal.

Despite, showing improvements, the transversal circular reinforcements were still not showing the desired results, even after thickness increments until 120 mm. Therefore, longitudinal reinforcements were also implemented. These reinforcements were assembled at the top and bottom of the MC, as these zones reveal much higher stresses than the intermediate zones. Figure 4.28 a) and b) show the use of the supports at top level and at the bottom, respectively. The longitudinal reinforcements have a thickness of 70 mm at the top of the MC, while the ones at the bottom have 100 mm.

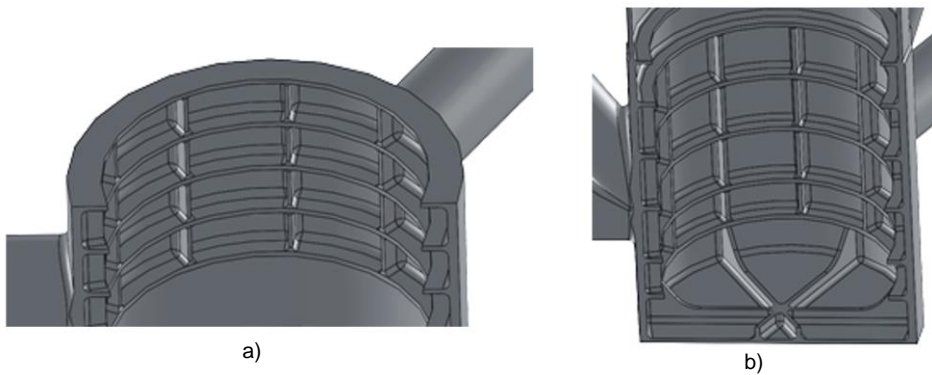


Figure 4.28 MC reinforcements. a) at the top; b) at the bottom.

Later on, the thickness segmentation was used. This allowed for high reduction of the total weight of this member while remaining structurally strong. Figure 4.29 shows this segmentation, with the red zone having 180 mm in thickness while the green zone presents 90 mm. The circular reinforcements at the top present 80 mm in thickness while the ones at the bottom have 100 mm. There are also two circular reinforcements, at thickness transition regions, with thickness of 80 mm, assigned by arrows in Figure 4.29. These transitional reinforcements are used to reinforce the regions of thickness variation.



Figure 4.29 MC segmentation.

The final analysis will show in detail the results of these final improvements.

4.2.2.5. Pontoons Improvement

The Pontoon members are identified in Figure 4.30. The connection of these members to the larger diameter columns was presented in the master thesis [79], as the most critical zones. The solution used was to increase the thickness of these members. However, as for this project the goal is to have the lowest weight, several layout alterations were tried in combination with the increments in thickness (that were found insufficient), without having a significant additional added weight.

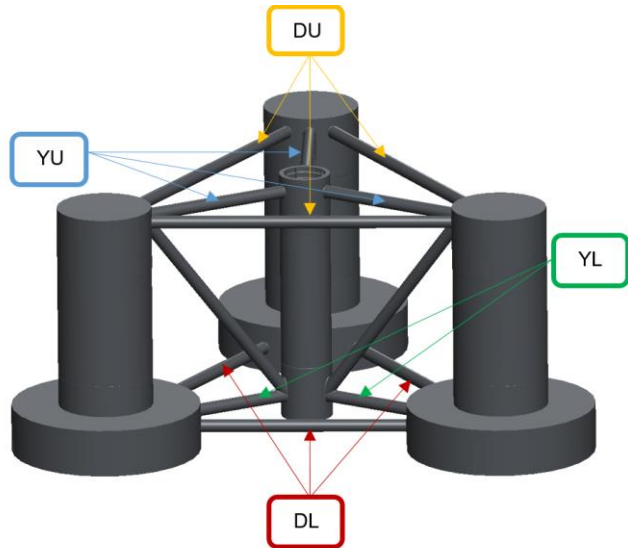


Figure 4.30 Pontoons identification.

The following layout options were evaluated using the exact same loads applied in each case, i.e., the only difference is the different layout. These analysis are to be considered more in a comparable qualitative way, verifying which option yields the best results.

4.2.2.5.1 Conical Connections

When the pontoons joints are produced, they are welded, thus creating a welding bead. Figure 4.31 shows a real welding bead on the left and a computational one on the right. These create a rounded profile that reduces the stress concentration, as it allows for a smoother stress flow. Otherwise, the stresses would be localized at the sharpest points.



Figure 4.31 Weld bead. Real weld bead on the left. Simulated one on the right.

As previously said, it was experimented to use reinforcements at the connections instead of just increasing the thicknesses. The first layout tried was the use of conical transitions, which would assist in enduring the applied loads. These types of connections are shown in Figure 4.32, with a) showing a connection of the DU member to UC and b) of the YL and CB to MC (the CB members themselves did not have conical transitions, as they would result in geometries of highly difficult production due to its shape). These connections would be hollow inside. Figure 4.33 show analyses of the concepts with and without conical transitions.

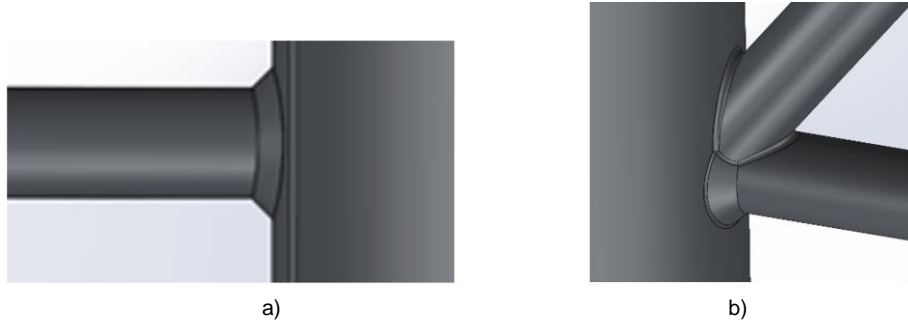


Figure 4.32 Conical connections. a) DU to UC; b) YL+CB to MC.

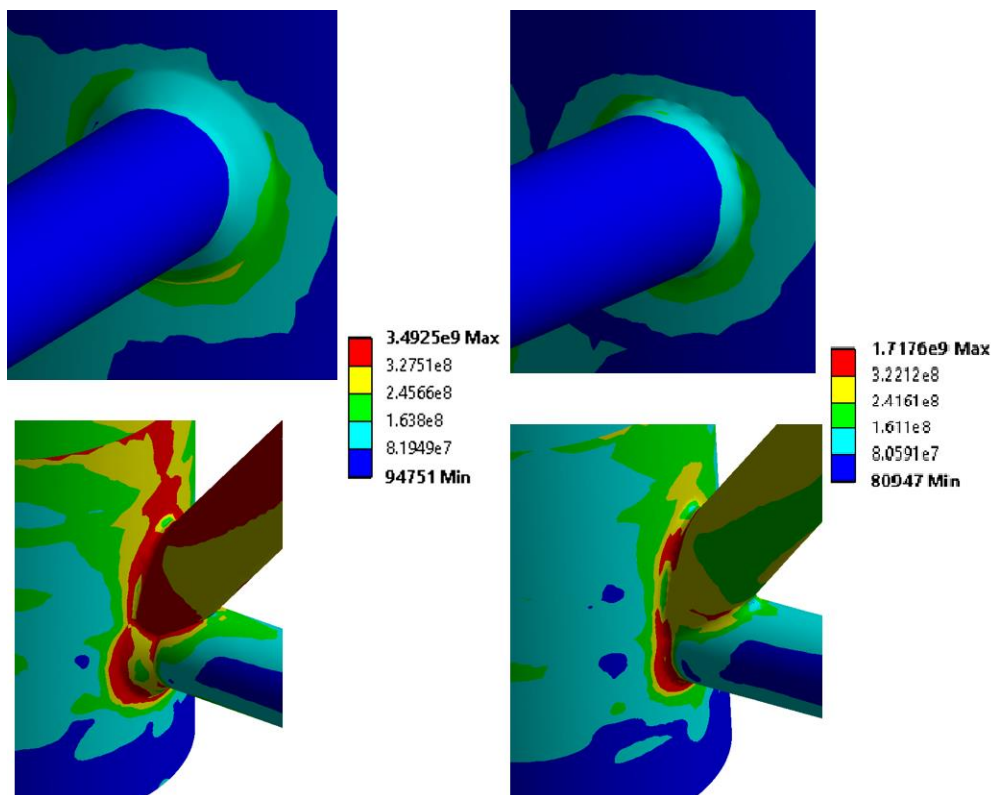


Figure 4.33 Conical connection analysis. With conical connections on the left and without on the right. Analysis at 11.4 m s^{-1} , with the displacements formulation. Units in Pascal.

The scales used, although not exactly, have transitions very close to one other, allowing for the direct comparison of each image. The highest stresses are very dissimilar, but these should not be considered as they are singularities. Instead, the general stress distribution should be considered.

After examination, it is clear that the conical transitions actually increased the stresses verified and predominantly increased the area affected by higher stresses. Thus, this layout is not favourable. These conclusions support the claim that joints should be as flexible as possible, specially if subjected to highly dynamic loads. This type of layout had several versions and analysis, being most of them present in Appendix B with further details.

4.2.2.5.2 Disjoint Connections

Other experiment examined the suitability of using a spread joint instead of an overlapped one for the CB members. This is shown in Figure 4.34 a) and b), with an overlapped solution and a spread solution, respectively.



Figure 4.34 Connection study. a) Joint connection; b) Disjoint connection.

Once again, the loads used were the same, being the connection the only alteration that was made, allowing for a direct comparison. (It should be noted that conical transitions were still under consideration at the time of this analysis, thus they are present; nevertheless, they are present in both versions, consequently they will have a low influence in results' variation) Figure 4.35 show the results from these analyses, with the use of overlapping and without it.

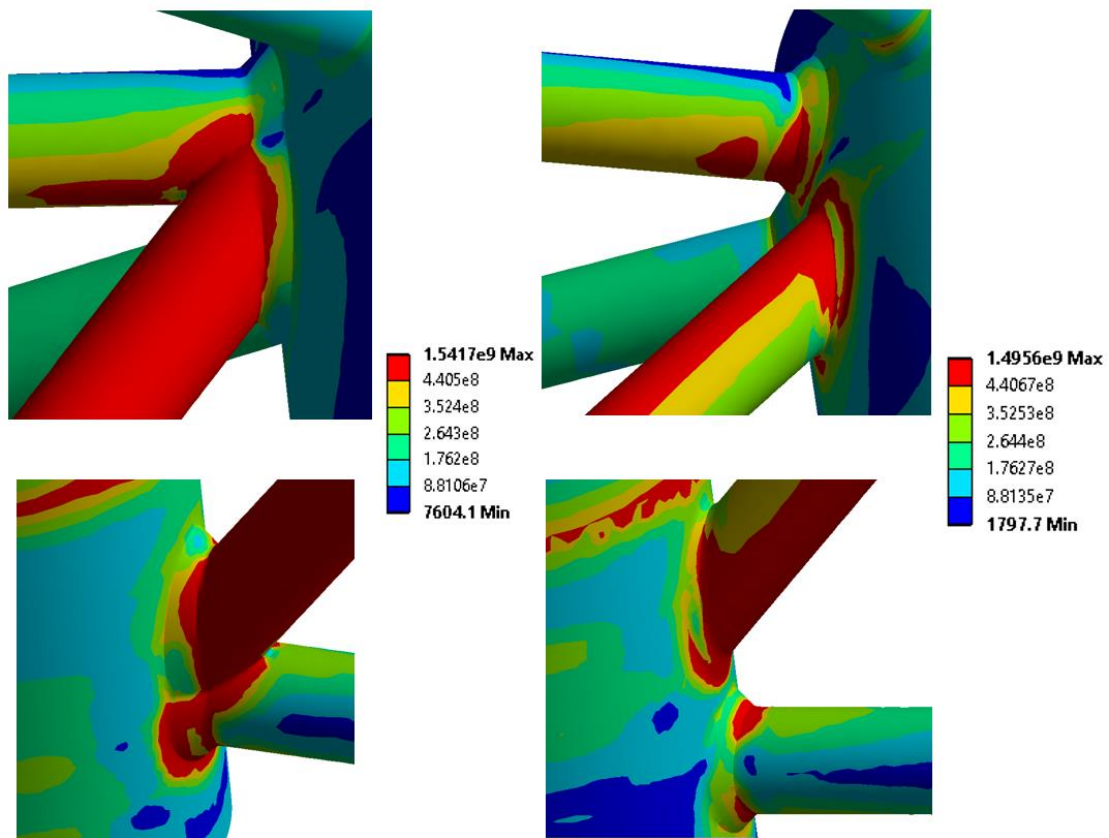


Figure 4.35 Joint analysis. Joint connection on the left and disjoint connection on the right.

After examination of the stress distribution, using disjoints connections shows no significant advantage. Furthermore, a closer look at specific points of interest shows a small increase in stresses when using connections that are not overlapped. This more careful examination can be seen in Appendix B. These results reinforce the claim by ARSEM⁷ in *Design Guides for Offshore Structures – Welded Tubular Joints* [113]:

"Overlap ensures that the common welded cross-section of the overlapping braces withstand part of the shear force transmitted by the braces. Hence, the cross-sectional area of the chord is not required to withstand the total shear force, and strains due to the shear force in the chord wall are thus limited. The overlapping of one tube on another improves the bending rigidity of the chord wall. This local stiffening of the chord wall is due to the presence of a continuous brace/chord junction zone."

4.2.2.5.3 Thickness Increment

The considered layout alterations were not adequate. Therefore, the increment in thickness was the chosen method to strengthen the pontoons. Thickness segmentation was considered but the analyses performed showed that it was not suitable for these members. This is most likely due to the structural importance of these members on performing the connections between each different elements.

Analyses were performed with thicknesses up until 220 mm. With the use of the displacement formulation, it was not possible to converge to an appropriate solution. Afterwards, the use of the springs formulation allowed for a more realistic examination and the thicknesses were optimized to: 160 mm in the YL member, 150 mm in CB and YU members and 100 mm for the DU and DL members.

The final analyses will show in detail the results of these final improvements.

4.2.3. Final Analysis

After the improvement process, the structure was examined with transient analysis, in order to evaluate its suitability for implementation. As previously mentioned, two wind speeds were evaluated, 11.4 m s⁻¹ and 25 m s⁻¹ (specifically, 24 m s⁻¹ were assessed as the turbine is stopped at 25 m s⁻¹) for 600 seconds. These analyses employed the shell-solid hybrid model, using quadrilateral elements for the shell sections, SHELL181, and tetrahedral elements for the solid sections, SOLID187. Further details on the following analysis may be consulted in Appendix C.

For simplification, the blades and the nacelle, are not represented, instead they are idealized as:

- **In the Springs Formulation:** their effects are included on the Force and Moment that are applied to the top of the tower;
- **In the Displacements Formulation:** their effects are not directly inserted, as the use of displacements at the tower cancel the effects of forces/point masses that could be

⁷ Association de Recherche sur les Structures Métalliques Marines

passed to the structure. Instead, the displacements make the structure move as it should when subjected to these forces.

4.2.3.1. Springs Formulation at 11.4 m s^{-1}

Figure 4.36 shows the results of the analysis at 11.4 m s^{-1} with the springs formulation, at the time of highest stress. Figure 4.37 shows a plot of the stresses verified during the time of the analysis. The initial 200 seconds are obscured as they represent the initial part of the analysis, which is not considered for the final 600 seconds (See section 3.12).

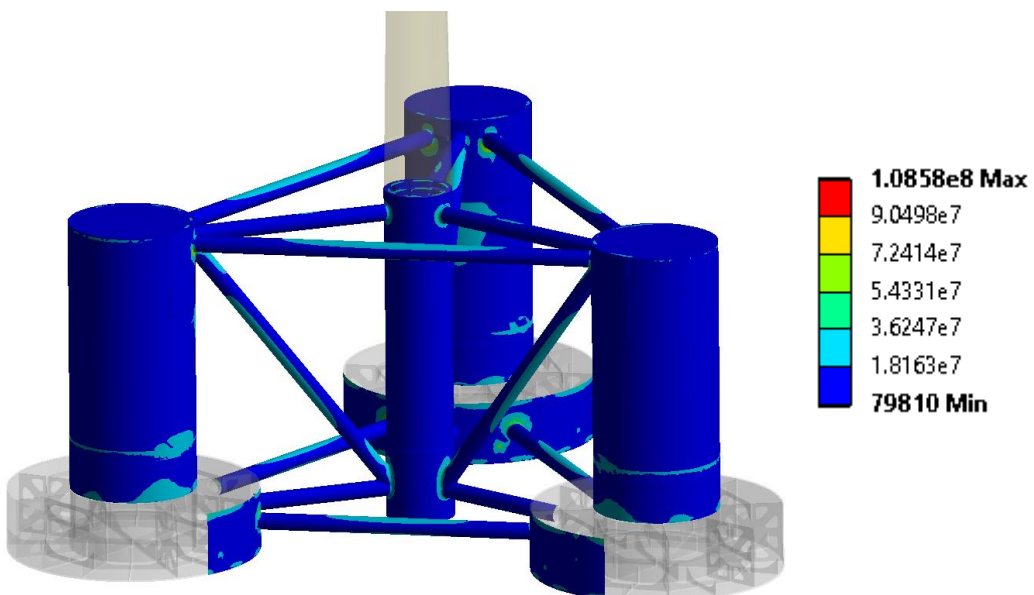


Figure 4.36 Global model analysis with springs formulation. Units in Pascal.

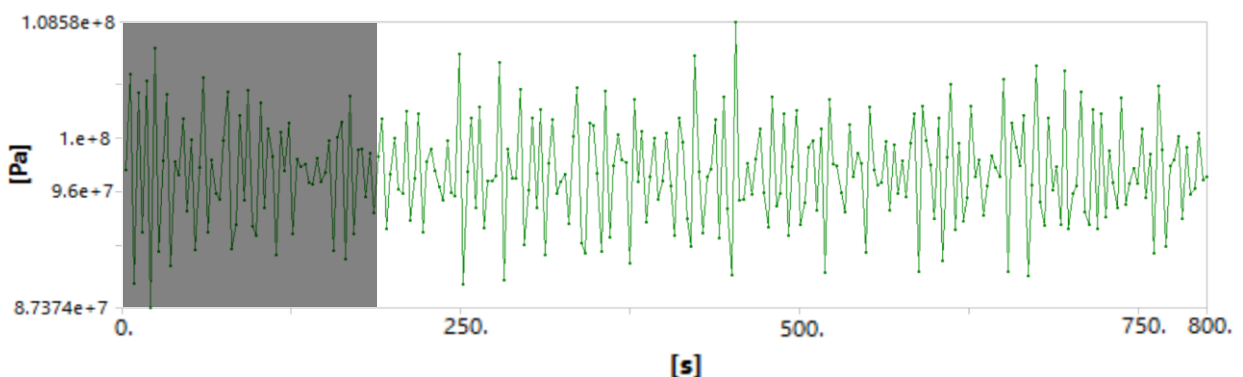


Figure 4.37 Plot of the highest stresses verified during the time of the analysis.

The highest stress verified is 109 MPa, which yields a safety coefficient of 3.2234. From Figure 4.37, it can be understood that the structure is not subjected to higher stresses during the examination period.

4.2.3.2. Displacements Formulation at 11.4 m s^{-1}

Figure 4.38 shows the results of the analysis at 11.4 m s^{-1} with the displacements formulation, at the time of highest stress. Figure 4.39 shows a plot of the stresses verified during the time of the analysis. As previously discussed, the displacements formulation is used to accurately evaluate the BC members.

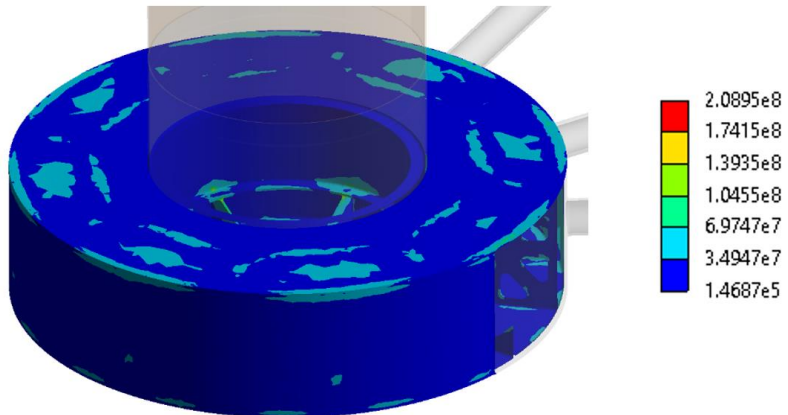


Figure 4.38 BC analysis with the displacements formulation. Units in Pascal

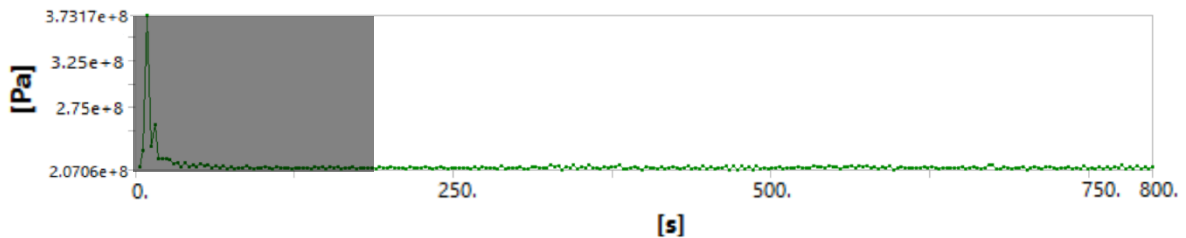


Figure 4.39 Plot of the highest stresses verified during the time of the analysis.

The highest stress verified is 209 MPa, which yields a safety coefficient of 1.67. In spite of largely succeeding in passing the required safety coefficient, it should be noted that the presence of singularities is increasing the highest stress. The singularities behaviour may be observed in Appendix D.

4.2.3.3. Springs Formulation at 24 m s^{-1}

Figure 4.40 shows the results of the analysis at 24 m s^{-1} with the springs formulation, at the time of highest stress. Figure 4.41 shows a plot of the stresses verified during the time of the analysis.

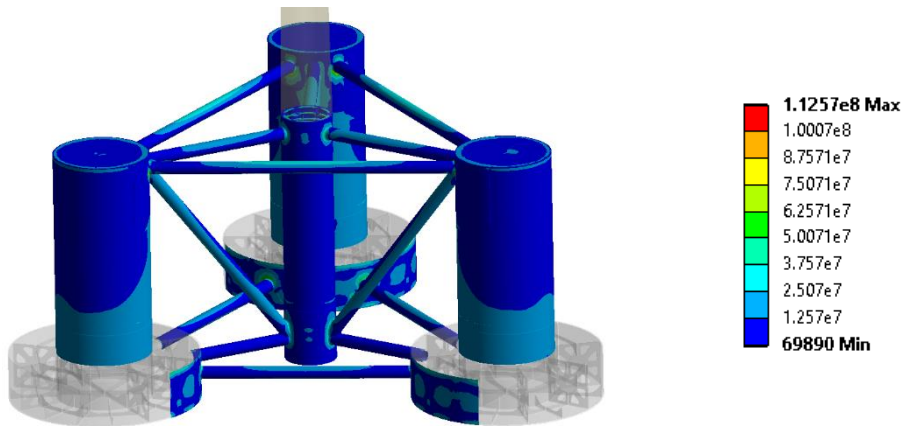


Figure 4.40 Global model analysis with the springs formulation. Units in Pascal.

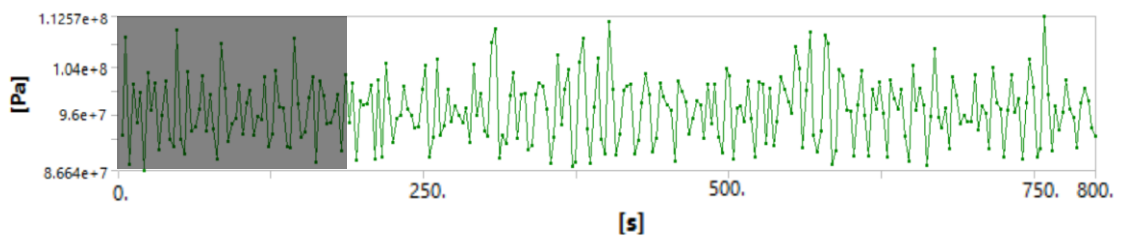


Figure 4.41 Plot of the highest stresses verified during the time of the analysis.

The highest stress verified is 113 MPa, which yields a safety coefficient of 3.1091.

4.2.3.4. Displacements Formulation at 24 m s^{-1}

Figure 4.42 shows the results of the analysis at 24 m s^{-1} with the displacements formulation, at the time of highest stress. Figure 4.43 shows a plot of the stresses verified during the time of the analysis.

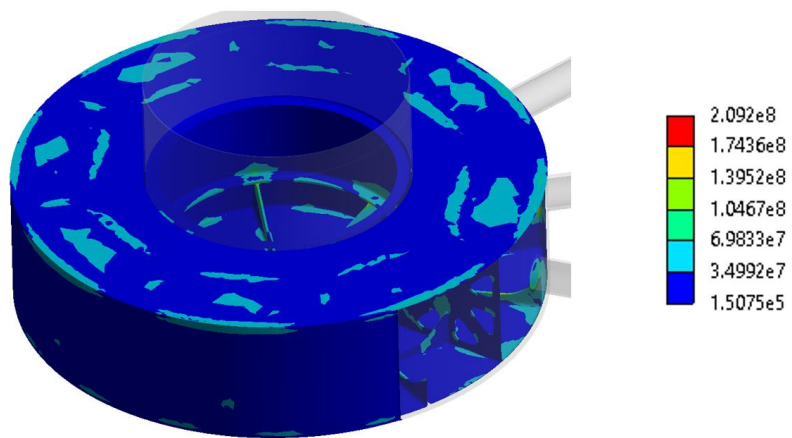


Figure 4.42 BC analysis with the displacements formulation. Units in Pascal

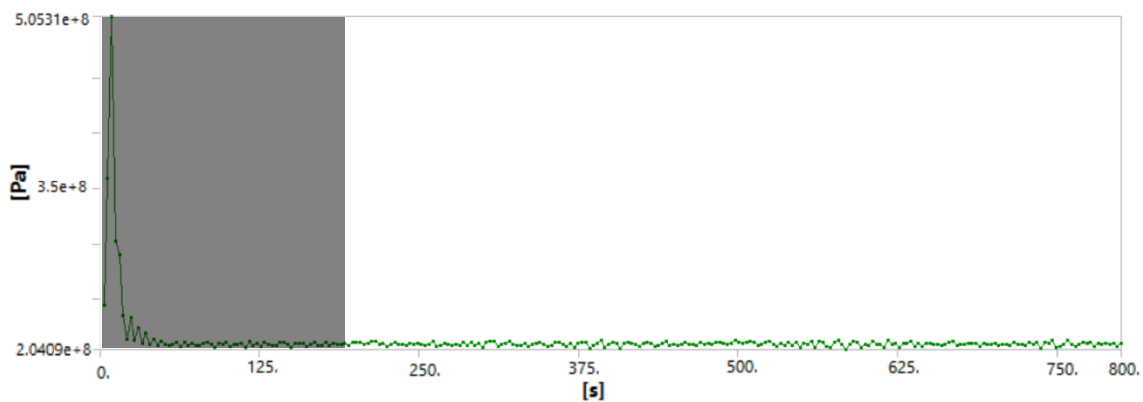


Figure 4.43 Plot of the highest stresses verified during the time of the analysis.

The highest stress verified is 210 MPa, which yields a safety coefficient of 1.668.

4.2.3.5. Modal

The reinforced structure presented higher stiffness relatively to the original platform. The fundamental frequency of the original structure was 0.278 Hz, thus being located, approximately, at the middle of the soft-stiff range. The improved structure was highly reinforced, in order to prevent the verified deformations, which led to a major increase in the structure's rigidity. On the other hand, the total mass of the structure, steel structure plus the ballast's water, remained constant. Therefore, the fundamental frequency was expected to increase. This was verified in the first analysis, yielding a fundamental frequency of 0.452 Hz. This frequency was located at the 3P region, thus resonance would be likely to occur. Figure 4.44 shows the deformation for this frequency. It can be seen that this fundamental frequency produces high deformations at the tower, not at the platform itself.



Figure 4.44 Structure Fundamental Frequency

The tower is part of the support system, thus it may also be altered. As previously discussed, the wind turbine used as reference was the 5 MW NREL Reference Turbine. In spite of this, when in production, turbines and tower may be custom-made, as it is said by *Aerodyn Company* [114]:

"You can select between ready developed and certified aeroMaster wind turbine models for onshore and offshore applications or we can perform a customized wind turbine design project which can be tailored to your specific needs."

As such, the thicknesses of the tower were altered. The original turbine possessed 19 mm at the top and 27 mm at the bottom. After several analysis, the updated tower had 19 mm at the top (it was decided to maintain this dimension) and 100 mm at the bottom, varying approximately in a linear way. This change in thickness had an impact of approximately 2.9 % in the total platform's mass, thus not having great importance.

Figure 4.45 shows the deformation shapes while Table 4.3 shows the frequencies of interest. Other frequencies of interest can be found in Annex D. As it is shown, the increment in thickness allowed for the dislocation of the fundamental frequency from the resonance region. This structure is of the stiff-stiff type.

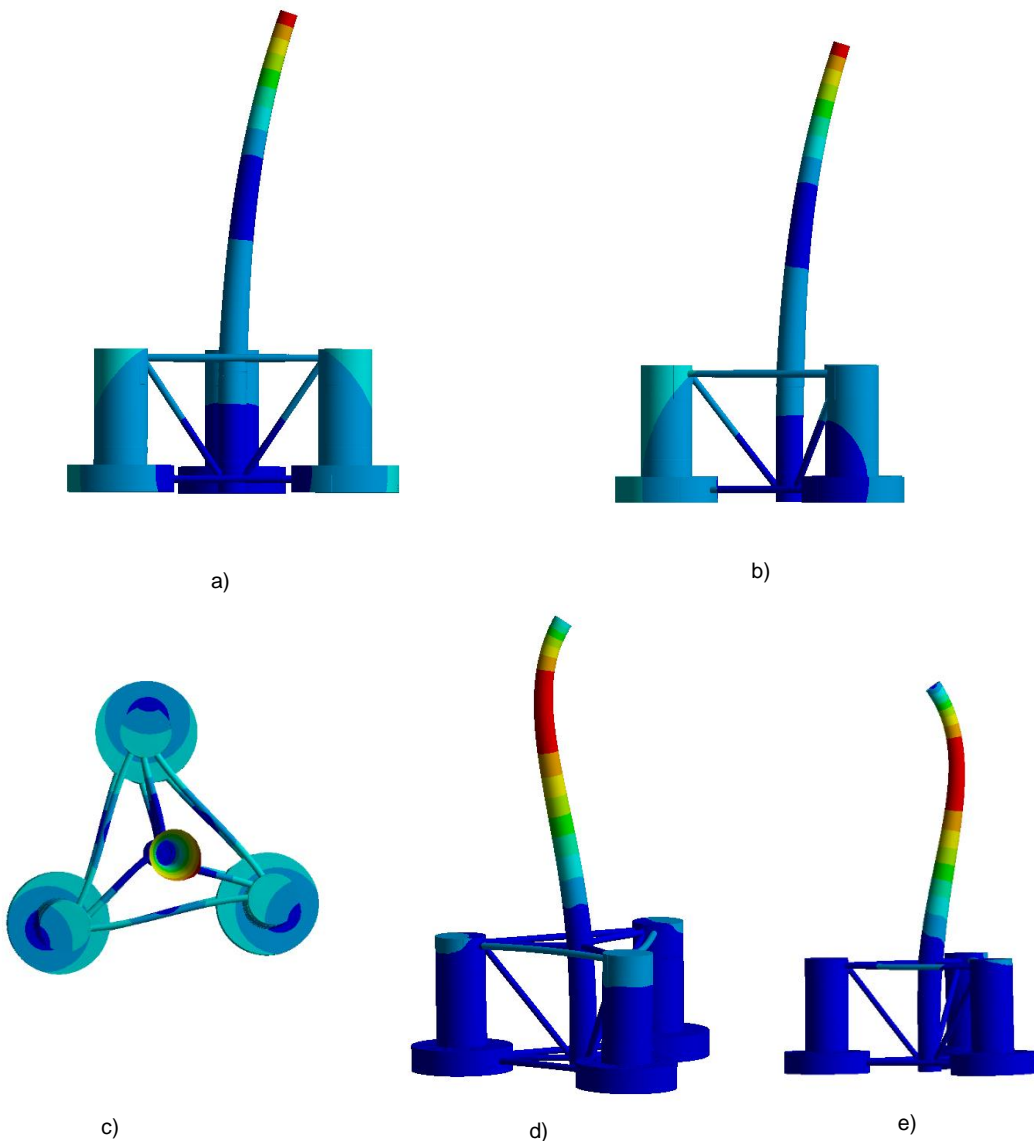


Figure 4.45 Figure Deformation Shapes from the Modal Analysis; a) Mode 1 – Side to Side; b) Mode 1 - Fore-Aft; c) Mode 2 – Torsion; d) Mode 2 - Fore-Aft; e) Mode 2 - Side-to-Side.

Table 4.3 Mode description and respective frequency.

Mode Description	Frequency [Hz]
Mode 1 – Side-to-Side	0.6896
Mode 1 – Fore-Aft	0.70212
Mode 2 - Torsion	1.8263
Mode 2 – Side-to-Side	2.1473
Mode 2 – Fore-Aft	2.5376

4.3. Comparison of Results

Table 4.4 shows the comparison of several properties of the obtained structure versus previous versions. From the comparison of these properties/results, it can be understood that the structure's performance was improved. However, the structure's steel mass was slightly increased.

Table 4.4 Platform versions comparison.

Properties	Original Structure	[79] Structure	Final Structure
Steel Mass	3 852 Tonnes	9 188 Tonnes	9 543 Tonnes
Overall Ballast's Water Mass	9 621 Tonnes	4 285 Tonnes	3 930 Tonnes
Fundamental Frequency	0.278 Hz	0.3094 Hz	0.6896 Hz
Lower Safety Coefficient at 11.4 m s⁻¹	0.032	1.57	1.67 ⁸
Lower Safety Coefficient at 24 m s⁻¹	Analysis not performed	0.94	1.668 ⁸

⁸Worth reminding, that these coefficient account for the presence of singularities. See Appendix D.

Chapter 5

5. Conclusions and Future Work

5.1. Conclusions

Wind power shows great potential as a clean technology used in energy production. Worldwide, onshore wind power is already established as a competitor at the energy production market. Going offshore presents great advantages and also allows for the expansion of the usable space for the exploration of this resource. Offshore wind power is already being used in several countries with a continental platform of low depth, such as Denmark, Netherlands, Germany or United Kingdom. Mostly, these wind farms make use of bottom fixed platforms and already have a key role in those countries electrical production.

The problem of going offshore is the increased depth of the sea for most locations, such as Portugal. The exploration of these zones seems to be only economically viable through the use of floating platforms. The association of a structurally successful platform with economical advantages has been the major problem. Although some solutions, such as the WindFloat or the Hywind, have already been implemented, these projects are still hugely funded.

The DeepCWind concept was developed with the objective of generating test data that would be suitable for the validation of modern floating offshore wind turbine modelling tools. Despite this, it was subjected to a structural analysis to examine how it endures the loads it was designed for. The original foundation showed an incapacity to produce successful results. It is worth noting that the DeepCwind Consortium did not partake on the development of the structure from a mechanical design perspective; instead, its intended use was only focused on the validation of hydrodynamic models. Therefore, no responsibility is credited to them for the structural results achieved by the original foundation.

After structurally improving the foundation, the requirements for successfully passing this part of the DLC 1.1 were achieved. However, only two wind speeds were considered as this is an academic research. For the completion of the whole DLC 1.1, a wide-spread of wind speeds must be used (inside the required interval), which results in the necessity of performing a large number of analysis for the certification of such a structure [91]. Other part of the DLC 1.1 also requires a fatigue analysis.

For both the wind speeds, 11.4 m s^{-1} and 24 m s^{-1} , the achieved lowest coefficient of safety is around 1.67. In spite of successfully passing the DLC requirements, this value may be influenced by the existence of singularities at certain regions of the BC member. Furthermore, it was established that the displacements formulation can have a majoring impact at the verified stresses. The modal analysis was also successfully passed through the alteration of the thicknesses used at the turbine tower.

The improved structure shows evidence of being capable of a practical implementation. It should be noted that the structure was improved with the objective of having the highest security coefficients while also considering the necessity for a possible decrease in mass. The structure was already partially optimized, in order to reduce the mass. However, it remained with thicknesses or layouts in some locations that may be further adjusted. It was decided to leave some regions with high strength, as the structure still has to successfully pass more demanding tests, such as fatigue analysis and other DLCs. It should also be reminded that the outside dimensions of the DeepCWind members were not to be changed. Also, the layout should only suffer minor changes.

Comparing these results to other existing options, the DeepCWind falls behind other solutions such as the WindFloat. The WindFloat owns a great advantage over the DeepCWind. Although it seems to give further instability to the WindFloat platform, the tower is located at one the corner columns of its layout. However, this is a great advantage as it avoids the use of a central column as the DeepCWind uses, thus avoiding many structural problems. At sea, the stability of the WindFloat is ensured just by adjusting the mass of water at the column that supports the tower.

5.2. Future Work

For future work, it is worth mentioning the following aspects, in decreasing order of importance:

- In order to have a more advantageous layout, the redesign of the structure to avoid the use of a central column would be far valuable;
- It should also be examined the suitability of using different outside diameters, more importantly changing the pontoons diameters;
- Fatigue analysis ought to be performed at critical sections, to fully evaluate the DLC 1.1;
- Further DLCs ought to be examined, in order to completely analyse the different conditions that the structure is subjected to;
- After successfully passing the required DLC's, the structure ought to be optimized in order to have the lowest steel mass.

Bibliography

- [1] International Energy Agency, "World Energy Outlook 2018 - EXECUTIVE SUMMARY," 2018.
- [2] U. S. Energy Information Administration, "Electricity and the Environment - Energy Explained, Your Guide To Understanding Energy - Energy Information Administration." [Online]. Available: https://www.eia.gov/energyexplained/index.php?page=electricity_environment. [Accessed: 08-Oct-2018].
- [3] "Wind Energy: Aims and Scope," *Wind Energy*.
- [4] "Where the Wind Blows – Onshore vs. Offshore Wind Energy | The Future of Energy." [Online]. Available: <http://futureofenergy.web.unc.edu/2016/04/06/where-the-wind-blows-onshore-vs-offshore-wind-energy/>. [Accessed: 09-Oct-2018].
- [5] U. S. Energy Information Administration, "How Electricity Is Generated - Energy Explained, Your Guide To Understanding Energy - Energy Information Administration." [Online]. Available: https://www.eia.gov/energyexplained/index.php?page=electricity_generating. [Accessed: 11-Oct-2018].
- [6] Engineering and Technology History, "Edison's Electric Light and Power System," 2018. [Online]. Available: https://ethw.org/Edison%27s_Electric_Light_and_Power_System. [Accessed: 09-Oct-2018].
- [7] U. S. Energy Information Administration, "Coal and the Environment - Energy Explained, Your Guide To Understanding Energy - Energy Information Administration." [Online]. Available: https://www.eia.gov/energyexplained/index.php?page=coal_environment. [Accessed: 10-Oct-2018].
- [8] Harvey, A.; Larson, A.; Patel, S., "History of Power: The Evolution of the Electric Generation Industry," *POWER Magazine*, 2017.
- [9] UNFCCC, "Kyoto Protocol Reference Manual On Accountin of Emissions and Assigned Amount," 2008.
- [10] UNFCCC, "ADOPTION OF THE PARIS AGREEMENT," 2015.
- [11] Green Rhino Energy, "What is Renewable Energy?" [Online]. Available: <http://www.greennrhinoenergy.com/renewable/>. [Accessed: 26-Apr-2019].
- [12] Wilson, A., "Physics 240 Coursework: The Grand Inga Dam Project," 2010.
- [13] "Joining the Energy Underground: Residential Geothermal Power Systems," *Scientific American*. [Online]. Available: <https://www.scientificamerican.com/article/earth-talks-geothermal/>. [Accessed: 14-Apr-2019].
- [14] "How do solar systems produce energy?," *Northwest Wind & Solar*. [Online]. Available: <https://www.nwwindandsolar.com/solar-power-in-seattle-and-the-northwest/how-do-solar-systems-produce-energy/>. [Accessed: 11-Oct-2018].
- [15] "Solar Power Information and Facts," *National Geographic*, 2019. [Online]. Available: <https://www.nationalgeographic.com/environment/global-warming/solar-power/>. [Accessed: 26-Apr-2019].
- [16] U. S. Energy Information Administration, "Wave Power - Energy Explained, Your Guide To Understanding

- Energy.” [Online]. Available: https://www.eia.gov/energyexplained/index.php?page=hydropower_wave. [Accessed: 14-Apr-2019].
- [17] TheGreenAge, “Agucadoura Wave Farm, Portugal.” [Online]. Available: <https://www.thegreenage.co.uk/cos/agucadoura-wave-farm-portugal/>. [Accessed: 26-Apr-2019].
- [18] Lewis, T.; Writer, S., “Underwater Ocean Turbines: A New Spin on Clean Energy?,” *Live Science*, 2014. [Online]. Available: <https://www.livescience.com/47188-ocean-turbines-renewable-energy.html>. [Accessed: 26-Apr-2019].
- [19] “The Basics of Wind Energy,” American Wind Energy Association. [Online]. Available: <https://www.awea.org/wind-101/basics-of-wind-energy>. [Accessed: 26-Apr-2019].
- [20] BP, “Electricity - BP Statistical Review of World Energy 2018.”
- [21] “Electricity Statistics,” International Energy Agency. [Online]. Available: <https://www.iea.org/statistics/electricity/>. [Accessed: 26-Apr-2019].
- [22] Stockton, N., “Electric Cars Could Destroy the Electric Grid—or Fix It Forever,” *WIRED*, 2018. [Online]. Available: <https://www.wired.com/story/electric-cars-impact-electric-grid/>. [Accessed: 11-Oct-2018].
- [23] Associação Portuguesa de Energias Renováveis, “Balanço da Produção de Electricidade de Portugal Continental.” [Online]. Available: <https://www.apren.pt/pt/energias-renovaveis/producao/>. [Accessed: 27-Apr-2019].
- [24] Marvel, K.; Kravitz, B.; Caldeira, K., “Geophysical limits to global wind power,” *Nature Climate Change*, vol. 3, no. 2, pp. 118–121, Feb. 2013.
- [25] Windpower Engineering & Development, “Vertical Axis Wind Turbines vs Horizontal Axis Wind Turbines,” 2009. [Online]. Available: <https://www.windpowerengineering.com/construction/vertical-axis-wind-turbines-vs-horizontal-axis-wind-turbines/>. [Accessed: 11-Oct-2018].
- [26] Maciel, G. da S. G., “Desenvolvimento e Projeto Mecânico de uma Fundação para uma Turbina Eólica Offshore Engenharia Mecânica,” 2017.
- [27] Lynn, P. A.; Wiley, J., *Onshore and Offshore Wind Energy An Introduction*. 2012.
- [28] Baghzouz, Y., “Characteristics of Wind Power Systems.”
- [29] Solon, O., “Giant inflatable wind turbine to soar to 300 metres,” *Wired UK*, 2014. [Online]. Available: <https://www.wired.co.uk/article/altaeros-wind-turbine>. [Accessed: 07-May-2019].
- [30] Thompson, A., “9 Weird Ways We Can Harness the Wind’s Energy,” *Popular Mechanics*, 2017. [Online]. Available: <https://www.popularmechanics.com/science/energy/g2944/9-alternative-wind-turbine-designs/>. [Accessed: 12-Oct-2018].
- [31] Ogura, J.; Marsh, J., “Typhoon turbine could power Japan for 50 years,” *CNN*, 2016. [Online]. Available: <https://edition.cnn.com/style/article/typhoon-catchers-japan-challenergy/index.html>. [Accessed: 07-May-2019].
- [32] Lloyd, D., “Wind Energy: Advantages and Disadvantages,” *PH240 Coursework, Standford University*, 2014. [Online]. Available: <http://large.stanford.edu/courses/2014/ph240/lloyd2/>. [Accessed: 27-Apr-2019].

- [33] U. S. Department of Energy, "The Inside of a Wind Turbine | Department of Energy." [Online]. Available: <https://www.energy.gov/eere/wind/inside-wind-turbine-0>. [Accessed: 15-Oct-2018].
- [34] de Vries, E., "How to service and maintain a wind turbine blade," *Windpower Monthly*, 2012.
- [35] Alternative Energy Tutorials, "Wind Turbine Blade Design, Flat Blades or Curved Blades." [Online]. Available: <http://www.alternative-energy-tutorials.com/energy-articles/wind-turbine-blade-design.html>. [Accessed: 15-Oct-2018].
- [36] Carlin, J., "Wind Turbine Blades 102."
- [37] Kerrigan, S., "The Scientific Reason Why Wind Turbines Have 3 Blades," *Interesting Engineering*, 2018. [Online]. Available: <https://interestingengineering.com/the-scientific-reason-why-wind-turbines-have-3-blades>. [Accessed: 15-Oct-2018].
- [38] "Wind Turbines: How Many Blades?," *Danish Wind Industry Association*, 2003. [Online]. Available: <http://drømstørre.dk/wp-content/wind/miller/windpower> web/en/tour/design/concepts.htm. [Accessed: 27-Apr-2019].
- [39] Aerotrope, "Riva Calzoni M33 Single Bladed Wind Turbine." [Online]. Available: <https://www.aerotrope.com/what-we-do/wind/wind-turbine-design-case-studies/riva-calzoni.html>. [Accessed: 07-May-2019].
- [40] Milborrow, D., "Are three blades really better than two?," *Windpower Monthly*, 2011. [Online]. Available: <https://www.windpowernonthly.com/article/1083653/three-blades-really-better-two>. [Accessed: 27-Apr-2019].
- [41] Bachynski, E. E.; Moan, T., "Design considerations for tension leg platform wind turbines," *Marine Structures*, vol. 29, no. 1, pp. 89–114, 2012.
- [42] GE Renewable Energy, "Wind Turbines." [Online]. Available: <https://www.ge.com/renewableenergy/wind-energy/onshore-wind/turbines>. [Accessed: 07-May-2019].
- [43] Cruz, J.; Atcheson, M.; Collu, M., *Floating Offshore Wind Energy - The Next Generation of Wind Energy*. 2016.
- [44] Hill, J. S., "World's First Ever Offshore Wind Farm Finally Dismantled," *CleanTechnica*, 2017. [Online]. Available: <https://cleantechnica.com/2017/09/11/worlds-first-ever-offshore-wind-farm-finally-dismantled/>. [Accessed: 12-Nov-2018].
- [45] Frangoul, A., "The largest offshore wind farm on the planet opens," *CNBC*, 06-Sep-2018.
- [46] Smith, R., "This giant offshore turbine could be the future of wind energy," *World Economic Forum*, 2018. [Online]. Available: <https://www.weforum.org/agenda/2018/03/giant-offshore-turbine-wind-energy-haliade-x/>. [Accessed: 23-Oct-2018].
- [47] "Offshore and Onshore Wind Farms," *NES Global Talent*, 2016. [Online]. Available: <https://www.nesgt.com/blog/2016/07/offshore-and-onshore-wind-farms>. [Accessed: 23-Oct-2018].
- [48] Delony, J., "Foundation First: Designing Offshore Wind Turbine Substructures for Maximum Cost

- Reduction," *Renewable Energy World*, 2016. [Online]. Available: <https://www.renewableenergyworld.com/articles/print/volume-19/issue-10/features/wind/foundation-first-designing-offshore-wind-turbine-substructures-for-maximum-cost-reduction.html>. [Accessed: 07-May-2019].
- [49] Peyrard, C., "OFFSHORE WIND TURBINE FOUNDATIONS," 1989.
- [50] Wind Europe, "Offshore Wind in Europe: Key trends and statistics 2018," 2019.
- [51] World Wind Technology, "Good foundations: the pros and cons of monopiles," 2013. [Online]. Available: <http://www.windpower-international.com/features/featuregood-foundations-the-pros-and-cons-of-monopiles-4158694/>. [Accessed: 16-Nov-2018].
- [52] Danish Wind Industry Association, "Offshore Foundations: Mono Pile," 2003. [Online]. Available: http://drømstørre.dk/wp-content/wind/miller/windpower_web/en/tour/rd/monopile.htm. [Accessed: 16-Nov-2018].
- [53] Foxwell, D., "Monopiles continue to evolve as search continues for optimised foundations," *Offshore Wind Journal*, 2018. [Online]. Available: https://www.owjonline.com/news/view,monopiles-continue-to-evolve-as-search-continues-for-optimised-foundations_50720.htm. [Accessed: 27-Apr-2019].
- [54] Copenhagen Infrastructure Partners, "First jacket installation in Beatrice Offshore Wind Farm," 2017. [Online]. Available: <http://cipartners.dk/first-jacket-installation-beatrice-offshore-wind-farm/>. [Accessed: 18-Nov-2018].
- [55] 4C Offshore, "Jacket or Lattice Structures," 2013. [Online]. Available: <https://www.4coffshore.com/windfarms/jacket-or-lattice-structures-aid5.html>. [Accessed: 18-Nov-2018].
- [56] 4C Offshore, "Suction Bucket or Caisson Foundations," 2016. [Online]. Available: <https://www.4coffshore.com/windfarms/suction-bucket-or-caisson-foundations-aid11.html>. [Accessed: 18-Nov-2018].
- [57] Institution of Civil Engineers, "The EDF Renewables Blyth Offshore Demonstrator Windfarm Project." [Online]. Available: <https://www.ice.org.uk/what-is-civil-engineering/what-do-civil-engineers-do/blyth-offshore-demonstrator-windfarm-project>. [Accessed: 19-Nov-2018].
- [58] BAM Nuttall Ltd, "Blyth Offshore Demonstrator Wind Farm Project: First Gravity Base Foundation lowered onto sea bed," 2017. [Online]. Available: <https://www.bam.com/en/press/press-releases/2017/8/blyth-offshore-demonstrator-wind-farm-project-first-gravity-base>. [Accessed: 19-Nov-2018].
- [59] 4C Offshore, "Alpha Ventus." [Online]. Available: <https://www.4coffshore.com/windfarms/alpha-ventus-germany-de01.html>. [Accessed: 19-Nov-2018].
- [60] 4C Offshore, "Tripod Support Structures," 2013. [Online]. Available: <https://www.4coffshore.com/windfarms/tripod-support-structures-aid7.html>. [Accessed: 19-Nov-2018].
- [61] EWEA, *The next step for offshore wind energy*, no. May. 2014.
- [62] equinor, "Hywind - leading floating offshore wind solution." [Online]. Available:

- <https://www.equinor.com/en/what-we-do/hywind-where-the-wind-takes-us.html#>. [Accessed: 04-Dec-2018].
- [63] equinor, "Hywind - facts and figures." [Online]. Available: <https://www.equinor.com/en/what-we-do/hywind-where-the-wind-takes-us/hywind-up-close-and-personal.html>. [Accessed: 04-Dec-2018].
- [64] Rigzone, "How Do Spars Work?" [Online]. Available: https://www.rigzone.com/training/insight.asp?insight_id=307. [Accessed: 04-Dec-2018].
- [65] Brito, A., "ASM Industries constrói plataformas para parque eólico no mar de Viana," *Publico*, 2018.
- [66] Diamond Offshore Drilling, "Offshore Rig Basics." [Online]. Available: <http://www.diamondoffshore.com/offshore-drilling-basics/offshore-rig-basics>. [Accessed: 05-Dec-2018].
- [67] Rigzone, "How Does a Tension Leg Platform (TLP) Work?" [Online]. Available: https://www.rigzone.com/training/insight.asp?insight_id=305&c_id=1. [Accessed: 05-Dec-2018].
- [68] "Produção de renováveis excedeu consumo em Portugal pela primeira vez," *Publico*, 03-Apr-2018.
- [69] Cabrita-Mendes, A., "Portugal é um dos campeões europeus de energia eólica," *Jornal de Negócios*, 19-Jun-2017.
- [70] Costa, P. A. da S., "Atlas do Potencial Eólico para Portugal Continental," 2004.
- [71] Rifer, M., "Extensão da plataforma continental vai estar fechada até 2021," *O Jornal Económico*, 19-Aug-2018.
- [72] Silva, C. A. S., "RoadMap para as Energias Renováveis Offshore em Portugal."
- [73] Cabrita-Mendes, A., "Projecto eólico no mar supera ondas de 17 metros e ventos de 111 quilómetros/hora," *Jornal de Negócios*, 02-Jun-2016.
- [74] EDP, "WindFloat." [Online]. Available: <https://www.edp.com/pt-pt/windfloat>. [Accessed: 15-Nov-2018].
- [75] Cabrita-Mendes, A., "Central eólica offshore ligada à rede em 2019," *Jornal de Negócios*, 24-Apr-2018.
- [76] Robertson, A. et al., "Summary Of Conclusions And Recommendations Drawn From The Deepcwind Scaled Floating Offshore Wind System Test Campaign," *Proceedings of the ASME 2013 32nd International Conference on Ocean, Offshore and Arctic Engineering*, no. July 2013, pp. 1–13, 2013.
- [77] "FAST 8." [Online]. Available: <https://nwtc.nrel.gov/FAST8>. [Accessed: 07-May-2019].
- [78] Robertson, A. et al., "Definition of the Semisubmersible Floating System for Phase II of OC4," 2014.
- [79] Dias, D. R., "Análise da Integridade Estrutural duma Fundação Flutuante para Energia Eólica Offshore Engenharia Mecânica," 2017.
- [80] SimScale, "What is FEA | Finite Element Analysis?" [Online]. Available: <https://www.simscale.com/docs/content/simwiki/fea/whatisfea.html>. [Accessed: 19-Feb-2019].
- [81] Ansys 2019R1 Help Section, "Transient Structural Analysis." [Online]. Available: https://www.sharcnet.ca/Software/Ansys/17.0/en-us/help/wb_sim/ds_transient_mechanical_analysis_type.html. [Accessed: 15-Feb-2019].
- [82] Thorby, D., *Structural Dynamics and Vibration in Practice: An Engineering Handbook*, 1st ed. ELSEVIER,

2008.

- [83] Jonkman, J.; Butterfield, S.; Musial, W.; Scott, G., "Definition of a 5-MW Reference Wind Turbine for Offshore System Development," 2009.
- [84] Jonkman, J. M., "Dynamics Modeling and Loads Analysis of an Offshore Floating Wind Turbine," 2007.
- [85] Simões Da Silva, L. *et al.*, *Design of Joints in Steel and Composite Structures*, 2nd ed. European Convention for Constructional Steelwork, 2016.
- [86] Jonkman, J. M.; Buhl, M. L., "FAST User's Guide," 2005.
- [87] Platt, A.; Jonkman, B.; Jonkman, J., "InflowWind User's Guide," 2016.
- [88] Jonkman, J. M.; Hayman, G. J.; Jonkman, B. J.; Damiani, R. R., "AeroDyn v15 User's Guide and Theory Manual," 2015.
- [89] Jonkman, J. M.; Robertson, A. N.; Hayman, G. J., "HydroDyn User's Guide and Theory Manual."
- [90] Hall, M., "MoorDyn User's Guide," 2017.
- [91] Germanischer Lloyd, "Guideline for the Certification of Offshore Wind Turbines," 2012.
- [92] Ansys 2019R1 Help Section, "Static Structural Analysis." .
- [93] Lee, H.-H., *Finite Element Simulations with ANSYS Workbench 17*. Stephen Schroff, 2017.
- [94] Harish, A., "What Is the Modal Analysis and Why Is It Necessary?," *SimScale*, 2019. [Online]. Available: <https://www.simscale.com/blog/2016/12/what-is-modal-analysis/>. [Accessed: 21-Feb-2019].
- [95] Divincenzo, N., "Natural Frequency and Resonance," *Siemens PLM Community*, 2018. [Online]. Available: <https://community.plm.automation.siemens.com/t5/Testing-Knowledge-Base/Natural-Frequency-and-Resonance/ta-p/498422>. [Accessed: 21-Feb-2019].
- [96] Letcher, T. M., *Wind Energy Engineering: A handbook for onshore and offshore wind turbines*. 2017.
- [97] DNV/Riso, "Guidelines for Design of Wind Turbines," 2002.
- [98] Ansys 2019R1 Help Section, "Shell Elements." [Online]. Available: https://www.sharcnet.ca/Software/Ansys/16.2.3/en-us/help/ans_elem/HIp_E_ShellElements.html. [Accessed: 21-Feb-2019].
- [99] Akin, J. E., "Finite Element Analysis Concepts via SolidWorks," 2009.
- [100] Ansys 2019R1 Help Section, "Submodeling." [Online]. Available: https://www.sharcnet.ca/Software/Ansys/17.0/en-us/help/wb_sim/ds_submodeling.html. [Accessed: 22-Feb-2019].
- [101] Ansys 2019R1 Help Section, "Modeling a Shell-Solid Assembly." [Online]. Available: https://www.sharcnet.ca/Software/Ansys/17.2/en-us/help/ans_ctec/HIp_ctec_solshel.html. [Accessed: 22-Feb-2019].
- [102] Adams, V.; Askenazi, A., *Building Better Products with Finite Element Analysis*, 1st ed. OnWord Press, 1998.
- [103] Veikos, N., "Verifying Your Finite Element Analysis Results," *engineering.com*, 2016. [Online]. Available: <https://www.engineering.com/DesignSoftware/DesignSoftwareArticles/ArticleID/11356/Verifying->

Your-Finite-Element-Analysis-Results.aspx. [Accessed: 12-Apr-2019].

- [104] Olivera, G. A., "Structural Dynamic Behaviour of a Floating Platform for offshore Wind Turbines."
- [105] Hordvik, T., "Design analysis and optimisation of mooring system for floating wind turbines Student: Open Floating wind turbine Mooring system Optimisation," Norwegian University of Science and Technology, 2011.
- [106] GL, "Guideline for the Certification of Wind Turbine," 2010.
- [107] Amzallag, C.; Gerey, J. P.; Robert, J. L.; Bahuaud, J., "Standardization of the rainflow counting method for fatigue analysis," *International Journal of Fatigue*, vol. 16, no. 4, pp. 287–293, 1994.
- [108] Budynas, R. G. (Richard G.; Nisbett, J. K.; Shigley, J. E., *Shigley's Mechanical Engineering Design*. 2008.
- [109] ASTM, "ASTM E 1049-85 - Standard Practices for Cycle Counting in Fatigue Analysis," 1997.
- [110] MATLAB Help Section, "Rainflow counts for fatigue analysis." [Online]. Available: <https://www.mathworks.com/help/signal/ref/rainflow.html>. [Accessed: 24-Mar-2019].
- [111] Mahran, M.; Elsabbagh, A.; Negm, H., "A comparison between different finite elements for elastic and aero-elastic analyses," *Journal of Advanced Research*, vol. 8, no. 6, pp. 635–648, Nov. 2017.
- [112] "Commercial Software ANSYS 16." .
- [113] ANSYS, "FEA Best Practices."
- [114] "Use Water Jet Cutting for Cutting Metal," *Water Jet Sweden*. [Online]. Available: <https://www.waterjetsweden.co.uk/materials/metal>. [Accessed: 28-Apr-2019].
- [115] "Grand Turn-key Delivery and Performance Testing."
- [116] Association de Recherche sur les Structures Métalliques Marines, *Design Guides for Offshore Structures Vol. 1 - Welded Tubular Joints*. Éditions Technip, 1987.
- [117] aerodyn, "Services - Wind turbines." [Online]. Available: <https://www.aerodyn.de/services/wind-turbines/wind-turbines/>. [Accessed: 03-May-2019].
- [118] "MIT Course Text - Design of electromechanical robotic systems," 2009.

Appendix A - Original Foundation Details

A.1. Static Shell Simulation – Displacement Formulation

Figure A.1 shows the overall result of the shell analysis, using the displacement formulation. Additionally, three points of interest were selected and their magnitudes expressed.

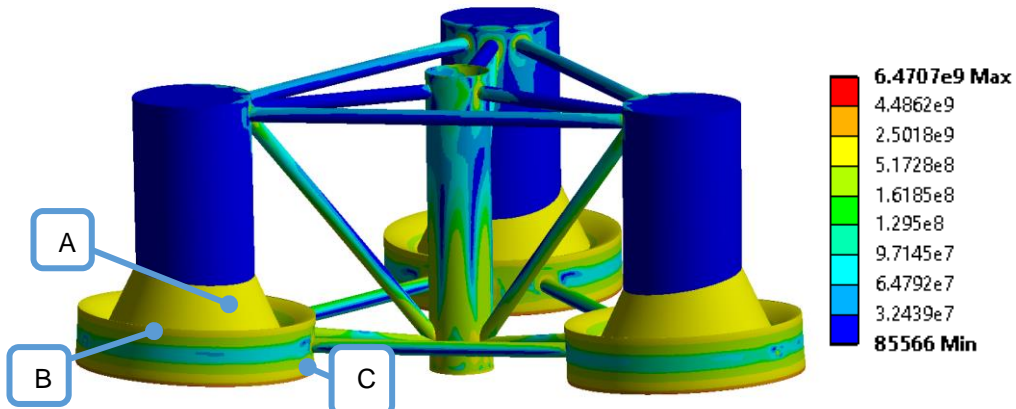


Figure A.1 Global model analysis. Units in Pascal.

The referred points have the following magnitudes: **A** is 1 713 MPa, **B** is 1 362 MPa and **C** is 875 MPa.

A.2. Submodel Analysis – Displacement Formulation

Figure A.2 shows a part of a submodel of one of the BC members. Four points were selected and their stress values stated.

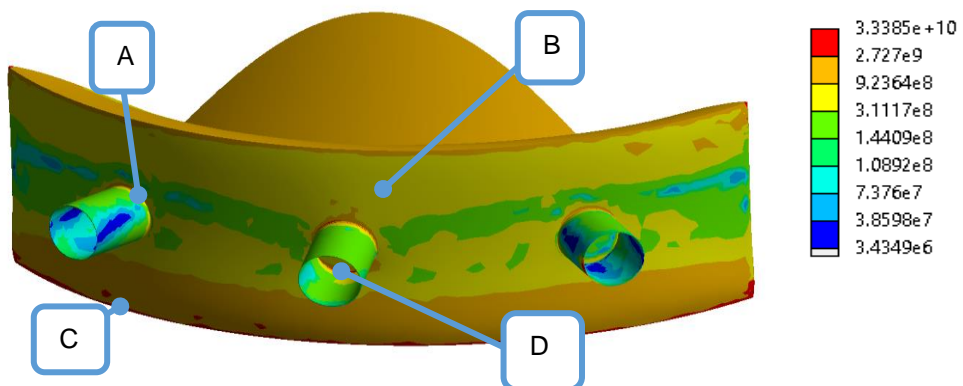


Figure A.2 BC Submodel analysis' details. Units in Pascal.

These points have the following magnitudes: **A** is 1 450 MPa, **B** is 734 MPa, **C** is 3 621 MPa and **D** is 3 728 MPa.

A.3. Static Shell Simulation – Springs Formulation

Figure A.3 shows two details of this analysis. Four points of interest were selected. On the left, the bottom of the MC column and on the right, the top of the UC.

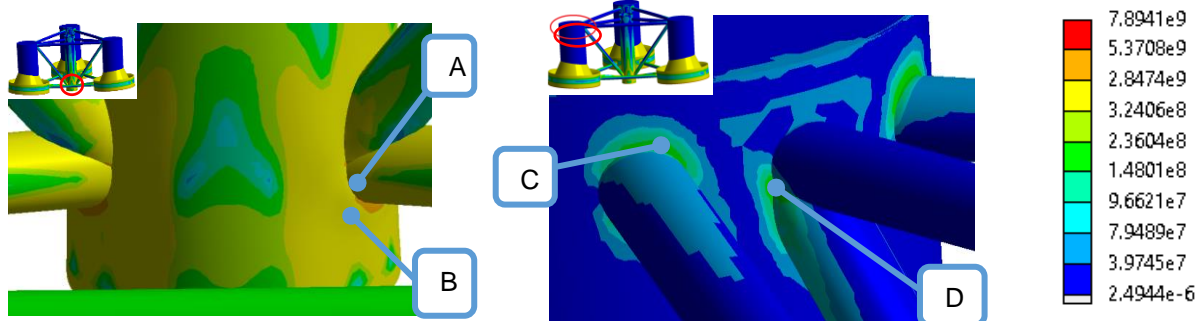


Figure A.3 Details of the global analysis with the springs formulation. Units in Pascal.

These points have the following magnitudes: **A** is 652 MPa, **B** is 2 170 MPa, **C** is 173 MPa and **D** is 392 MPa.

A.4. Submodel Analysis – Springs Formulation

Figure A.4 and Figure A.5 show the submodels with the greatest importance. Several points of interest were selected. On the left of Figure A.4, the top of the MC column and on the right, the top of the UC. Figure A.5 shows the bottom of the MC member.

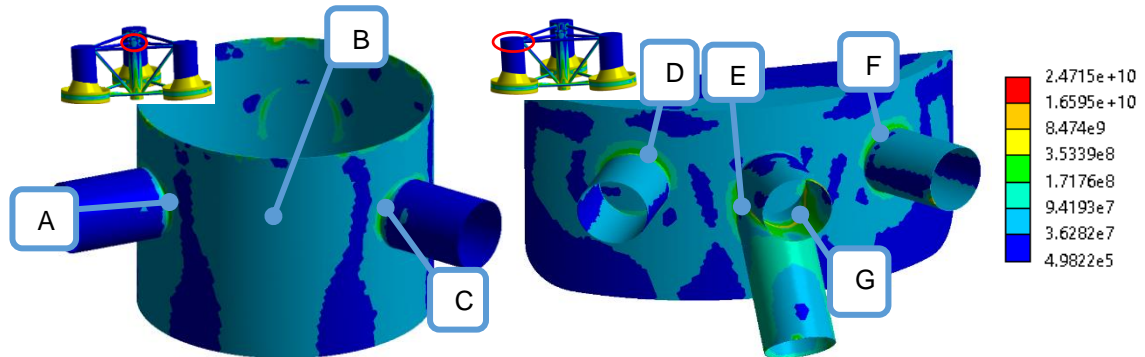


Figure A.4 Submodel Analysis' details. Units in Pascal.

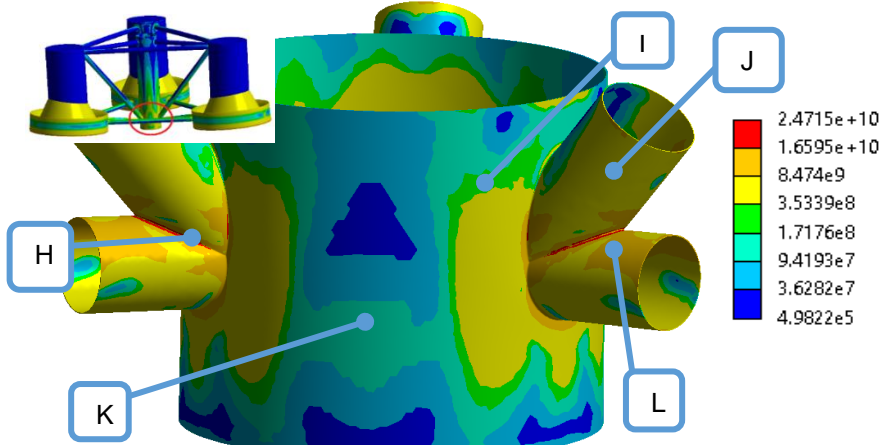


Figure A.5 Submodel Analysis' details. Units in Pascal.

These points have the following magnitudes: A is 294 MPa, B is 45 MPa, C is 337 MPa, D is 390 MPa, E is 450 MPa, F is 327 MPa, G is 717 MPa, H is 14 061 MPa, I is 565 MPa, J is 2 373 MPa, K is 377 MPa and L is 4 141 MPa.

Appendix B - Improvement Process Details

This appendix shows details on previously discussed analyses while showing other analysis formerly omitted.

B.1. Pontoons Disjoint and Joint Connection Comparison

Figure B.1 shows details and reference points of the disjoint (at the top) and overlapped (at the bottom) connections analyses. Table B.1 shows the comparison of these points.

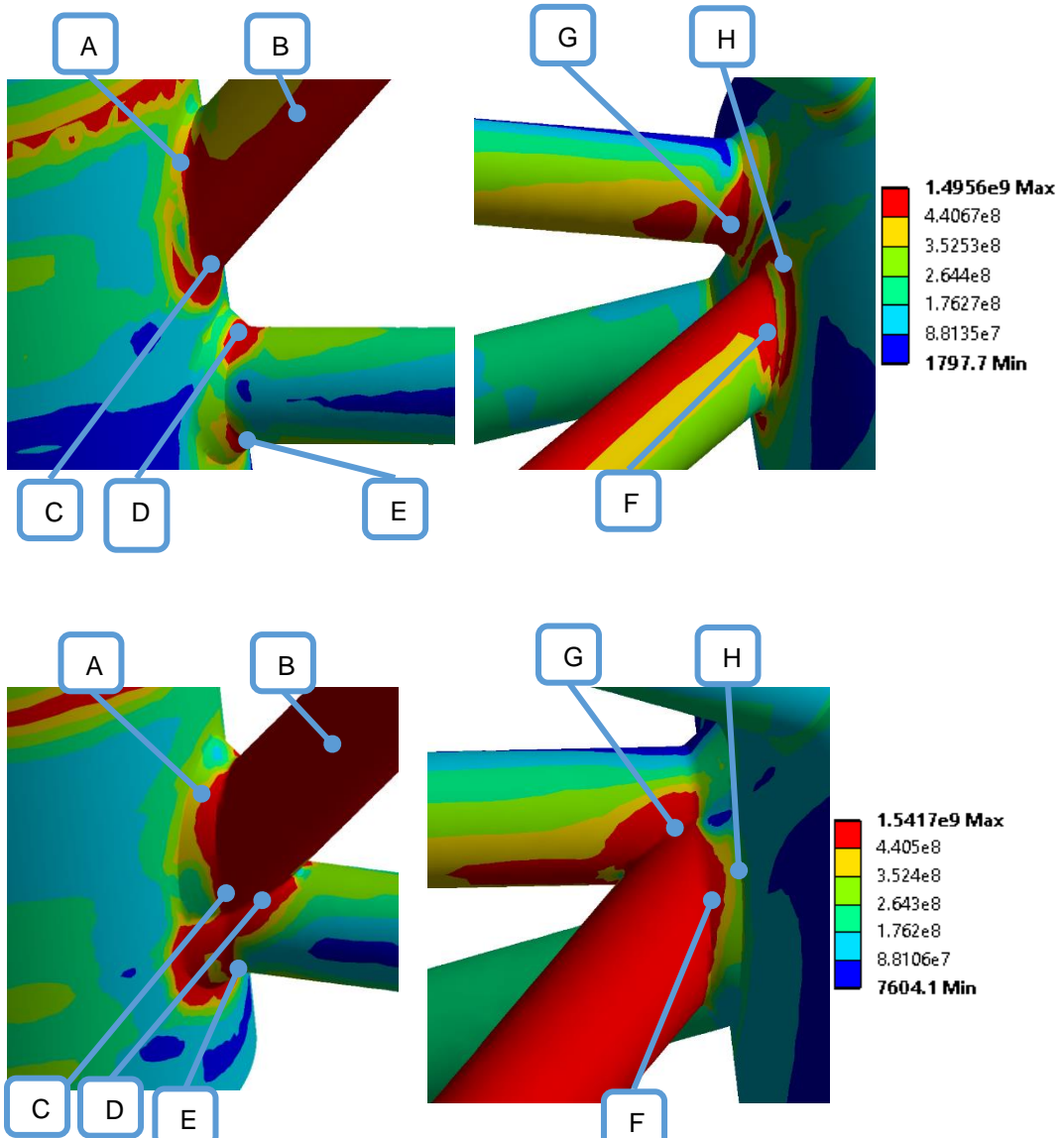


Figure B.1 Pontoons disjoint and joint connection comparison. Units in Pascal.

Table B.1 Comparison of disjoint and joint connections.

	Disjoint	Joint
A	506 MPa	477 MPa
B	468 MPa	510 MPa
C	826 MPa	724 MPa
D	892 MPa	634 MPa
E	546 MPa	536 MPa
F	652 MPa	498 MPa
G	1 041 MPa	720 MPa
H	509 MPa	344 MPa

From the general examination of both analyses, it may seem that the use of disjoint connections is favourable, as the areas affected by high stresses are reduced. In spite of this, on the layout with disjoint connections, the highest stresses increase relatively to the overlapped joints. Therefore, it was decided to use the overlapped joints.

B.2. Pontoons Conical Transitions with Triangular Reinforcements

At first, it was considered to use conical transitions around all members. Although, as referred, conical transitions around the CB members would produce high eccentricity that would create major problems for the production of these reinforcements. This eccentric reinforcement is shown in Figure B.2, marked by a red circle.



Figure B.2 BC member conical transition.

Instead, triangular reinforcements were used at the CB joints, as shown in Figure B.3 a). For further support, triangular reinforcements were also used inside the conical transitions, as shown in Figure B.3 c) while b) shows the outside view of the reinforced conical transition.

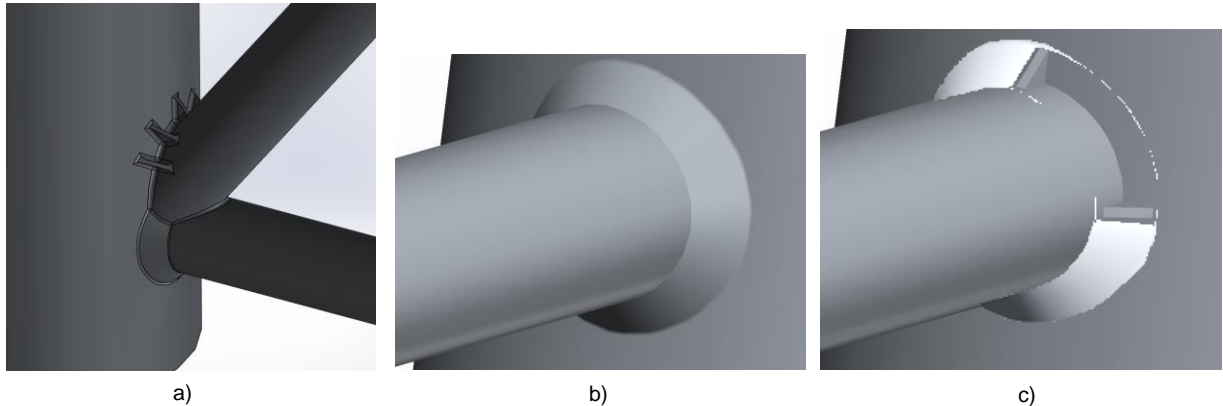


Figure B.3 Conical connections with triangular reinforcements. a) triangular reinforcement at the CB members; b) exterior view of reinforced conical connection; c) interior view of reinforced conical connection (the conical transition is partially transparent, allowing to see the reinforcements inside).

Figure B.4 shows details and reference points of these analysis, with the use of triangular reinforcements, at the top, and without them, at the bottom. Table B.2 shows the comparison of these points.

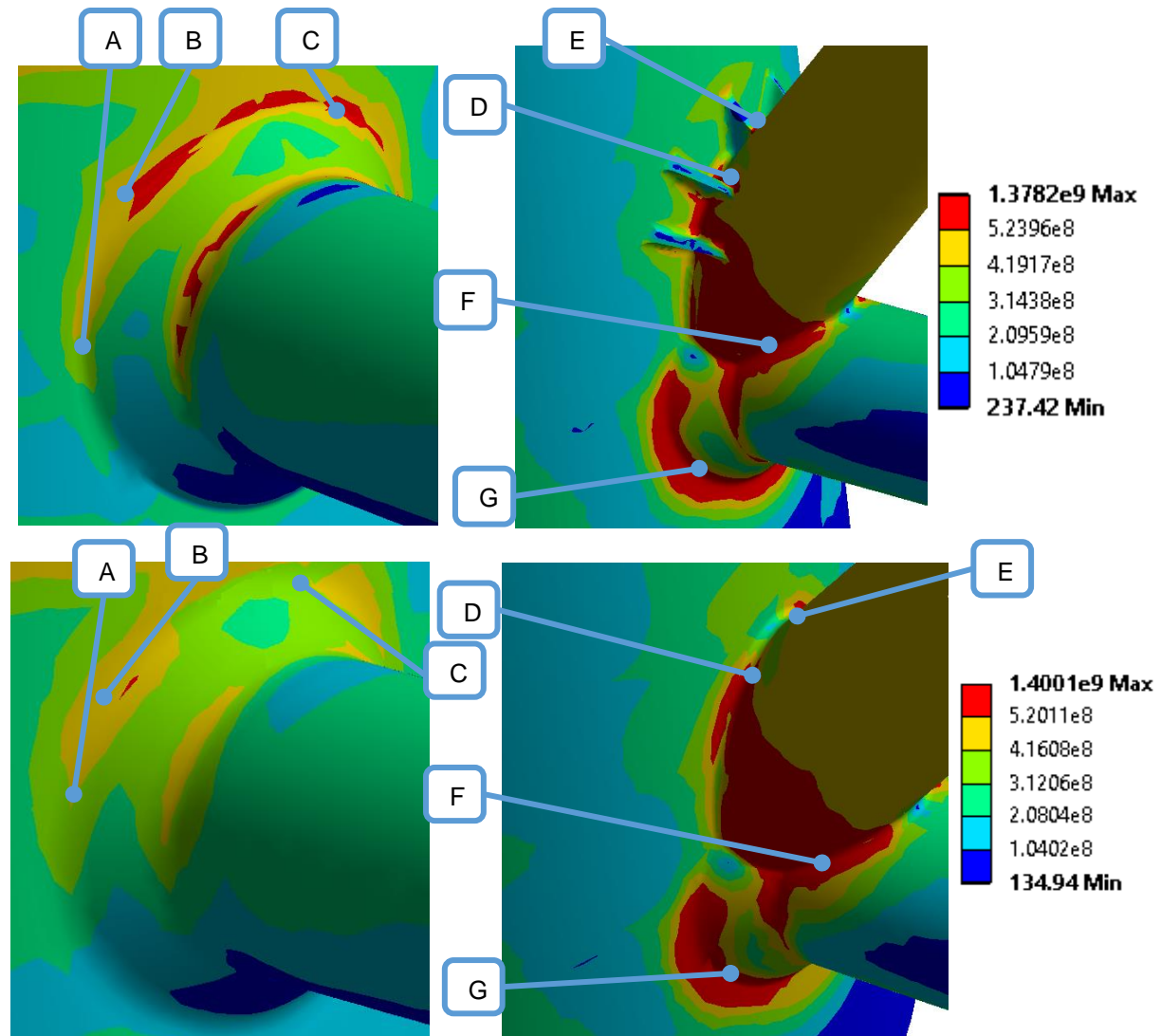


Figure B.4 Comparison of reinforced conical transitions with simple conical transitions. Units in Pascal.

Table B.2 Comparison of reinforced and simple conical transitions.

	With Triangle Reinforcements	Without Triangle Reinforcements
A	400 MPa	389 MPa
B	548 MPa	478 MPa
C	542 MPa	359 MPa
D	983 MPa	610 MPa
E	455 MPa	382 MPa
F	681 MPa	647 MPa
G	892 MPa	666 MPa

As it is perceptible, the use of triangular reinforcements is not advantageous.

B.3. Pontoons Simple Conical Transitions

These analyses compare the use of conical transitions without other reinforcements to not using conical transitions at all. At the CB members' joint, no reinforcements were used. Figure B.5 and Figure B.6 show details and reference points of the reinforced and not reinforce analyses, respectively. Table B.3 shows the comparison of these points.

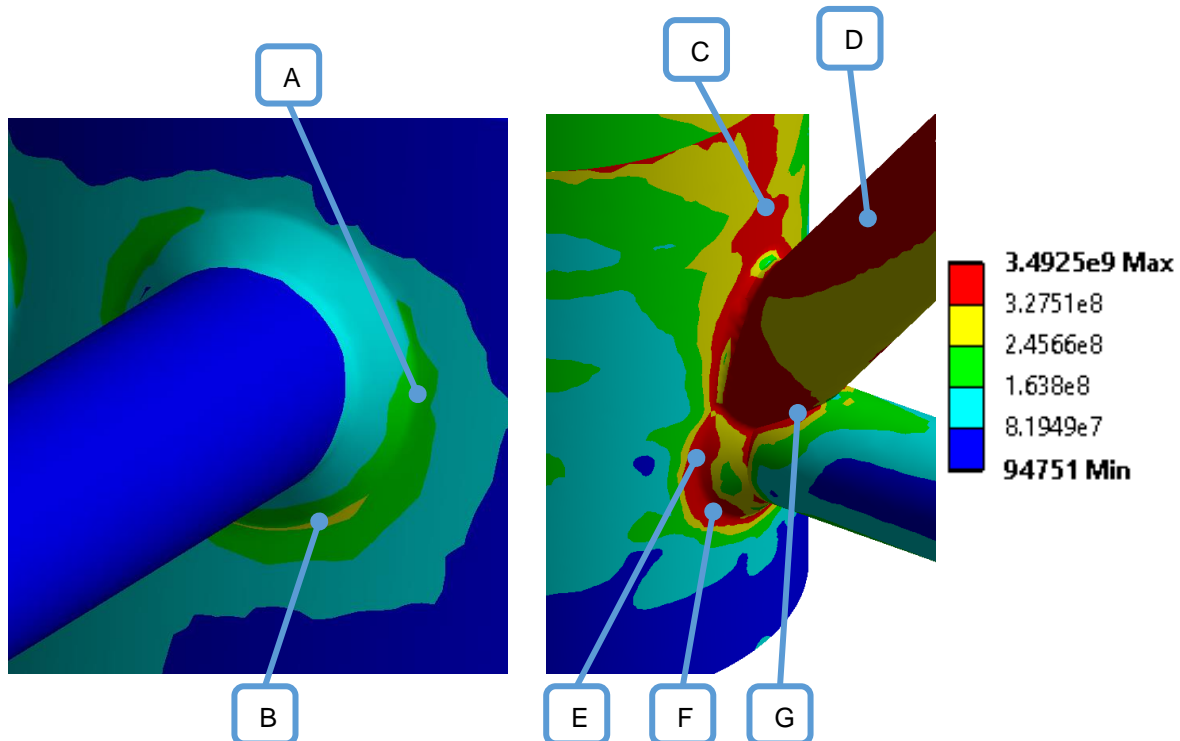


Figure B.5 Simple conical transitions. Units in Pascal.

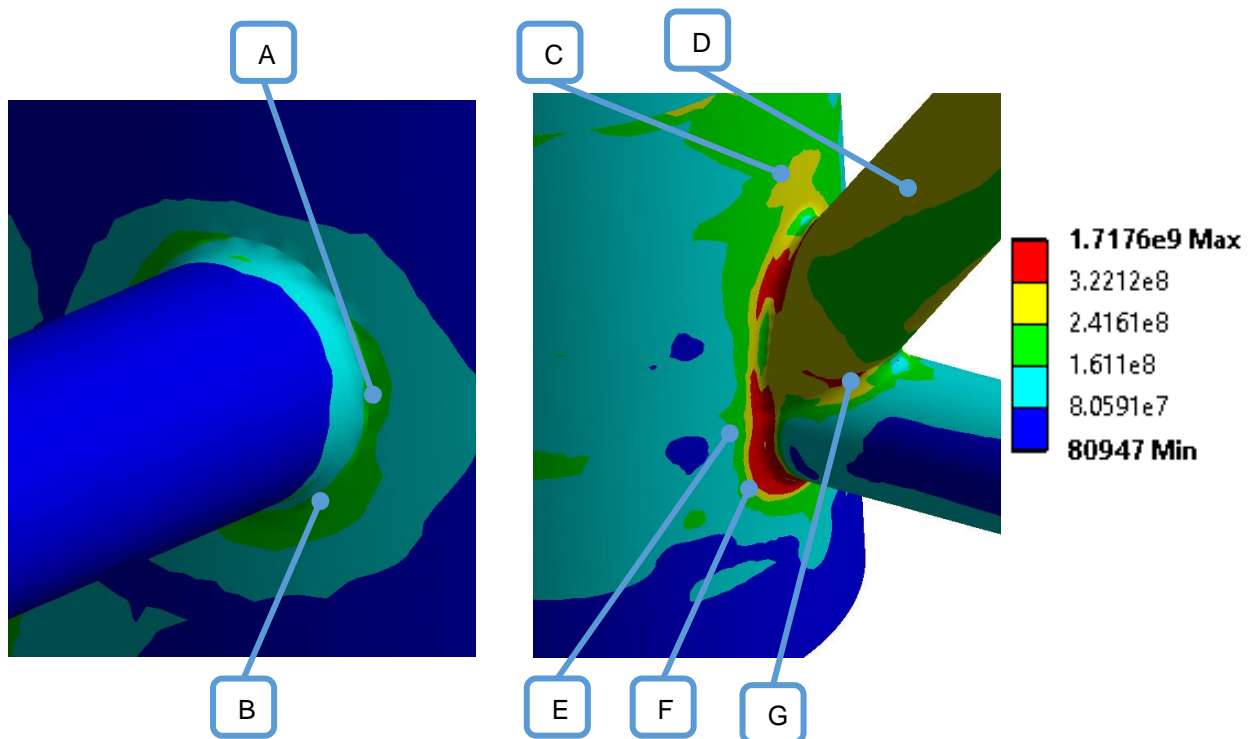


Figure B.6 Without conical transitions. Units in Pascal.

Table B.3 Comparison of conical transitions and no conical transitions.

	With Conical Transitions	Without Conical Transitions
A	201 MPa	196 MPa
B	260 MPa	222 MPa
C	450 MPa	298 MPa
D	365 MPa	266 MPa
E	549 MPa	182 MPa
F	635 MPa	224 MPa
G	461 MPa	349 MPa

It was concluded that the use of conical transitions was not beneficial for this application.

Appendix C - Final Analysis Details

This section shows details and reference points of the final analyses. Its intended use is for a better understanding of the stresses verified at certain locations.

C.1. Springs Formulation at 11.4 m s^{-1}

Figure C.1 shows the top of the UC with some highlighted points. The scale is the same for all pictures.

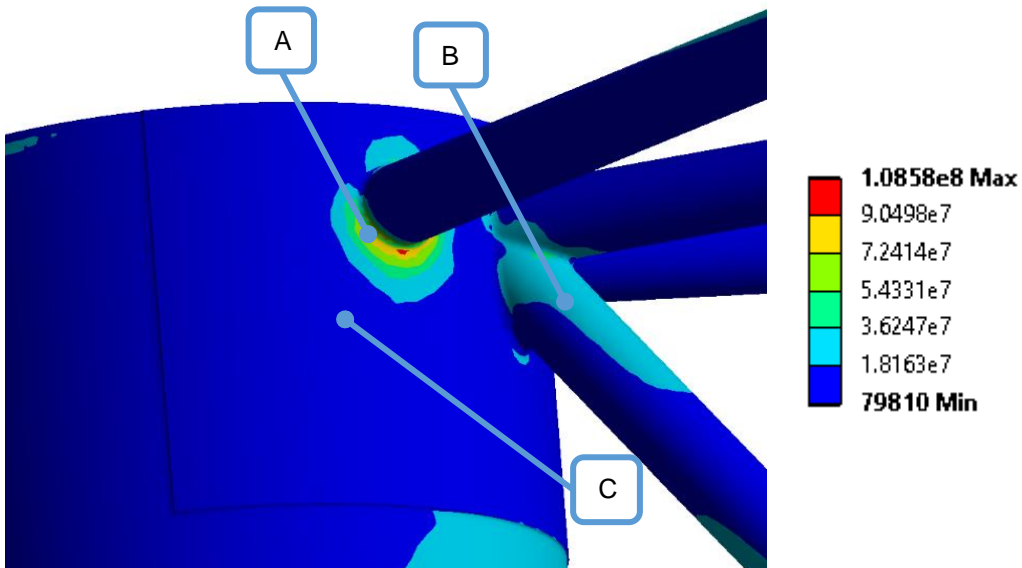


Figure C.1 UC detail. Units in Pascal.

The selected points have the following magnitudes: A is 82 MPa, B is 18 MPa and C is 4 MPa. Figure C.2 shows the connections at the BC.

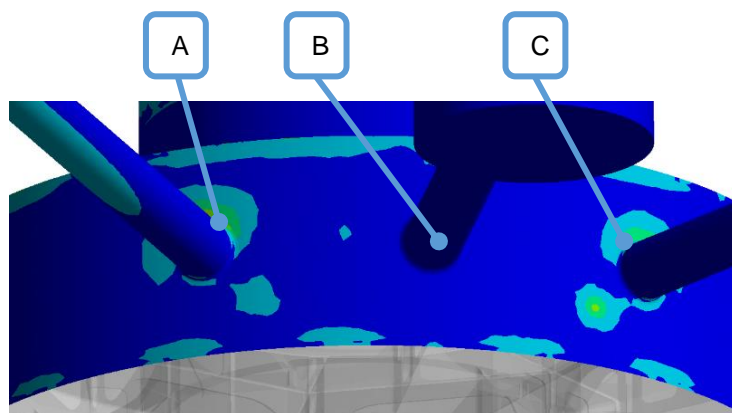


Figure C.2 BC connections detail.

The selected points have the following magnitudes: A is 26 MPa, B is 6 MPa and C is 36 MPa. Figure C.3 shows the top of the MC.

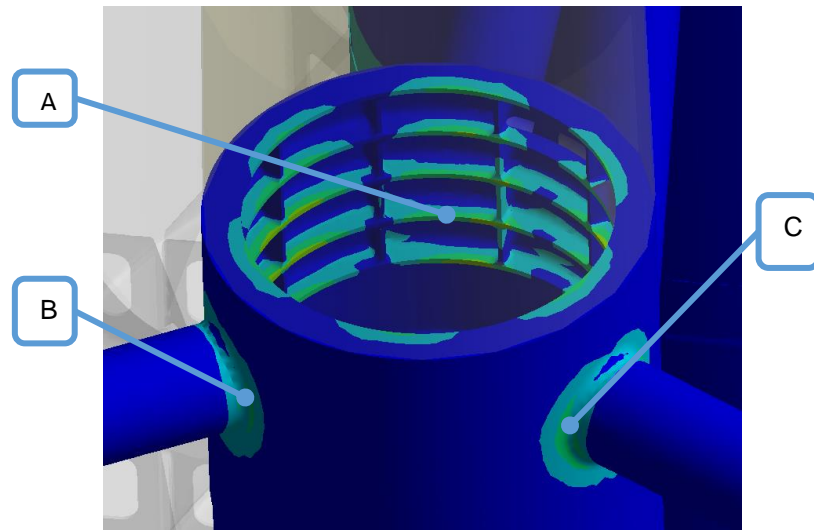


Figure C.3 MC top detail.

The selected points have the following magnitudes: **A** is 46 MPa, **B** is 29 MPa and **C** is 32 MPa.

Figure C.4 shows a section cut of the bottom of the MC.

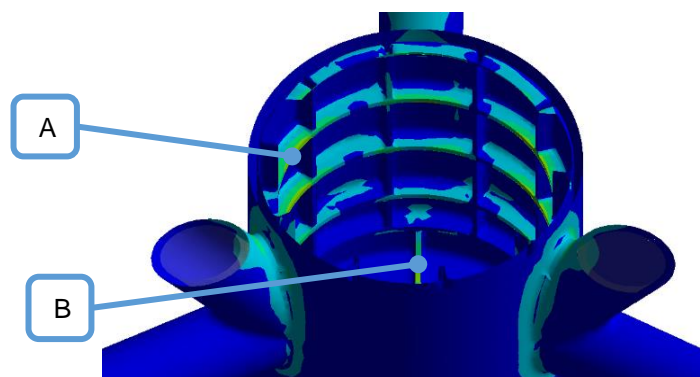


Figure C.4 MC bottom cut view detail.

The selected points have the following magnitudes: **A** is 61 MPa and **B** is 68 MPa. Figure C.5 shows the bottom of the MC.

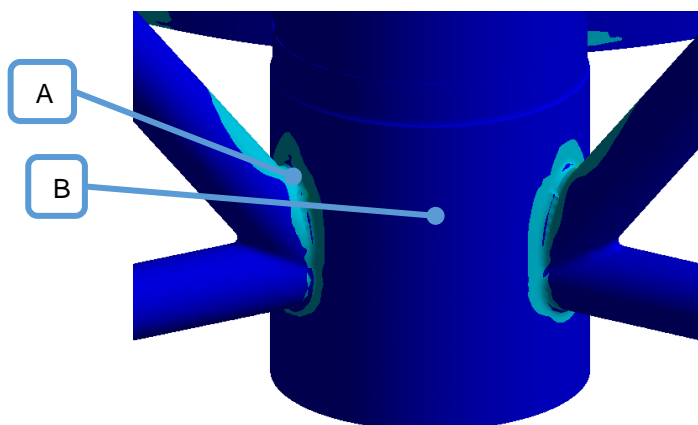


Figure C.5 MC bottom detail.

The selected points have the following magnitudes: **A** is 23 MPa and **B** is 21 MPa. **Figure C.6** shows the variation of the safety coefficient for this analysis.

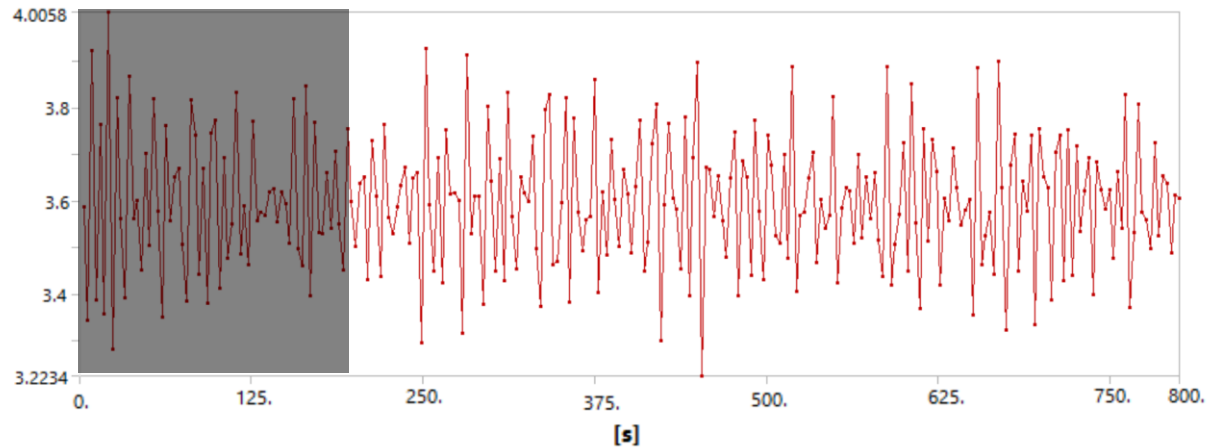


Figure C.6 Time series of the safety coefficient.

C.2. Displacements Formulation 11.4 m s^{-1}

Figure C.7 shows a BC's section cut, along with some highlighted points.

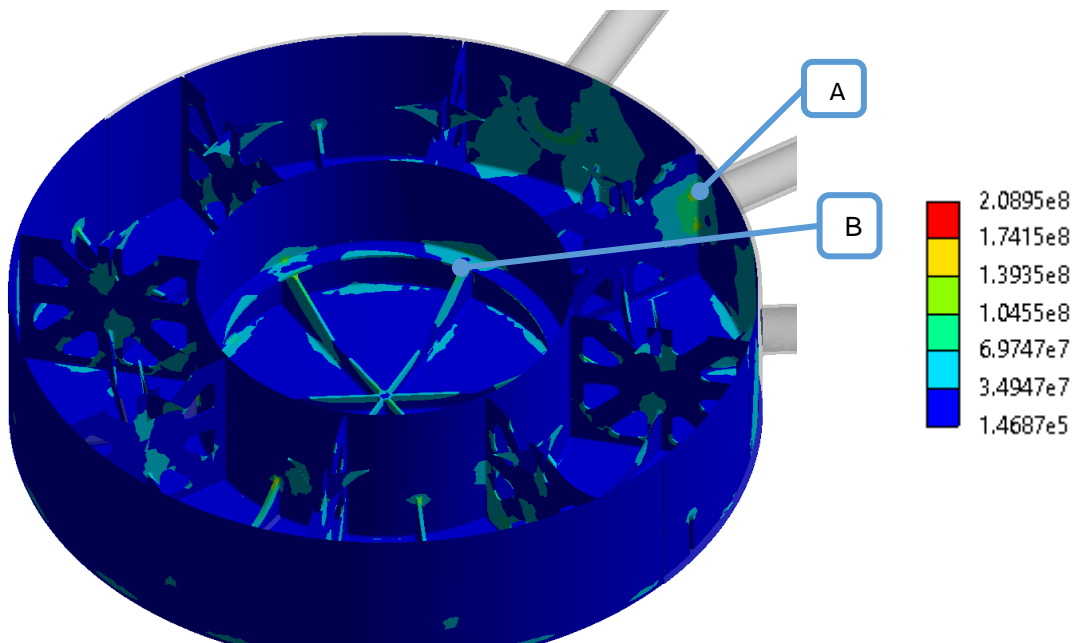


Figure C.7 BC cut view. Units in Pascal.

The selected points have the following magnitudes: **A** is 153 MPa and **B** is 85 MPa. Figure C.8 shows the variation of the safety coefficient for this analysis.

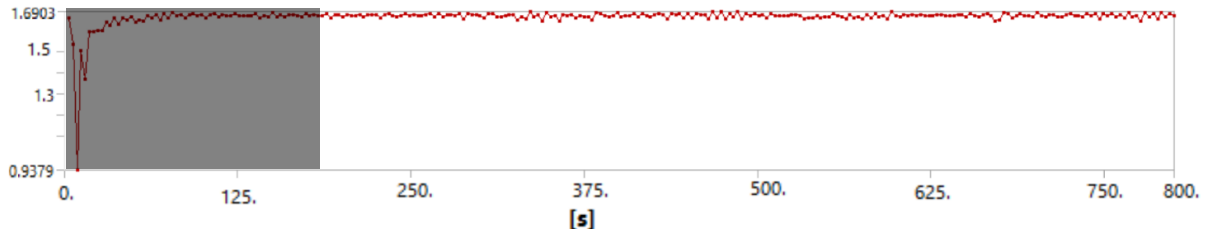


Figure C.8 Time series of the safety coefficient.

C.3. Springs Formulation at 24 m s^{-1}

Figure C.9 shows the top of the UC with some highlighted points. The scale is the same for all pictures.

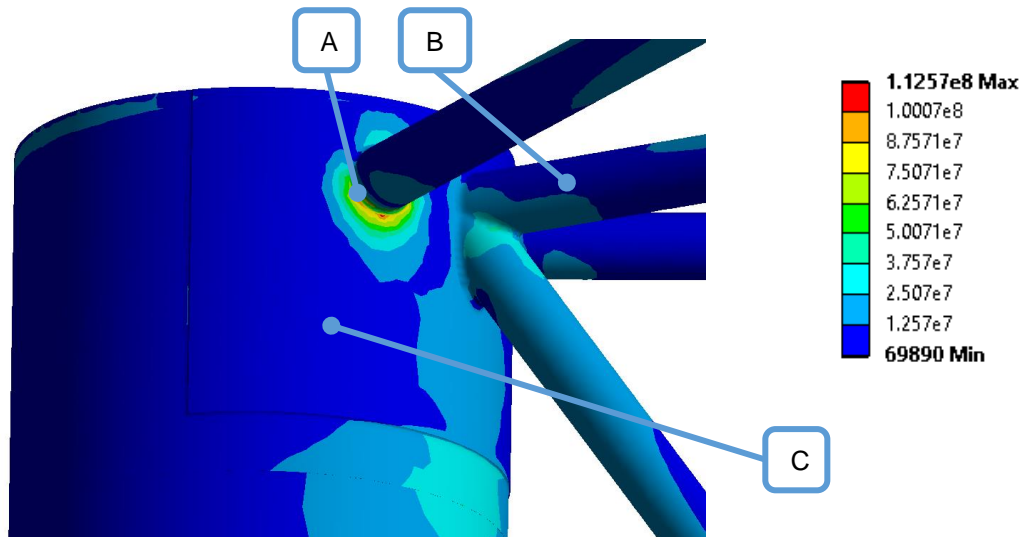


Figure C.9 UC detail. Units in Pascal.

The selected points have the following magnitudes: **A** is 94 MPa, **B** is 10 MPa and **C** is 6 MPa. Figure C.10 shows the connections at the BC.



Figure C.10 BC connections detail.

The selected points have the following magnitudes: **A** is 37 MPa and **B** is 40 MPa. Figure C.11 shows the top of the MC.

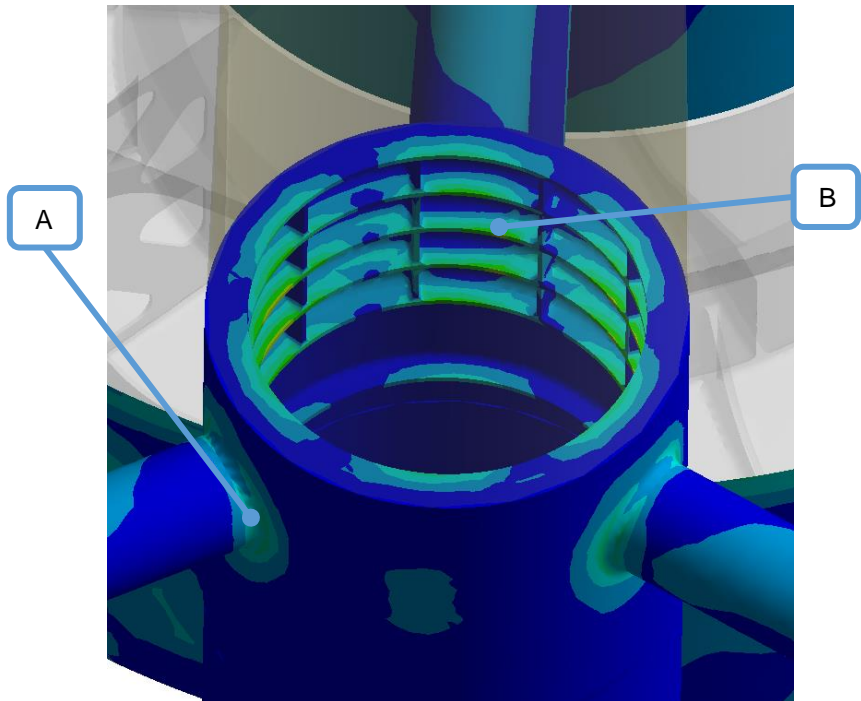


Figure C.11 MC top detail.

The selected points have the following magnitudes: **A** is 27 MPa and **B** is 42 MPa. Figure C.12 shows a section cut of the bottom of the MC.

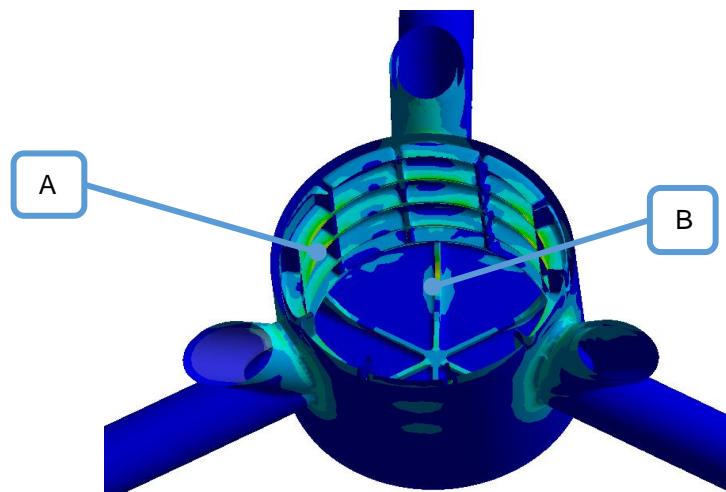


Figure C.12 MC bottom cut view detail.

The selected points have the following magnitudes: **A** is 58 MPa and **B** is 67 MPa. Figure C.13 shows the bottom of the MC.

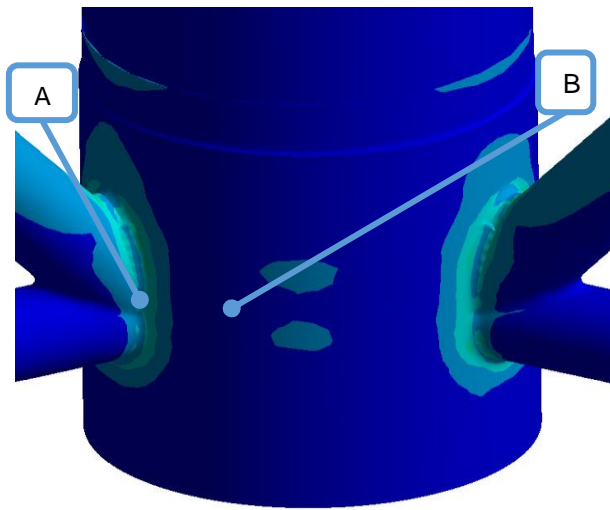


Figure C.13 MC bottom detail.

The selected points have the following magnitudes: **A** is 24 MPa and **B** is 7 MPa. Figure C.14 shows the variation of the safety coefficient for this analysis.

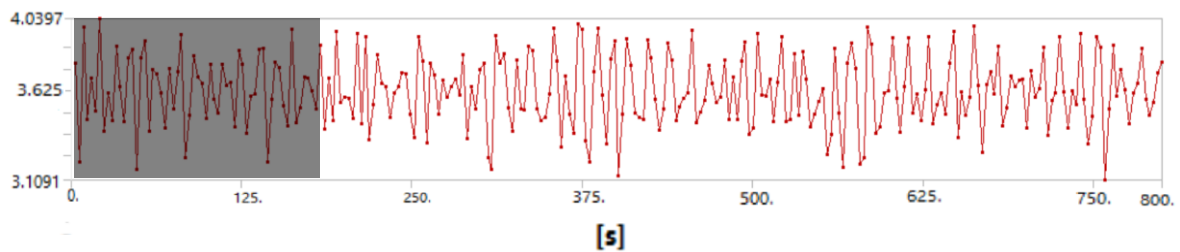


Figure C.14 Time series of the safety coefficient.

C.4. Displacements Formulation at 24 m s^{-1}

Figure C.15 shows a BC's section cut, along with some highlighted points.

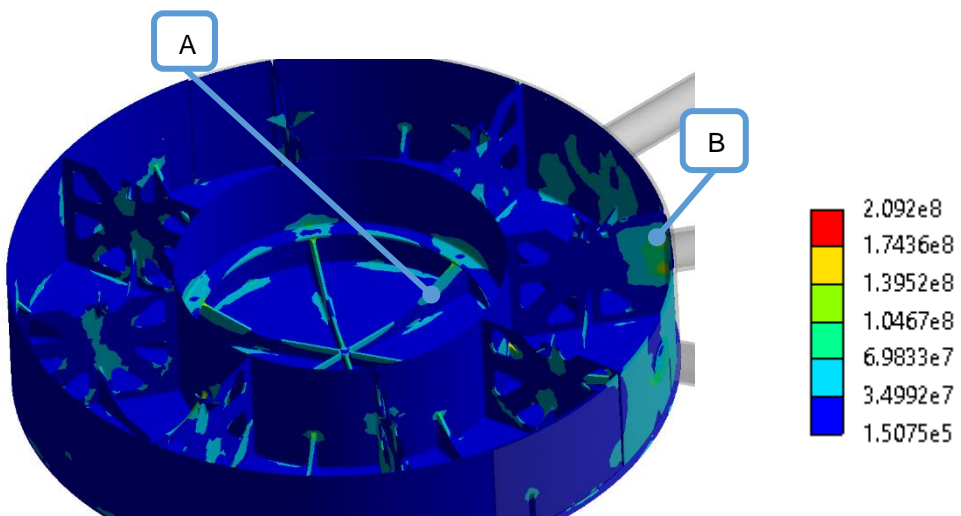


Figure C.15 BC cut view. Units in Pascal.

The selected points have the following magnitudes: **A** is 43 MPa and **B** is 123 MPa. Figure C.16 shows the variation of the safety coefficient for this analysis.



Figure C.16 Time series of the safety coefficient.

C.5. Modal Analysis Supplement

As previously described at the modal analysis section, the first and second bending mode and/or torsion modes are usually examined for onshore wind power towers. However, the present structure is offshore and of the floating type, thus other frequencies may be of concern. Therefore, Table C.1 and Figure C.17 show the data of other frequencies, as well as their deformation shapes. These resonance frequencies affect specifically the platform, instead of being more damaging for the tower as the other aforementioned.

Table C.1 Platform's Natural Frequencies

Mode Description	Frequency [Hz]
Platform 1 st Torsion Mode	1.0581
Platform 1 st Bending Mode Fore-Aft	2.023
Platform 1 st Bending Mode Side-to-Side	2.0241

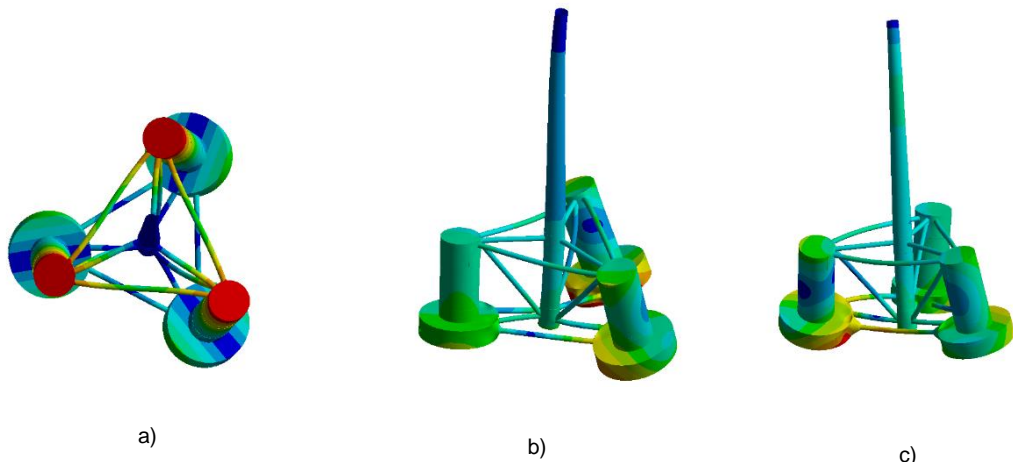


Figure C.17 Deformation shapes. a) Mode 1 - Torsion; b) Mode 1 - Bending Fore-Aft; c) Mode 1 - Bending Side-to-Side.

Appendix D - Singularities

As previously discussed, the results of the analysis of the BC members using the displacements formulation may be influenced by the presence of singularities, consequently yielding a relatively low coefficient of safety when compared to other regions of the structure. In spite of this, the yielded results allow for the structure to fulfil the required criteria. Figure D.1 shows the location of these singularities at the BC member, marked by a red circle while Figure D.2 shows a detail of one of these locations with some points of interest.

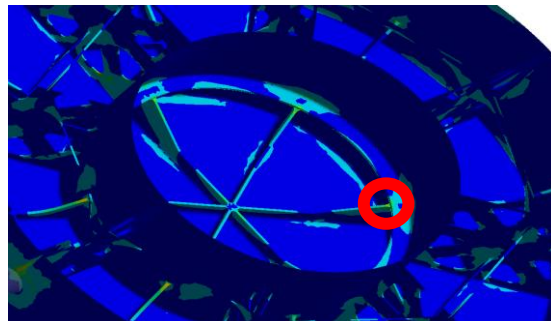


Figure D.1 BC detail.

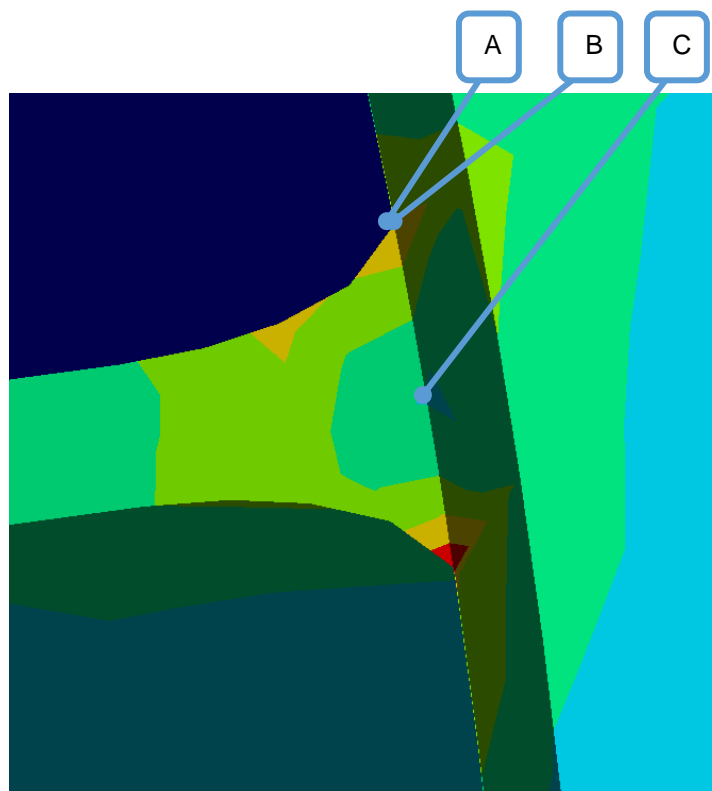


Figure D.2 Singularity detail.

The highlighted points of interest have the following magnitudes: **A** is 176 MPa, **B** is 160 MPa and **C** is 69 MPa. It is worth mentioning that the reinforcement section has 100 mm, thus the variation from A to B occurs is 50 mm. Further analysis, with higher refinements of these locations made the point of high stress to be further isolated at the sharp edge, while its influence decreased in its vicinities. In future works, these locations should be examined carefully.